DET NORSKE VERITAS

Final Report
Effect of Ethanol Blends and Batching Operations on SCC of Carbon Steel

Pipeline & Hazardous Materials Safety Administration
U.S. Department of Transportation

Consolidated Program for Development of Guidelines for Safe and Reliable Pipeline Transportation of Ethanol Blends – WP#325
Report No.: 2010-9362 (86082756)
February 8, 2011

Effect of Ethanol Blends and Batching Operations on SCC of Carbon Steel	DET NORSKE VERITAS USA, INC. 5777 Frantz Road Dublin, OH 43017-1386, United States Tel: (614) 761-1214 Fax: (614) 761-1633 http://www.dnv.com
For: Pipeline & Hazardous Materials Safety Administration U.S. Department of Transportation East Building, 2nd Floor 1200 New Jersey Ave., SE Washington, DC 20590	
Account Ref.: DTPH56-08-T-000013	

Date of First Issue:	October 30, 2010	Project No.	86082756
Report No.:	2010-9362	Organization Unit:	SRIUS915
Revision No.:	1	Subject Group:	

Summary:

This is the draft final report of the project on blending and batching (WP#325) of the Consolidated Program on Development of Guidelines for Safe and Reliable Pipeline Transportation of Ethanol Blends. The other two aspects of the consolidated program, ethanol source effects (WP#323) and monitoring (WP#327) are reported separately.

Prepared by:	Narasi Sridhar	*Signature* 
Verified by:	Arun Agarwal	*Signature* 
Approved by:		*Signature*

Indexing Terms

Key Words

Service Area

Market Segment

Rev. No. / Date:	Reason for Issue:	Prepared by:	Approved by:	Verified by

Executive Summary

Pipeline companies have a keen interest in assessing the feasibility of transporting fuel grade ethanol (FGE) and ethanol blends in existing pipelines. Previous field experience and laboratory research, funded by PRCI and API, has shown that steel can suffer stress corrosion cracking (SCC) when exposed to FGE in the presence of oxygen. Though cracking was prevalent under some conditions, variability in cracking susceptibility of steel was noted with different ethanol chemistries. Additionally, the effects of residence time of FGE or its blends on SCC (i.e. crack initiation time and growth rate) had not yet been determined. Finally, the effects of ethanol on other materials used in the pipelines, such as elastomeric seals, had to be evaluated. Thus, the major objectives of the program are to:

1. Develop data necessary to make engineering assessments of the feasibility of transporting FGE and FGE blends in existing pipelines. The transportation may be in a dedicated pipeline or in a batching mode.
2. Identify ethanol blends that can be transported in existing pipelines without significant modification of the system and operations (Case 1), blends that require significant modifications (Case 2) and blends that cannot be transported in existing pipelines, but could be moved in specially designed systems (Case 3).
3. Characterize the time to initiation of SCC in a range of potent ethanol environments and identify safe operating and or batching practices that prevent the initiation and growth of SCC.

The project accomplished substantially all of these objectives. The following were the major conclusions of the program:

- Although slow strain rate tests (SSRT) are considered to be conservative (i.e. if SCC is not observed in SSRT, it is unlikely to occur in the field, but SCC detected in SSRT does not necessarily mean SCC will occur in the field), the results of SSRT in terms of the effects of various factors on ethanol SCC were in agreement with the more realistic fracture mechanics based crack growth measurements.

- No SCC was observed in aerated ethanol less than about 15 percent (by volume) blend (E-15), prepared with SFGE. These results were consistent between slow stran rate tests and the long-term crack growth tests performed under loading conditions that simulate pipeline operating conditions.

- Significant SCC was observed with both simulated and one lot of corn-based FGE but the simulated FGE was a slightly more potent SCC agent. The increased chloride concentration in the simulated ethanol could be a significant factor in increasing the susceptibility to SCC.

- Dissolved oxygen is necessary for causing SCC under natural exposure conditions. SCC can be prevented by removing dissolved oxygen. If dissolved oxygen cannot be removed, certain inhibitors may be effective in mitigating SCC.

- Although some proprietary commercial inhibitors were shown to be effective in mitigating SCC, ammonium hydroxide (a non-proprietary chemical) is the most effective in mitigating SCC. It is not clear whether the addition of these inhibitors will take the ethanol out of ASTM Specification since the D-4806 specification includes inhibitors. However, these inhibitors are only effective in mitigating corrosion of automotive components and not SCC of pipe steel. T

- The base metal of all of the steels evaluated (X42, X46, X52, and X60) and cast steel exhibited measurable susceptibility to SCC and the differences probably are not significant from an integrity standpoint.

- Crack growth rates for the seamless, the cast steel, and the low frequency electric resistance welded (LFERW) line pipe steels were somewhat lower than for the double submerged arc welded (DSAW) and two other ERW line pipe steels but all steels exhibited relatively deep cracks.

- No major effect of weld metallurgy on SCC behavior was observed in SSR tests of base metal, weld metal, and heat affected zone specimens from girth welds and DSAW long seam welds. The crack depths in the tests were similar for the three different metallurgies, although the weld metals appeared to be somewhat more resistant to cracking.

- The absence of SCC in several tests with high frequency electric resistance welded (HFERW) and LFERW specimens, where the notch was located at or near the bond line of the long seam weld, was attributed to the poor mechanical properties of the bond line.

- In two SSR tests with one LFERW pipe steel, the bond line did appear to be more resistant to SCC in the ethanol-gasoline blends than the base metal of that steel.

- The results of the batching tests were not promising. For the long (twelve-day) batch cycle, the average crack-growth rate could be reasonably estimated based on the exposure time to the SFGE. This rate is too high to be considered a reasonable mitigation method. For the short (twenty-four hour) batch cycle, even short times of exposure to SFGE resulted in measurable SCC crack growth. This behavior indicates that SCC initiation times are short for sharp cracks.

- Significant volumetric swelling in ethanol-fuel blends was observed for some elastomeric materials. The swelling was greater for E-20 than either neat gasoline or E-95.

Recommendations for future activities include

- Further evaluation of SCC of steel in blends around E-15 to determine whether SCC can occur in blends higher than e-15 but lower than E-20.
- Evaluation of the inhibitor effectiveness under flowing conditions and the effect of ammonium hydroxide on downstream applications (these activities are being conducted in another on-going PHMSA project).
- Further evaluation of elastomeric seals under dynamic loading conditions in different blends.

Table of Contents

1.0 BACKGROUND 1

1.1 Project Objectives 3

2.0 TASKS 1 AND 2: EFFECT OF ETHANOL BLENDS AND STEEL MICROSTRUCTURE – SCREENING TESTS 5

2.1 Experimental Approach 5

2.2 Results 6

2.2.1 Un-notched Specimens 6

2.2.2 Notched SSR Tests 7

2.2.3 Effect of Blend Ratio and Dissolved Oxygen 13

3.0 TASK 3 – EFFECT OF RESIDENCE TIME AND BATCHING ON CRACK GROWTH 14

3.1 Experimental Approach 14

3.2 Results and discussion 15

3.2.1 Threshold Stress Intensity 16

3.2.2 Effect of Metallurgy 16

3.2.3 Effect of Blend Ratio 19

3.2.4 Effect of Batching 21

4.0 TASK 4 - ELASTOMERIC MATERIALS 24

4.1 BACKGROUND 24

4.2 Experimental Procedures 25

4.2.1 Testing Conditions 26

4.2.2 Results and discussion 26

4.2.3 Summary of Elastomer Testing 34

5.0 TASK 5 - EVALUATION OF MITIGATION METHODS FOR EXISTING PIPELINES 35

5.1 Results 36

5.1.1 Crack Growth Test Results 38

6.0 SUMMARY AND RECOMMENDATIONS 38

7.0 REFERENCES 40

Appendix A: Screening Tests

Appendix B: Crack Growth Tests

List of Tables

Table 1. Gaps addressed by the projects in this consolidated program 3

Table 2. Chemical compositions of steels used in SSR testing. 3

Table 3. Matrix of Slow Strain Rate SCC Tests for Task 1..... 4

Table 4. Additives used to prepare SFGE 6

Table 5. Target composition of SFGE. 6

Table 6. Summary of results of SSR tests performed with un-notched base metal specimens..... 7

Table 7. Summary of results of SSR tests performed with notched test specimens. 8

Table 8. Summary of results of SSR tests performed in Task 5. All testes were performed in SFGE unless noted. 11

Table 9. Summary of results of Phase 2 crack growth tests. 2

List of Figures

Figure 1. Renewable fuel standard volumes of biofuels. Lifecycle greenhouse gas reduction thresholds are specified compared to the 2005 baseline gasoline or diesel fuel. 1

Figure 2. Major gasoline refining and consumption areas in the U.S. (top) versus major ethanol (bottom) production and consumption regions [2]. 2

Figure 3. Effect of chloride in SFGE on SCC of steel. 7

Figure 4. Effect of ethanol concentration in blends on SCC in notched SSR tests. The crack growth rates are average rates calculated over the entire test time. 8

Figure 5. Crack growth rate as a function of notch location for notched specimens removed from the seam weld of an X 46 DSAW tested in two SFGE-ethanol blends. 9

Figure 6. Crack growth rate as a function of pipe steel for notched base metal specimens tested in two SFGE-ethanol blends. 10

Figure 7. Crack growth rate as a function of notch location for notched specimens removed from the girth weld of an X 46 HFERW pipe, tested in two SFGE-ethanol blends. 11

Figure 8. Crack growth rate versus time to failure for notched specimens removed from the seam weld of HFERW and LFERW line pipe in two SFGE-ethanol blends. 12

Figure 9. Crack growth rate as a function of notch location for notched specimens removed from the seam weld of an X 46 DSAW, tested in two SFGE and FGE blends 13

Figure 10. Effect of ethanol concentration in blend and dissolved oxygen (related to oxygen concentration in the gas phase) on SCC. 14

Figure 11. Crack growth rates for tests performed on base metal specimens in SFGE. 17

Figure 12. Probability plot of crack-growth rates for tests performed on base metal specimens in SFGE. 17

Figure 13. Crack growth rates for test periods in which Specimen 4-4-HAZ 1 was exposed to SFGE 18

Figure 14. Changes in crack growth rate in response to environmental and loading changes 20

Figure 15. Average crack growth rate as a function of percent ethanol in the blend. 21

Figure 16. Crack growth rate changes due to different batching cycles. 22

Figure 17. Time average crack-growth rate for various batch cycles. Value for SFGE (no batching) is an average for a number of observations. 23

Figure 18. Comparison of the swelling of non-metallic materials upon 28 days of exposure to E95 Fuel Blend with that of E20 Fuel Blend and the Neat Gasoline. 27

Figure 19. Effect of sequential fuel transitions from E95 fuel blend to neat gasoline followed by E95 fuel blend on the swelling of non-metallic materials. 28

Figure 20. Effect of Sequential Fuel Transitions from E20 Fuel Blend to Neat Gasoline followed by E20 Fuel Blend on the Swelling of Non-Metallic Materials..... 28

Figure 21. Comparison of the swollen elastomeric samples upon exposure to sequential fuel immersions of E95 fuel and gasoline (a) Viton Sample after 28 days of exposure to E95 followed by 28 days in Gasoline & 7 days in E95, (b) Low-Swell Buna N Sample after 28 days of exposure to E95 followed by 7 days of exposure to Gasoline and (c) Initial dimensions of a Viton sample. 29

Figure 22. Tearing of a Low-swell Buna N sample after 28 days of exposure to E95 Fuel followed by 28 days of exposure to Neat Gasoline. 30

Figure 23. Effect of leaching of non-metallic materials on the immersion test fluids at the end of the last E95 fuel exposure, Phase III. 31

Figure 24. Effect of Sequential Fuel Transitions from E95 Fuel to Neat Gasoline followed by E95 Fuel for 28 days on the Hardness Loss of Non-Metallic Materials. 32

Figure 25. Effect of sequential fuel transitions from E20 Fuel to neat gasoline followed by E20 Fuel for 28 days on the hardness loss of non-metallic materials. 32

Figure 26. Comparison of hardness retention of non-metallic materials upon 28 days of exposure to E95 fuel blend with that of E20 fuel blend and the neat gasoline..... 33

Figure 27. Comparison of compression-set properties of non-metallic materials upon 28 days of exposure to E95 fuel blend followed by neat gasoline and E95 fuel blend. 33

Figure 28. Drawing of un-notched SSR test specimen. 12

Figure 29. Drawing of notched SSR test specimen. 13

Figure 30. Photograph of cell used for testing the notched specimens; RE – Reference Electrode, LVDT – Displacement transducer, RCS – Connection to rusted carbon steel sample, SSR Specimen – Slow Strain Rate specimen. 14

Figure 31. Optical Photograph of gage section of SSR Specimen (4-4)-X4, showing severe cracking..... 15

Figure 32. Optical Photograph of gage section of SSR Specimen (4-4)-X1, showing very minor crack-like fissures (arrow) in necked region of gage section. 15

Figure 33. Low magnification SEM photograph of the fracture surface of base metal Specimen (4-4)-X4, tested in SFGE containing 4 ppm Cl, showing SCC crack depth measurements..... 16

Figure 34. Low magnification SEM photograph of the fracture surface of Specimen (4-4)-1, with notch located in base metal, tested in SFGE containing 5 ppm Cl (E-95), showing SCC crack depth measurement. 16

Figure 35. High magnification SEM photograph of the fracture surface of Specimen (4-4)-1, with notch located in base metal, tested in SFGE containing 5 ppm Cl (E-95), showing mixed mode cracking. 17

Figure 36. Schematic drawing of the crack growth specimen and photograph. 7

Figure 37. Photograph of cell used for crack-growth testing..... 8

Figure 38. Photograph of the inside of the test cell used for crack-growth testing, showing the test specimen and cell internals; RCS –Rusted Carbon Steel Sample, EPD – Electric Potential Drop. 9

Figure 39. Crack length as a function of time for Specimen 4-4 Base 3. 10

Figure 40. Low magnification SEM photograph of fracture surface of Specimen 4-4 Base 3..... 1

Figure 41. SEM photograph of fracture surface of Specimen 4-4 Base 3 showing the SCC zone. 1

Figure 42. Crack length as a function of time for Specimen 4-4 Base 4 (0 to 240 hours). 2

Figure 43. Crack length as a function of time for Specimen 4-4 Base 4 (200 to 325 hours). 2

Figure 44. Crack length as a function of time for Specimen 4-4 Base 2 (0 to 190 hours). 3

Figure 45. Crack Length as a function of time for Specimen 4-4 Base 14 (65 to 130 hours). 3

Figure 46. Crack length as a function of time for Specimen 4-4 HAZ 1. Long batch cycle (5 days SFGE – 7 Days Gasoline) started on Day 237..... 4

Figure 47. Crack length as a function of time for Specimen 4-4 Base 7. Short batch cycle (1 hour SFGE – 23 hours Gasoline) started on Day 234. 4

1.0 BACKGROUND

The U.S. Energy Independence and Security Act of 2007 established a nationwide renewable fuels standard, starting from 9 billion gallons (34 billion liters) of all biofuels in 2008 to 36 billion gallons (136 billion liters) in 2022. The most recent Renewable Fuel Standards issued by the U.S. Environmental Protection Agency [1] specifies a number of alternative biofuels, including corn-based ethanol, cellulosic ethanols, biodiesels, and other advanced biofuels that may be manufactured in the future using hitherto unknown technologies (Figure 1).

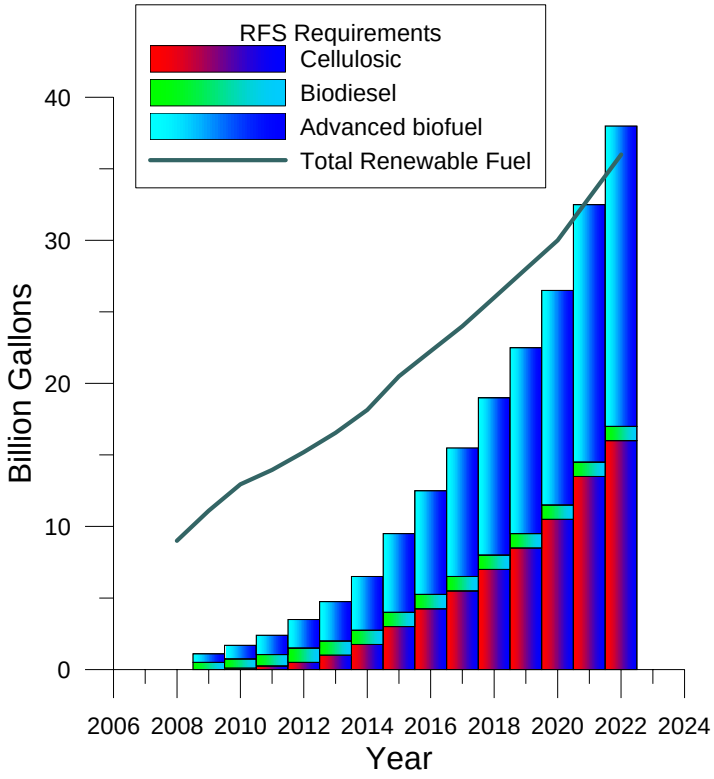

Lifecycle GHG Thresholds Specified in EISA

(Percent reduction from 2005 baseline)

Renewable fuel[a]	20%
Advanced biofuel	50%
Biomass-based diesel	50%
Cellulosic biofuel	60%

[a] The 20% criterion generally applies to renewable fuel from new facilities that commenced construction after December 19, 2007.

Figure 1. Renewable fuel standard volumes of biofuels. Lifecycle greenhouse gas reduction thresholds are specified compared to the 2005 baseline gasoline or diesel fuel.

EPA determined that the current corn-based ethanol meets the 20 percent GHG reduction threshold whereas ethanol produced from sugar cane meets the 50% GHG threshold, thus enabling it to be applicable to the advanced biofuel category.

At present, ethanol is first sent to blending terminals through tanker trucks, rail cars, and barges, where they are blended with gasoline or diesel and then sent to consumer filling stations via trucks. In the U.S. 67 percent of the ethanol is transported to blending terminals via trucks, 31 percent by rail cars, and 2 percent by barges. Ethanol is also exported through ships to receiving terminals which then blend them with gasoline and then transport them to filling stations using

trucks. The U.S. National commission on Energy Policy's Task Force on biofuels Infrastructure [2] defined the biofuels expansion into two major phases from an infrastructure perspective. During Phase 1 (concluding in 2015), existing multi-modal transportation infrastructure will continue to play a major role, but will require additional infrastructure investment. In Phase II (after 2015), the volume of biofuel production will expand beyond 15 billion gallons per year, but the infrastructure needs will depend on the mix of biofuels, geographical distribution of production and consumption centres, availability of flex fuel vehicles, etc. For example, Figure 2 shows the current gasoline consumption and distribution infrastructure. In comparison, the ethanol production centres are located at the geographic centre and needs a different distribution pathway.

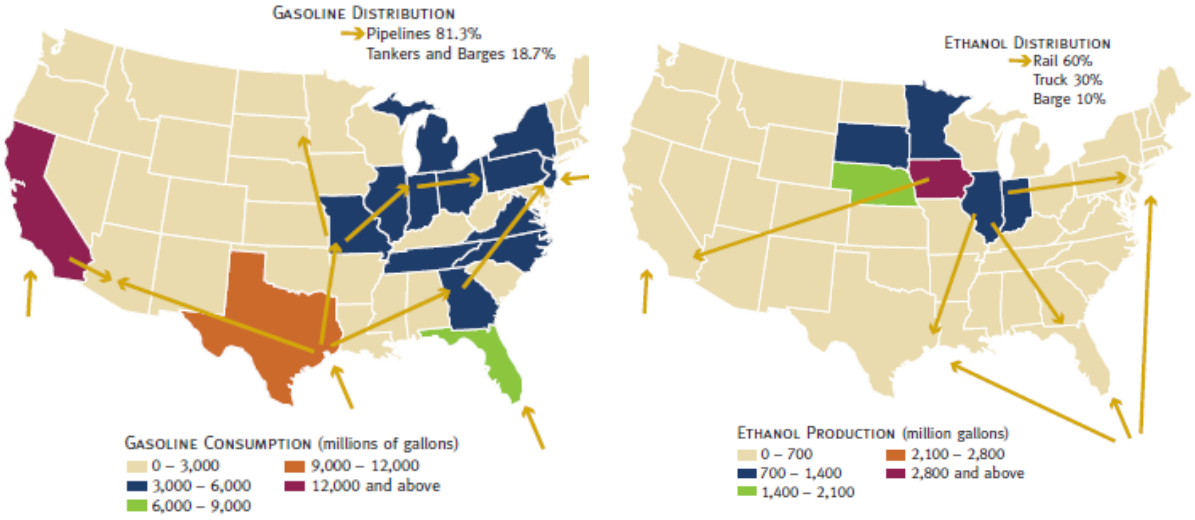

Figure 2. Major gasoline refining and consumption areas in the U.S. (top) versus major ethanol (bottom) production and consumption regions [2].

It should be noted that while pipelines form the bulk of the transportation of petroleum fuels, rail, truck and barges currently serve as the main transportation modalities for ethanol. The rail, truck, and barge transport modes are more costly and less efficient than pipeline transport for long distances. Construction of new pipelines will require significant investment and therefore careful assessment of enterprise-wide risk is needed. It has been estimated that for long-distance transportation of fuel, pipeline is less hazardous than trucks or rail cars based on frequency of fatalities per distance transported. While the pipeline infrastructure in the U.S. is still nascent, Brazil has a well-established ethanol pipeline already and is planning to expand this infrastructure even further.

Reliable and safe transportation of ethanol is critical to the viability of pipelines as the primary transportation mode. A 2003 survey of industry, reported in API Technical Report 939-D (2nd edition), indicates that stress corrosion cracking (SCC) has been observed primarily in user

terminals exposed to ethanol products, but not in ethanol producer tanks, rail/tank car/shipping transportation, nor end-user systems (e.g., gas tanks). More recently, a short segment of pipeline transporting FGE in North America was reported to have suffered SCC. In contrast, Brazil, which has transported anhydrous and hydrous ethanol for many years, has not reported any SCC in their pipeline system. At present, there is an incomplete understanding of why the occurrence of SCC differs so significantly in different parts of the supply chain.

1.1 Project Objectives

A Roadmap meeting, held on October 25-26, 2007, identified several gaps related to ethanol transportation in pipelines. A Consolidated Program, consisting of three projects, is being conducted to address several of these gaps:

WP#323 – Effect of ethanol source on SCC of carbon steel

WP#325 – Effect of Ethanol Blends and Batching Operations on Stress Corrosion Cracking of Carbon Steel

WP#327 – Monitoring Conditions Leading to SCC/Corrosion of Carbon Steel

The specific gaps addressed by WP#325 are shown in Table 1. The red dots indicate their priority/importance

Table 1. Gaps addressed by the projects in this consolidated program

Proposed Project	Gaps Addressed
WP#325	• Define safe operating limits: chemistry to prevent cracking (O_2, water), stress, etc. ●●●●●●● • Knowledge gap on what blends cause SCC. Threshold level of ethanol in gasoline blend to prevent cracking ●●●●●●. • Limited understanding of how fast SCC develops ●●●●● • Lack of understanding of steel microstructure-contaminant interactions during SCC • Swelling and permeation in seals and gaskets ●●●● • Elastomer and non-metallic compatibility with ethanol ●● • Batch tests on neat (E95) and blends ●● • Limited understanding of pressure fluctuations— can they accelerate pipeline stress? ●● • Limited understanding of flow issues—will stagnation be a problem? ●

The major goals of Project WP # 325 reported here are to:

- Develop guidelines to assess the safety and reliability issues associated with the transportation of Fuel Grade Ethanol (FGE) and its blends through existing and new pipelines.

- Develop data necessary to make engineering assessments of the feasibility of transporting FGE and FGE blends in existing pipelines in a batching or dedicated mode. Included in this will be batching of hydrous and anhydrous ethanol.

- Evaluate the performance of non-metallic pipeline components, such as static and dynamic seals, in FGE and its blends.

- Evaluate the implementation of various SCC/corrosion mitigation strategies (e.g., oxygen scavenging, inhibitors, coatings) that can enable transportation of all ethanols in existing or new pipelines. Such an evaluation would consider the practical aspects of scaling up laboratory studies to pipeline situations to ensure effective implementation.

The work scope consists of five major technical tasks, primarily focused on SCC/corrosion issues of carbon steel in ethanol blends for a variety of applicable steel metallurgical conditions – welds, castings, and steel grades. Attention is also given to the effect of FGE on seals and gaskets. Finally, for those FGE/FGE blends that cannot be transported without mitigation or modifications, various mitigation methods are being considered. The five technical tasks are:

Task 1 – Screening SCC Tests to Determine Different FGE Blends that Can Be Transported in Existing Pipelines,

Task 2 – Effect of Steel Microstructure on Performance,

Task 3 – Effect of Residence Time and Batching of FGE on Steel Performance,

Task 4 – Interaction of FGE with Seals and Chemicals Present in Pipelines, and

Task 5 – Evaluation of Mitigation Methods for Existing and New Pipelines

Tasks 1 and 2 have been completed and draft reports for the work have been issued as part of the PRCI SCC 4-4, Phase 1 project. This report is in the process of being finalized. Task 4 has been completed and the final report will be issued separately. The results are also presented in the form of a conference Paper in Corrosion/2010. During this reporting period, the research has focused on Tasks 3 and 5. The results from this also form part of a draft report of the PRCI SCC 4-4, Phase 2 project. Once finalized, the reports will be uploaded separately.

2.0 TASKS 1 AND 2: EFFECT OF ETHANOL BLENDS AND STEEL MICROSTRUCTURE – SCREENING TESTS

2.1 Experimental Approach

Two types of screening tests were performed: un-notched and notched slow strain rate (SSR) tests. The advantage of an un-notched SSR tests are that it is easier to observe signs of SCC through secondary cracks on the gage, it is less severe and is able to distinguish environmental effects better, and the specimens are less expensive. However, un-notched slow strain rate tests are not suitable to study the effect of welding because the differential yield strengths of the welds and base metal often results in the preferential cracking of the base metal, which has generally lower yield strength. In such cases, a notched SSR test can be performed whereby the notch is located at the desired metallurgical region forcing failure in that region.

Several initial SSR tests were performed with un-notched base metal specimens to establish the optimum chloride concentration for the subsequent tests. These tests were performed with two line pipe steels with established susceptibility to ethanol SCC. The chemical compositions of all of the steels tested in Task 1 are given in Appendix A, Table 2. The main matrix of tests in Task 1 was performed with SSR specimens containing notches in the gage section. Table 3 shows the matrix of tests performed with these notched specimens. Variables in the matrix included long seam weld type, location of the notch with respect to the seam weld (in the weld metal, in the heat-affected zone (HAZ), or in the base metal), ethanol source, and the ethanol-gasoline blend ratio.

The majority of the tests were performed using the simulated fuel grade ethanol (SFGE) containing 5 ppm Cl, as shown in Table 4. The additives used to prepare the SFGE are shown in Table 4 and the target composition is shown in Table 5. Several tests also were performed with one lot of actual fuel grade ethanol acquired from an ethanol producer (FGE).

The un-notched test specimens had a gage length of 25 mm (1 inch) and a gage diameter of 3.2 mm (0.125 inches), see Appendix A, Figure 28. A strain rate of 1×10^{-6} sec^{-1} was used for all of the SSR tests with smooth specimens. The notched specimens had a gage length of 12.5 mm (0.5 inches) and a gage diameter of 4.75 mm (0.187 inches). The notch had a depth and width of 0.25 mm (0.01 inches) and a radius of 0.127 mm. (0.005 inches). Appendix A, Figure 29 is a drawing of the notched specimen. A displacement rate of 9.53×10^{-6} mm/s (3.75×10^{-7} inches/s) was used for all of the SSR tests with notched specimens.

The tests with un-notched specimens were performed in stainless steel test cells with a total volume of 400 ml; 350 ml of solution was filled and the vapor space was 50 ml. The tests with notched specimens were performed in stainless steel test cells with a total volume of 800 ml; 700

ml of solution was filled and the vapor space was 100 ml. A photograph of the test cell used for the notched specimens is shown in Appendix A, Figure 30.

Specimens were tested under freely corroding conditions and the corrosion potential was monitored in each test using an Ag/AgCl/EtOH reference electrode. In all tests, a piece of rusted pipe steel was placed in the test cell and galvanically connected to the test specimen to more closely simulate the native corrosion potential of a mill scaled/rusted pipe wall. The rusted steel to specimen area ratio was approximately 5 to 1. The specimen and rusted steel piece were electrically isolated from the specimen grips and test cell in the SSR test machine. The tests were performed at room temperature and the cell was actively sparged with breathing air at a flow rate of approximately 4 ml/minute. Ethanol bubbler traps were used on the inlet and outlet to the test cell to remove/exclude any moisture, see Appendix A, Figure 30. Based on independent measurements of chloride leakage rate from the reference electrode, it is estimated that the chloride concentration in the test cell increased by about 1 ppm during the course of the SSR test.

After testing, the specimens were examined and optically photographed. The fracture surfaces were examined in the scanning electron microscope (SEM) and the maximum depth of SCC was measured. Other parameters that were recorded for each test included the maximum load and the time to failure.

2.2 Results

2.2.1 Un-notched Specimens

The details of the test results are shown in Appendix A, Table 6. Tests X0 and X7 were control tests performed in air with no solution. Tests X1 to X5 were performed with different chloride concentrations to evaluate the effect of chloride on the SCC potency of the simulated FGE. In the previous research [4], a chloride concentration of 50 ppm was used in the SFGE. This is slightly above the specification in ASTM 4806-01 (40 ppm) and well above typical values expected for FGE. The effect of chloride on SCC is shown in Figure 3.

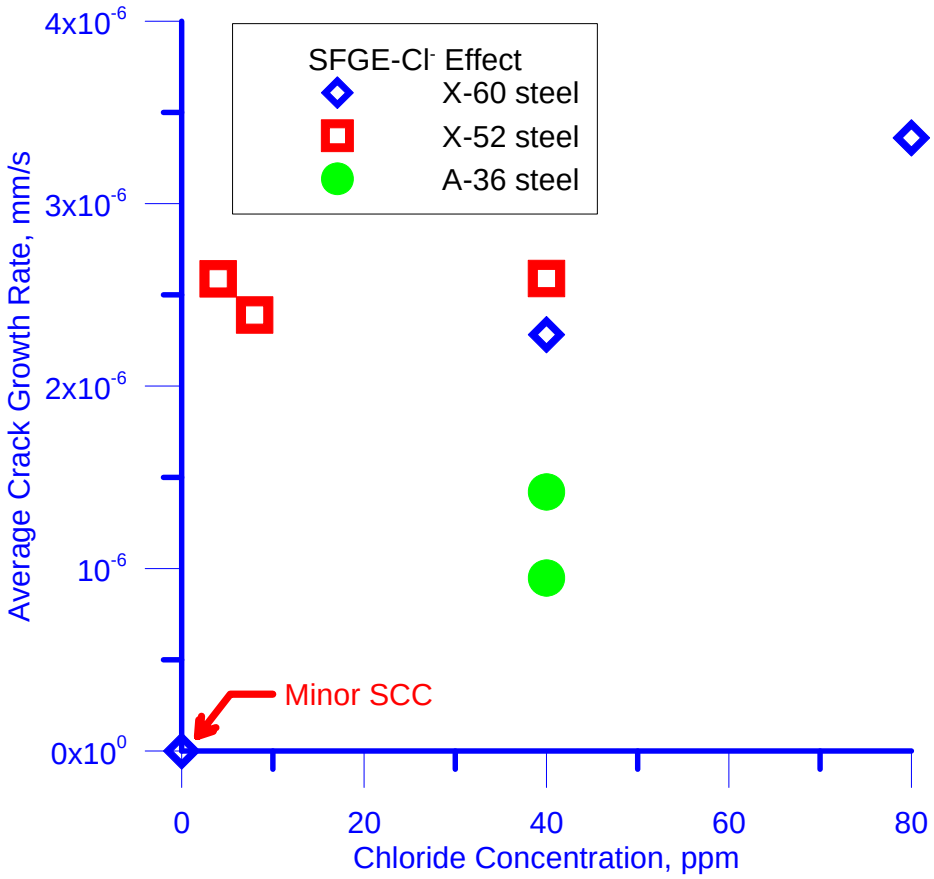

Figure 3. Effect of chloride in SFGE on SCC of steel.

No SCC was observed on the fracture surface of the SSR specimen tested in SFGE with no added chloride, but there was minor surface cracks on the gage section of the specimen. Over the range of 4 ppm to 40 ppm chloride, there did not appear to be any clear trend in crack growth rate with increasing chloride concentration. The cracking was judged to be severe in all of the tests, based on the high crack growth rate and the presence of cracking along most of the gage section of the specimens. Based on these results, a concentration of 5 ppm chloride was selected for all subsequent SSR tests with notched specimens performed in the SFGE.

2.2.2 Notched SSR Tests

The results of these tests are detailed in Appendix A, Table 7. Tests (4-4)-1 to (4-4)-5 were performed with X46 DSAW line pipe steel, with the notches located in the base metal, over a range of blend ratios from E-10 to E-95. Figure 4 shows the effect of ethanol concentration on the SCC crack growth rate measured in these tests. No SCC was observed below E-15. The

average crack growth rate was highest at about E-50, but there is a significant scatter in crack growth rate with increasing ethanol concentration blends.

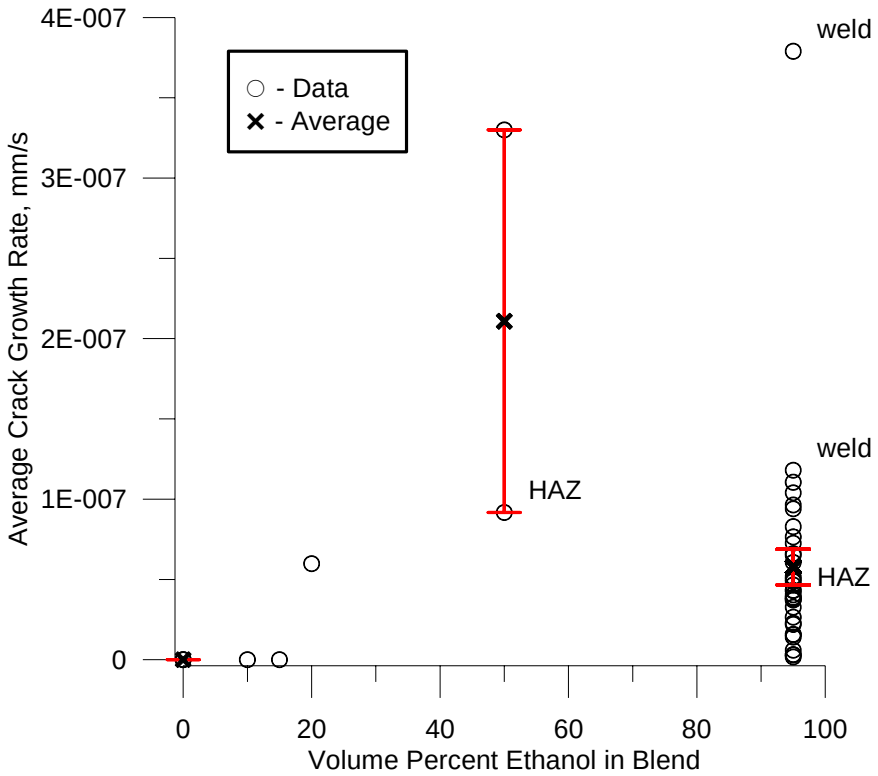

Figure 4. Effect of ethanol concentration in blends on SCC in notched SSR tests. The crack growth rates are average rates calculated over the entire test time.

In Appendix A, Table 7, tests (4-4)-8 to (4-4)-14 were performed with X46 DSAW line pipe steel, with the notches located in the HAZ and weld metal in E-30 and E-95 blends. The results of the tests, summarized in Figure 5, show that there was not a large effect of weld metallurgy or blend ratio on the SCC behavior.

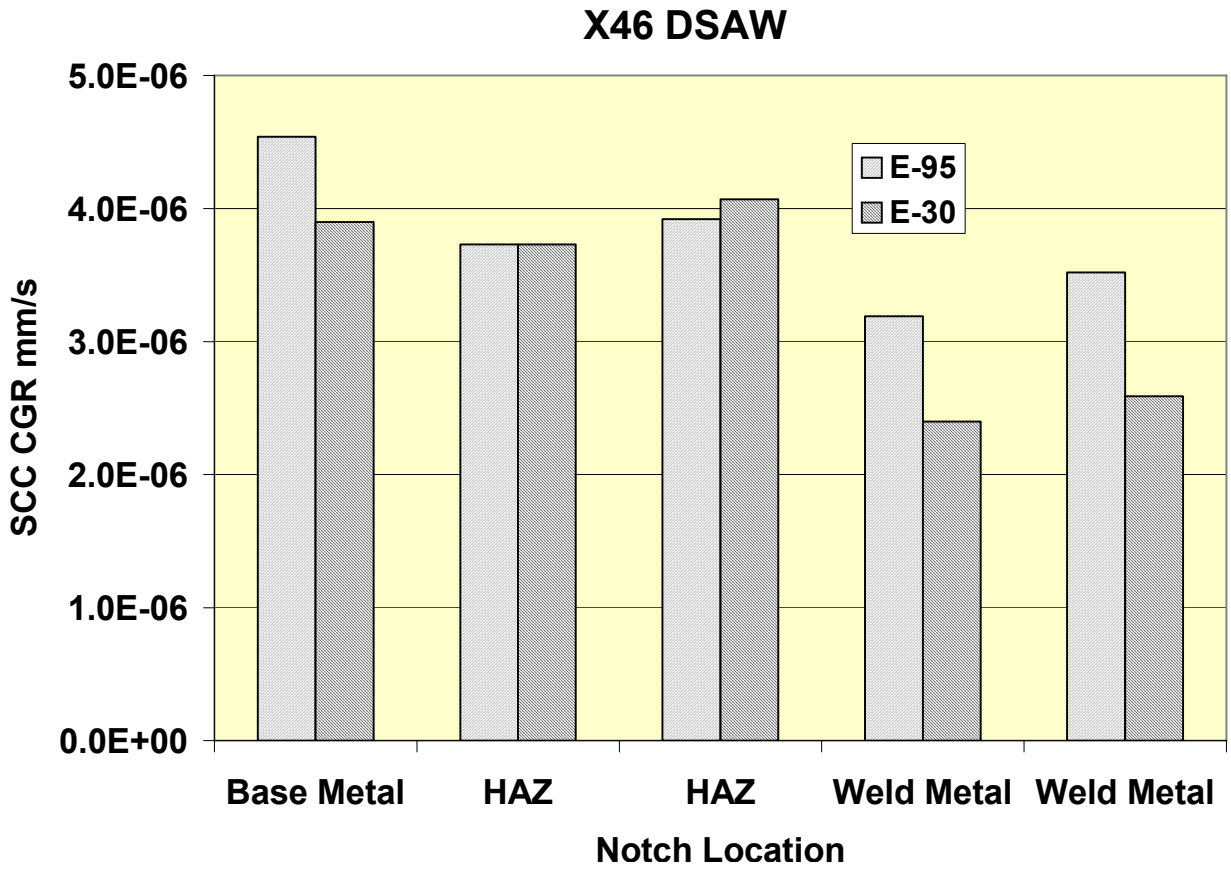

Figure 5. Crack growth rate as a function of notch location for notched specimens removed from the seam weld of an X 46 DSAW tested in two SFGE-ethanol blends.

In the majority of tests, the E-30 blend was slightly less potent as an SCC agent than the E-95 blend, but the difference was not large. In these tests, the HAZ exhibited similar SCC susceptibility to that of the base metal while the weld metal appeared to be slightly less susceptible to SCC.

Figure 6 summarizes the crack growth rate data for the base metal specimens for the different pipe steels evaluated on the project. All of the steels exhibited measurable susceptibility to SCC and the differences probably are not significant from an integrity standpoint. Crack growth rates for the seamless, the cast steel, and the LFERW pipe were somewhat lower than for the DSAW and two other ERW pipes but all steels exhibited relatively deep cracks. In the case of the cast steel, the lower crack growth rate was the result of the high ductility of the steel, which produced a long time to failure.

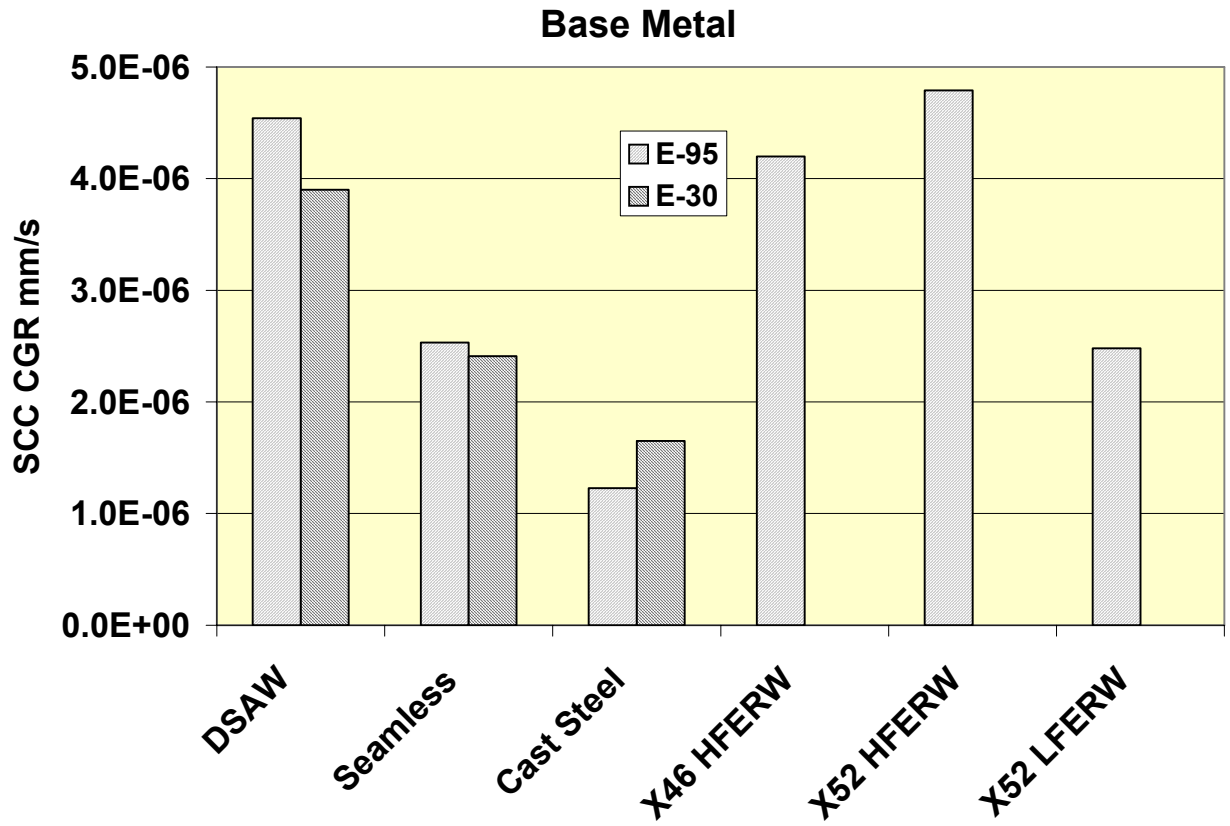

Figure 6. Crack growth rate as a function of pipe steel for notched base metal specimens tested in two SFGE-ethanol blends.

Figure 7 summarizes the crack growth rate data for SSR tests performed on notched girth weld specimens from an X46 HFERW line pipe steel. The behavior is similar to that observed in the tests of the X46 DSAW long seam weld. The weld metal was somewhat less susceptible to SCC than the HAZ or base metal and the cracking was slightly more severe in the E-95 blend than in the E-30 blend.

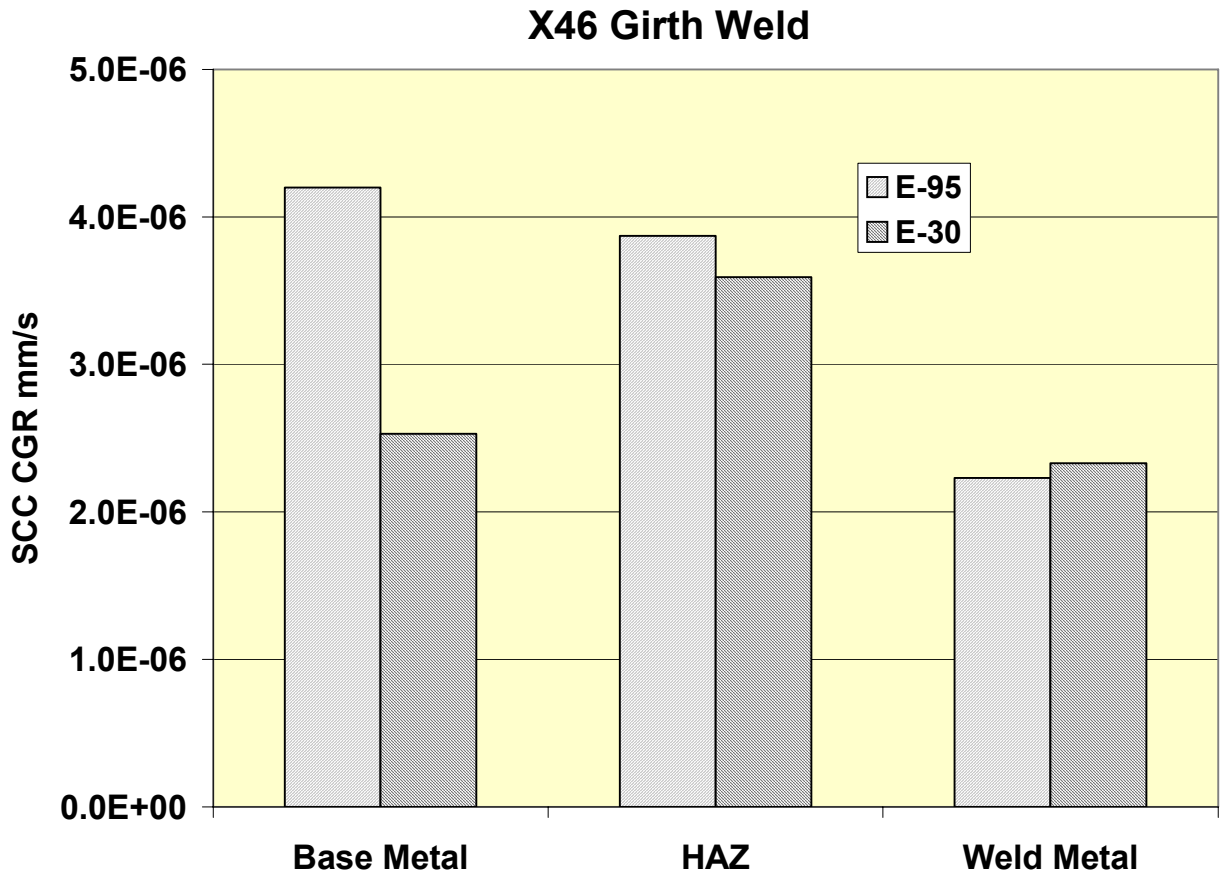

Figure 7. Crack growth rate as a function of notch location for notched specimens removed from the girth weld of an X 46 HFERW pipe, tested in two SFGE-ethanol blends.

Appendix A, Table 7 shows that no SCC was observed in several tests with HFERW and LFERW specimens where the notch was located at the bond line of the weld or in the HAZ, which is very close to the bond line. This is more a reflection of the short failure times of the specimens, as opposed to an inherit resistance to SCC. These specimens essentially failed mechanically at the bond line of the welds, because of poor mechanical properties. This behavior is shown graphically in Figure 8. There were two exceptions to this trend. The two LFERW specimens with the notch located at the weld both exhibited long failure times; one specimen, tested in E-95, had a moderate crack growth rate while the 2nd specimen, tested in E-30, exhibited no SCC. This behavior suggests that the welds in this ERW line pipe steel are more resistant to ethanol SCC than the base metal.

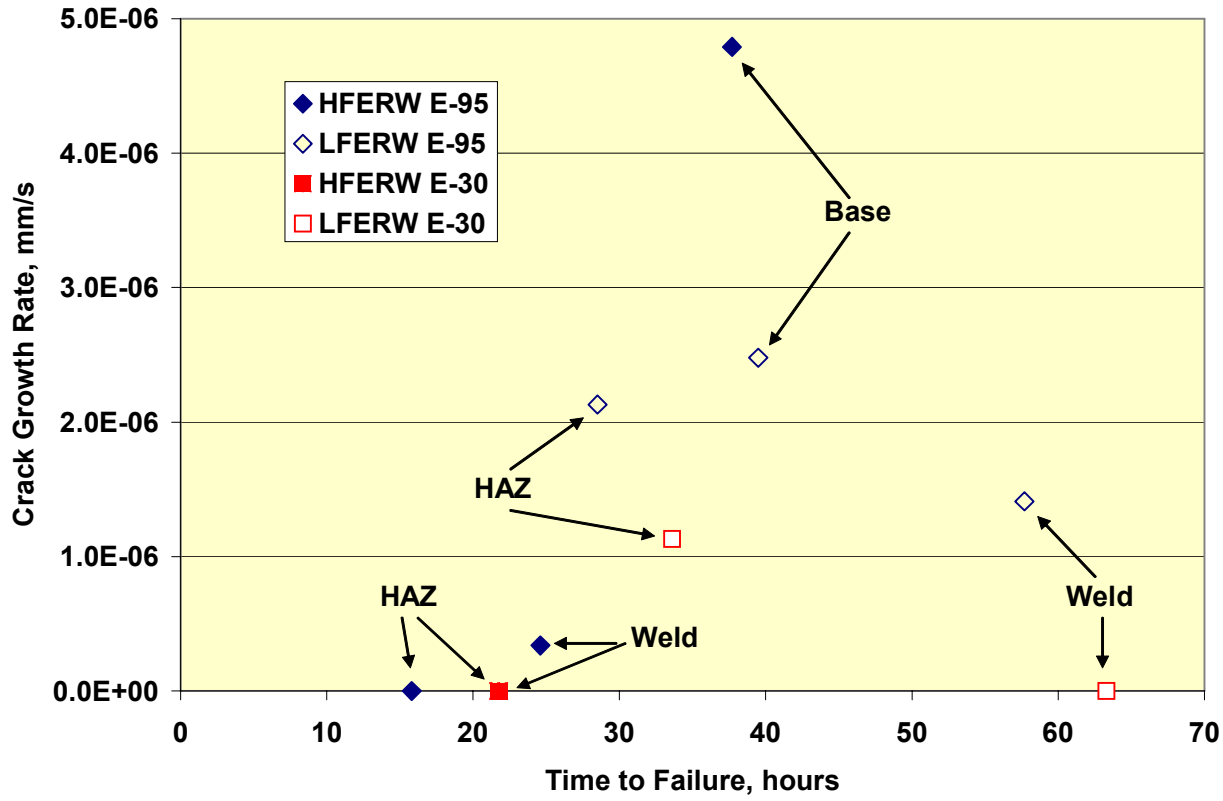

Figure 8. Crack growth rate versus time to failure for notched specimens removed from the seam weld of HFERW and LFERW line pipe in two SFGE-ethanol blends.

Figure 9 compares the SCC crack growth rates for notched specimens of the X46 DSAW line pipe steel in simulated and actual FGE. Only base metal and weld metal specimens were evaluated. In general, SCC potency was slightly lower in the actual FGE than the simulated FGE and in the lower ethanol concentration (E-30). However, significant SCC was observed in all of the tests.

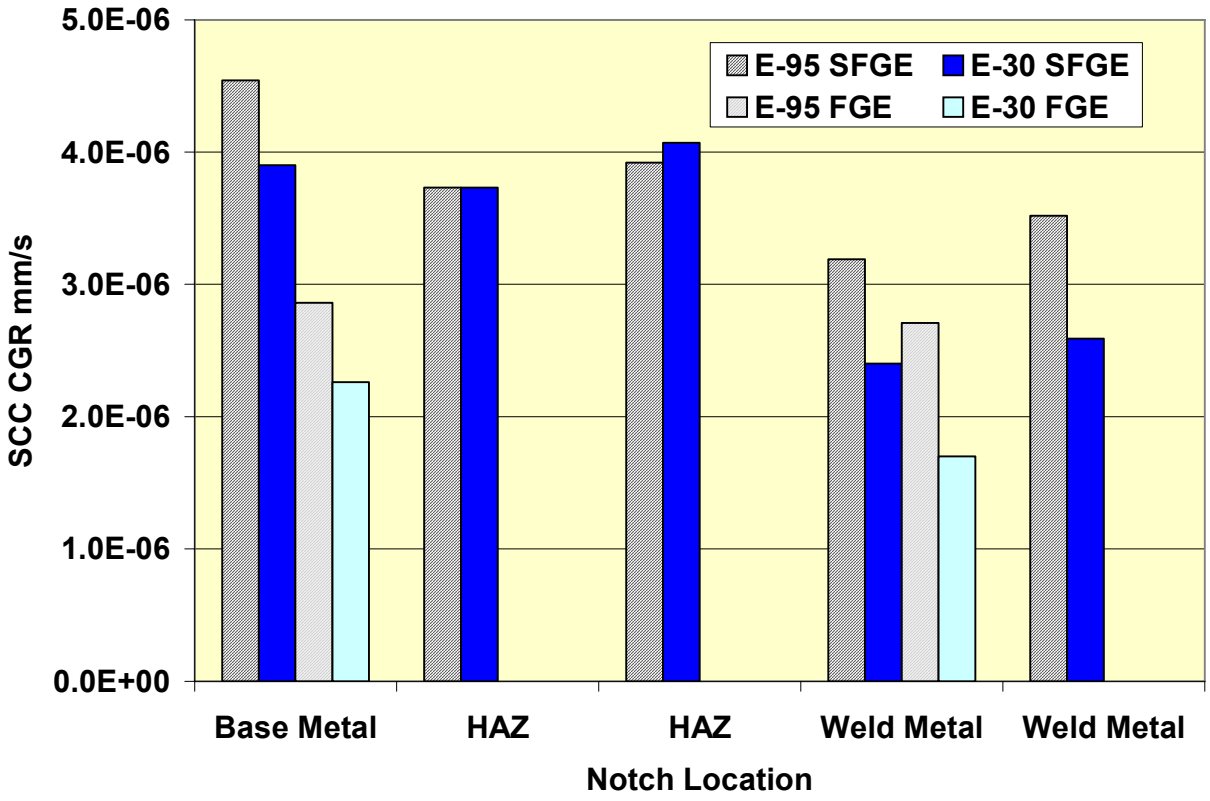

Figure 9. Crack growth rate as a function of notch location for notched specimens removed from the seam weld of an X 46 DSAW, tested in two SFGE and FGE blends.

2.2.3 Effect of Blend Ratio and Dissolved Oxygen

Several notched and un-notched SSR tests were conducted in different FGE and SFGE-gasoline blends purged with N_2 + O_2 mixtures containing different O_2 levels. The results are summarized in Figure 10. These tests indicate that for ethanol concentrations less than about 15 volume percent, no SCC is observed even at high O_2 concentrations, whereas for ethanol concentrations above 15 volume percent, the oxygen concentration needed to cause SCC is rather low. The 50 volume percent ethanol blend appears to show the most severe SCC (i.e. lowest oxygen concentration below which no SCC is observed). At present, there is no ASTM or any other specification for maximum dissolved oxygen concentration because there are no standards specifically meant to address SCC of steel. Thus lowering the dissolved oxygen levels to avoid SCC will not impact the current ASTM specification.

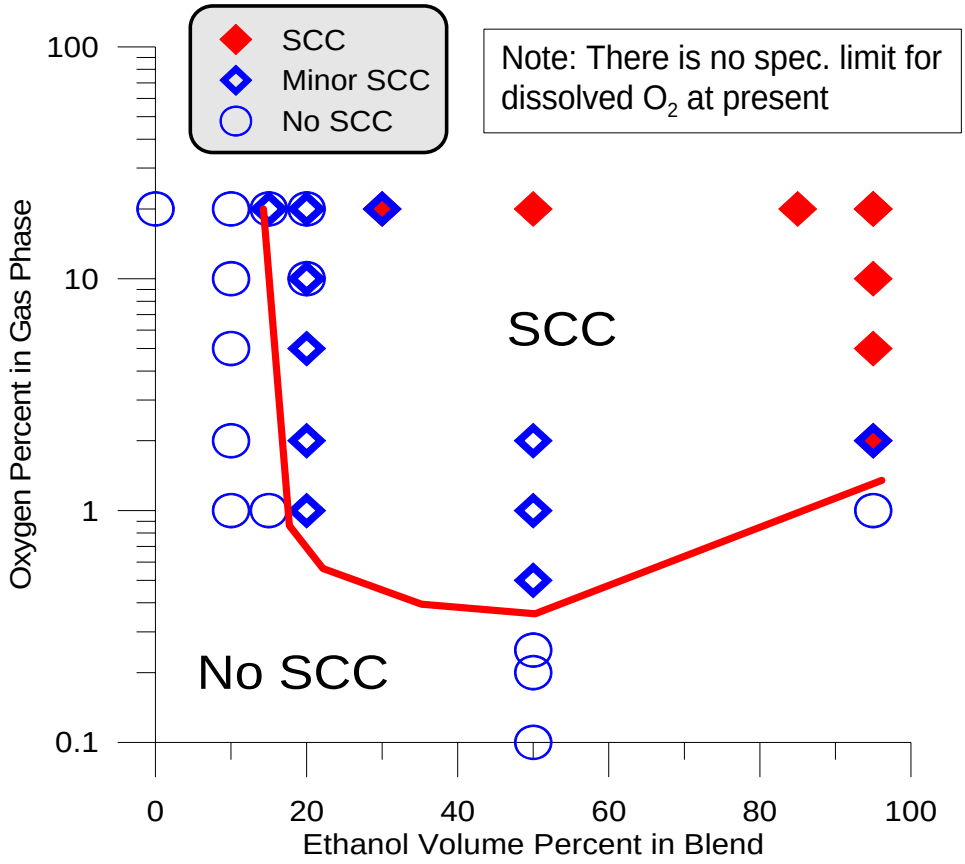

Figure 10. Effect of ethanol concentration in blend and dissolved oxygen (related to oxygen concentration in the gas phase) on SCC.

3.0 TASK 3 – EFFECT OF RESIDENCE TIME AND BATCHING ON CRACK GROWTH

3.1 Experimental Approach

The tests were performed at room temperature in a 4L stainless steel cell. An ethanol bubbler trap was used on the outlet of the test cell to exclude moisture. The SCC tests were performed under freely corroding conditions and the corrosion potential was periodically monitored in each test using an Ag/AgCl EtOH/0.1M LiCl reference electrode. A piece of rusted pipe steel was placed in the test cell and galvanically connected to the test specimen to more closely simulate the native corrosion potential of a mill scaled/rusted pipe wall. The rusted steel to specimen area ratio was approximately 5 to 1. The specimen and rusted steel piece were electrically isolated from the specimen grips and test cell in the test machine. The drawing of the speciment and photographs of the test set up are shown in Appendix B, Figure 36 through Figure 38.

Crack growth tests were performed using cyclic load conditions designed to simulate the loading conditions on a just- surviving crack in a pipeline that has been previously hydrostatically tested. The ratio of the minimum to maximum load (R ratio) in the tests ranged from 0.6 to 0.8 and the cyclic frequency was 1.2×10^{-4} Hz (one cycle every 2.3 hours) to simulate the ripple load effect from pressure fluctuations on an operating pipeline. For each specimen, cracking was initiated in SFGE under aerated conditions and propagated for approximately one-month period. The test conditions were changed periodically to evaluate the effect of blending, deaeration, or inhibitors on crack growth. In some tests, it was necessary to temporarily increase the cyclic frequency (to approximately 7.6 X 10^{-3} Hz) or apply an unload-reload cycle to initiate cracking. Using this method, a number of conditions could be investigated with a single specimen. The crack growth in the tests was monitored continuously using the electric potential drop (EPD) technique. With this technique, a direct current of 20 amperes was passed through the specimen and the change in resistance of the specimen, as a result of crack extension, was monitored. The resistance was converted to a crack length using the Johnson equation found in ASTM E647 [3]. At the end of the crack growth tests, selected specimens were electric discharge machined (EDM) in half. One-half was metallographically prepared and examined. The other half was broken open and the fracture surface was examined optically and in the scanning electron microscope (SEM). The total crack growth measured from the SEM matched reasonably well with the integrated crack length from the EPD measurements.

In addition to crack growth tests, the threshold stress intensity factor for SCC (K_{thSCC}) was estimated using an essentially monotonic loading followed by constant displacement procedure. With this test technique, the compact tension specimen is strained at a constant displacement rate of approximately 6 x 10^{-7} mm/s, using a slow strain rate (SSR) test frame. The displacement is stopped at a specified maximum $K_{applied}$, or when there is evidence of crack extension from the EPD measurements. The specimen is left in the loading frame under this constant displacement (static) loading for hold times ranging from 20 to 50 days. If SCC growth has occurred during the constant displacement rate step, then the crack will extend and the load will drop during the constant displacement step. This process will continue until K_{thSCC} has been reached. Once no additional load drop or increase in EPD is measured for one to two months, the specimen is removed from the test frame and examined as described above. The K_{thSCC} value is calculated based on the final load and crack length. The longer hold time was used to determine whether K_{thSCC} decreased with an increase in exposure time at maximum K value.

3.2 Results and discussion

The detailed results are shown in Appendix B.

3.2.1 Threshold Stress Intensity

Crack length versus time data for one of the two specimens (SCC 4-3, Table 9) used in the threshold stress intensity tests are shown in Appendix B, Figure 39. The figure shows that there was a large jump in the measured crack length after about five days of straining. This likely was the result of some initial tearing of the pre-existing fatigue crack, or a significant increase in the plastic zone size. There was then a steady increase in the crack length for the next ten days, with an average crack-growth rate of 5.5×10^{-8} mm/s. The crosshead was stopped on Day 16 of the test. The crack continued to extend for another four days, at an average crack-growth rate of 2.4×10^{-8} mm/s. The total amount of SCC crack extension was estimated to be approximately 120 μm, based on the EPD data. There was no evidence of additional growth for the remaining 15 days of the test. Appendix B, Figure 41 is an SEM view of the fracture surface between the fatigue pre-crack and the rapid fracture region. Intergranular facets characteristic of SCC are evident. The width of the SCC zone is 100 to 120 μm at this location, confirming the total SCC growth estimated from the EPD readings.

The threshold stress intensity factor for SCC, K_{thSCC}, was calculated based on the final crack length and load, giving a value of 33.3 MPa.m$^{0.5}$ (30.3 ksi in$^{1/2}$). A similar procedure was used in the longer-term test, 4-4 Base 5 and a K_{thSCC} value of 36.8 MPa.m$^{0.5}$ (33.5 ksi in$^{1/2}$) was estimated based on the final crack length and load. Note that all of the cyclic load tests were performed at K_{max} values above these threshold K values.

3.2.2 Effect of Metallurgy

Eight tests were initiated with base metal specimens in SFGE (1,2,4,6,7,9,10, and 11). For these specimens, there were 32 test periods in which crack growth was monitored in SFGE. These periods varied in length from two to twelve weeks. Appendix B, Table 9 and Figure 11 summarize the crack growth rates for these tests. Crack growth rates for base metal specimens in SFGE ranged between 0 mm/s and 1.43×10^{-7}mm/s (4.48 mm/y), the latter is nearly an order of magnitude higher rate than that typically measured for external near neutral pH SCC of pipelines.

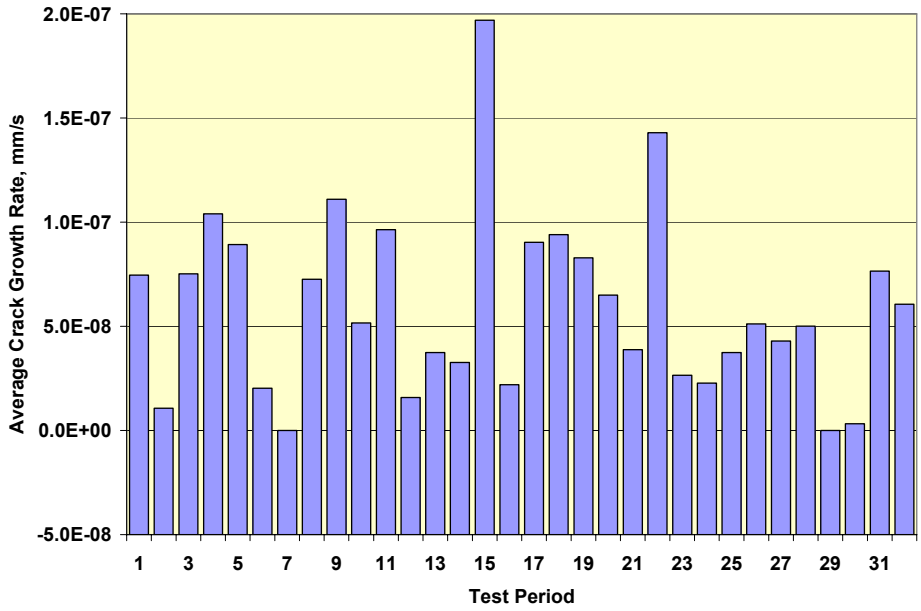

Figure 11. Crack growth rates for tests performed on base metal specimens in SFGE.

The average crack growth rate for the base metal specimens was 5.92×10^{-8} mm/s and the median crack growth rate was 5.14×10^{-8} mm/s. The zero (crack growth rate) data were excluded from the data set and the remainder of the data was statistically analyzed.

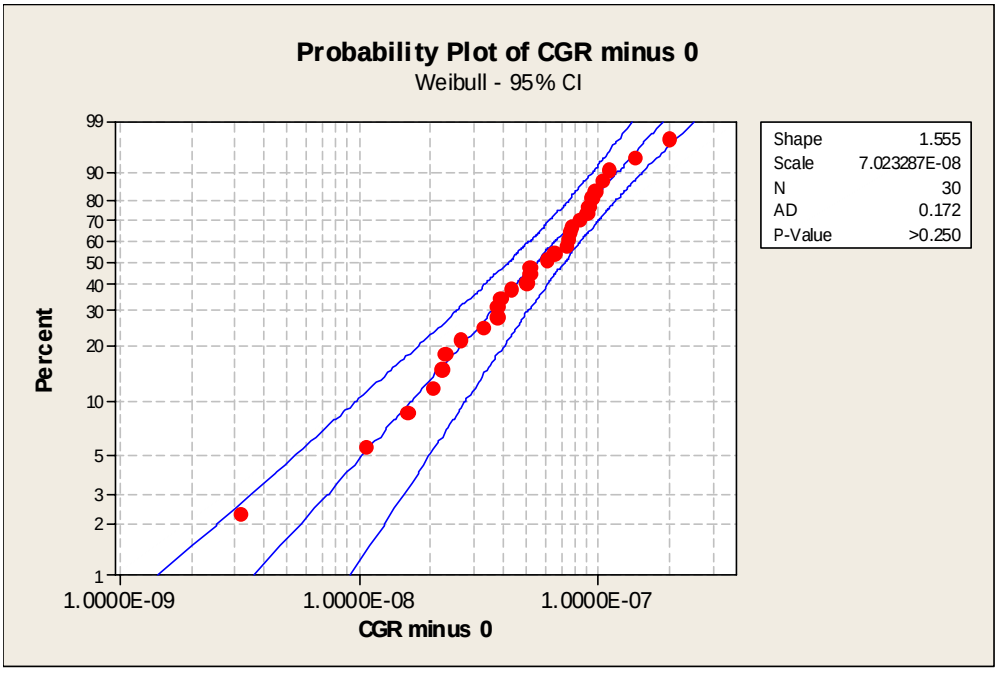

Figure 12. Probability plot of crack-growth rates for tests performed on base metal specimens in SFGE.

A Probability Plot of the data is shown in Figure 12. The fit to a Weibull distribution was excellent, passing the Anderson-Darling goodness of fit test at the 95% confidence level. The 50th percentile for the distribution was 5.55×10^{-8} mm/s, the 95% Upper Confidence Limit (UCL) was 7.27×10^{-8} mm/s, and the 95% Lower Confidence Limit (LCL) was 4.24×10^{-8} mm/s.

One HAZ specimen was tested and there were five separate test periods, over 475 days, in which the specimen was exposed to SFGE. Between these periods, the specimen was exposed to E-50, gasoline, batching with gasoline, and one inhibitor. Appendix B, Table 9 and Figure 13 summarize the crack growth rates for these test periods.

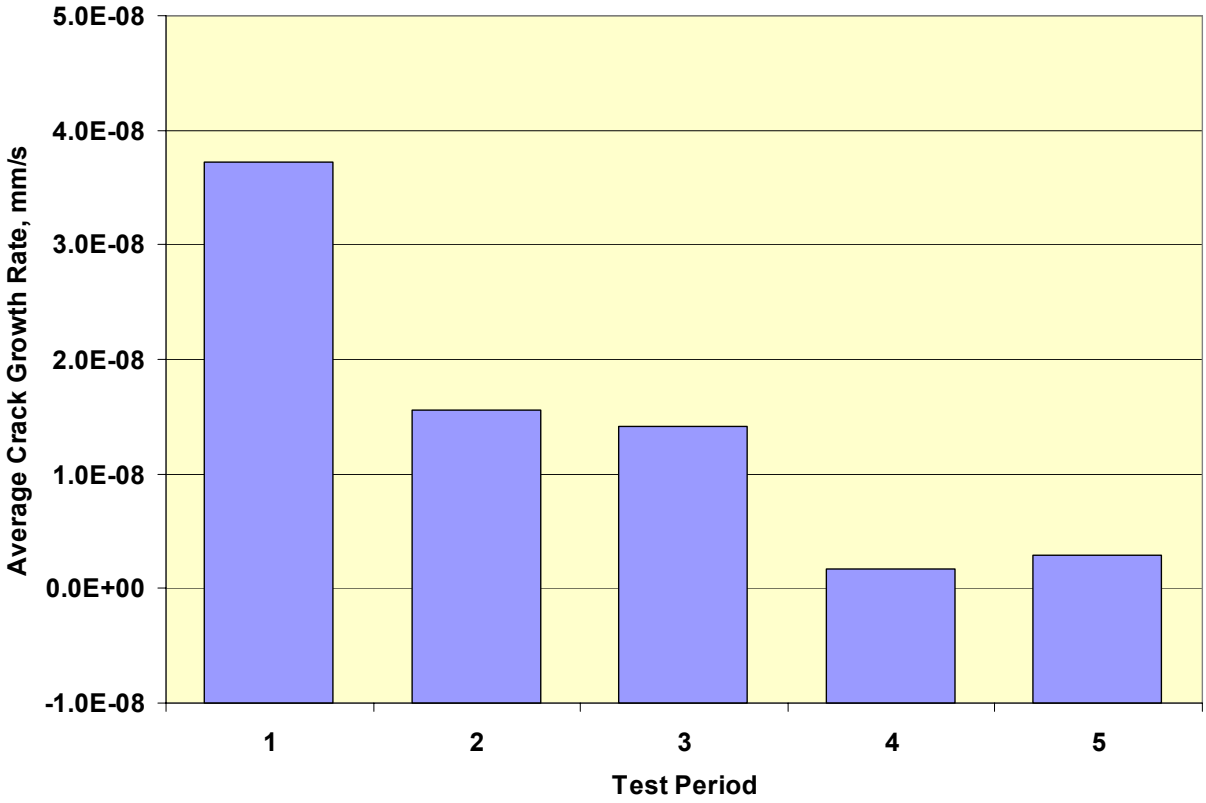

Figure 13. Crack growth rates for test periods in which Specimen 4-4-HAZ 1 was exposed to SFGE.

Crack growth rates ranged between 1.7×10^{-9} mm/s and 3.72×10^{-8} mm/s (1.17 mm/y). The average crack-growth rate was 1.43×10^{-8} mm/s and the median crack growth rate was 1.41×10^{-8} mm/s. These values are considerably lower than those measured for the base metal specimens but the sample size was considerably smaller and the R ratio was higher than for most base metal tests. An analysis of the means was performed comparing the crack growth rate data for the HAZ specimen and the base metal specimens and the differences was not significant at a

95% confidence level (alpha = 0.05). Given the small sample size, the data were analyzed at a 90% confidence level (alpha = 0.1) and the difference was significant at this lower confidence level.

Three weld metal specimens were tested and there were six separate test periods, over 84 days, in which the specimens were exposed to SFGE. Between these periods, the specimens were exposed to gasoline, or unload – reload transients were applied to the specimens to initiate cracking. No cracking could be initiated in one of the specimens (Weld 1) in spite of the fact that two unload reload transients were applied and the solution was changed.

The other two specimens exhibited cracking and a very high crack growth rate (1.18×10^{-7} mm/s) was observed for one of those specimens. This rate is at the upper end of rates observed for the base metal specimens, as show in Figure 11. An analysis of the means was performed comparing the crack growth rate data for the weld specimens and the base metal specimens and the differences were not significant at a 90% or 95% confidence level.

These two weld specimens also exhibited crack growth in the gasoline, following initiation in the SFGE. In the case of specimen Weld - 2, the cracking did not arrest. It is highly likely that the crack growth in the gasoline phase was the result of crack growth under cyclic loading in the inhomogeneous weld, since this type of behavior was never observed with HAZ or base metal specimens. However, this theory could not be confirmed from the fractography because of the mixed mode of the SCC region. Unfortunately, the quasi-cleavage in the mixed mode SCC cracking could not be distinguished from the quasi-cleavage associated with crack growth under cyclic loading.

3.2.3 Effect of Blend Ratio

The results of the crack growth tests were generally consistent with the results of the SSR tests performed in Task 1. Evidence of crack growth was observed in blends containing 20% (by volume) and higher concentrations of ethanol (prepares with SFGE and gasoline); whereas, continued crack growth was not observed in E-15, E-10, or in gasoline. Typical test data are shown in Appendix B (Figure 42 and Figure 43), for sample Base 4, which is a base metal sample. These data are replotted in Figure 14.

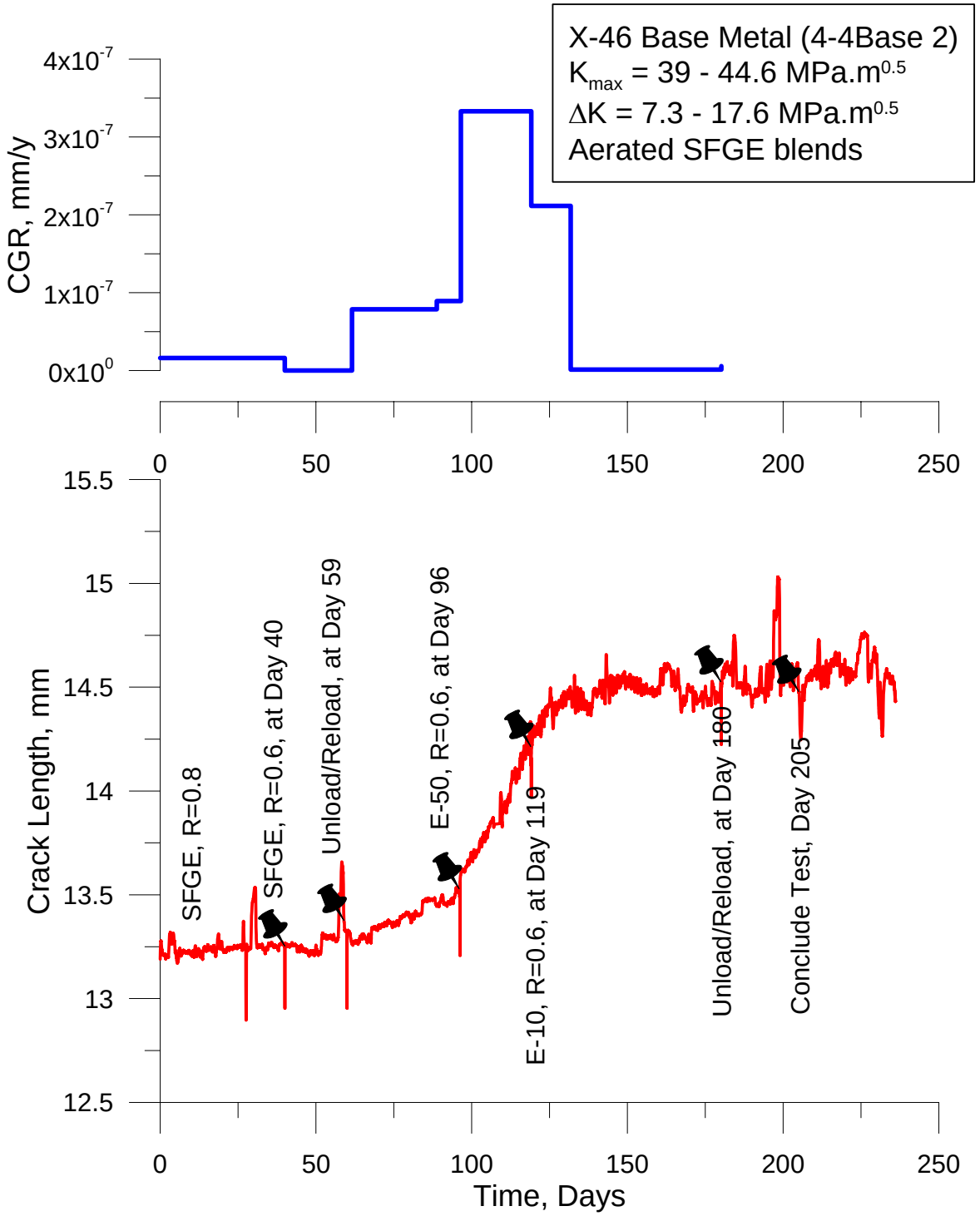

Figure 14. Changes in crack growth rate in response to environmental and loading changes.

Figure 12 shows the average crack-growth rate as a function of the ethanol concentration in the ethanol-gasoline blends.

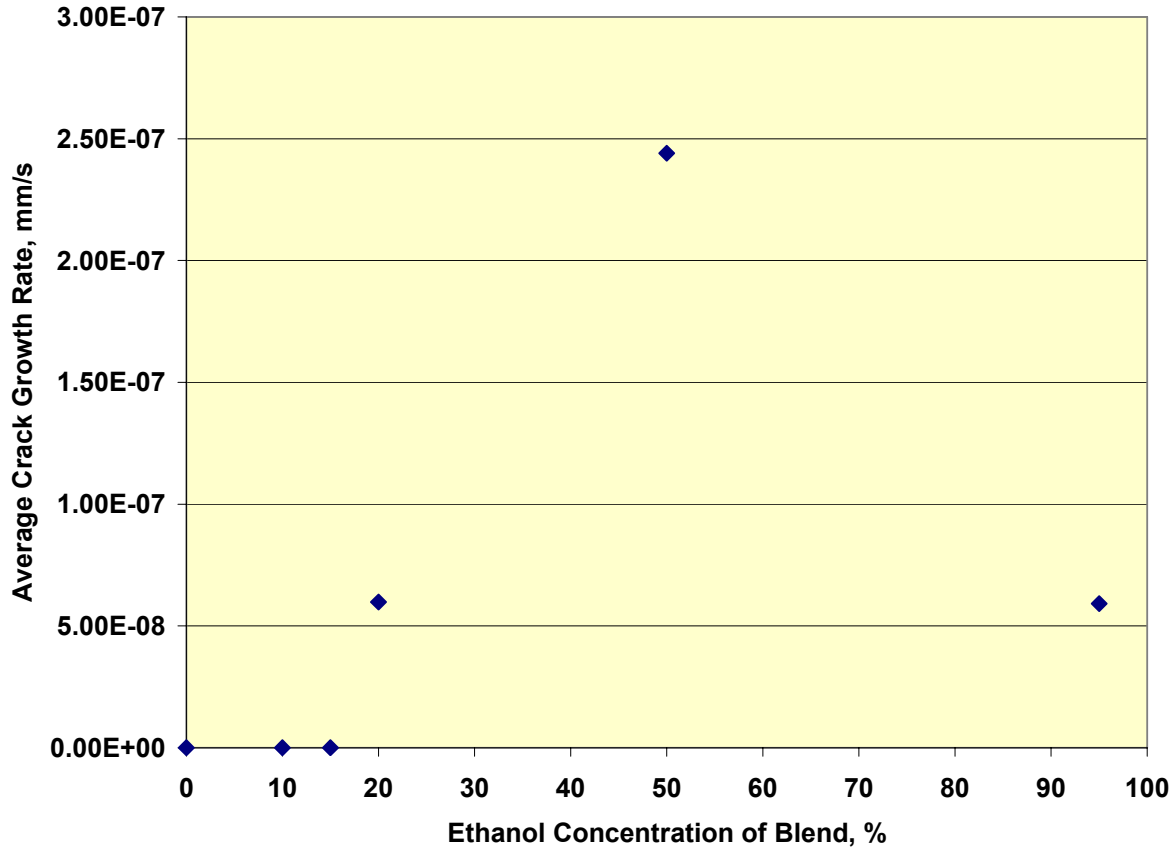

Figure 15. Average crack growth rate as a function of percent ethanol in the blend.

These data show that the crack growth rate in E-20 is comparable to that in E-95 while the rate is actually measurably higher in E-50. These data are consistent with overall crack growth rate derived from SSR tests (Figure 4)

3.2.4 Effect of Batching

Three batch cycles were evaluated in the project; two short cycles with a twenty-four hour period and one long cycle with a twelve-day period:

Cycle 1: One hour SFGE: 23 hours gasoline
Cycle 2: One hour gasoline: 23 hours SFGE
Cycle 3: Five Days SFGE: 7 Days gasoline

One long cycle test was performed with Sample (4-4 HAZ-1). One short cycle test, with 23 hours of SFGE exposure, was performed with one sample (4-4 Base 7). Three short cycle tests with 1 hour of SFGE exposure were performed (Samples 4-4 Base 6, 4-4 Base 7, and 4-4 Base 11). The results are summarized in Appendix B (Table 9) and Appendix B (Figure 46 and Figure 47). One such series of data is illustrated in Figure 16.

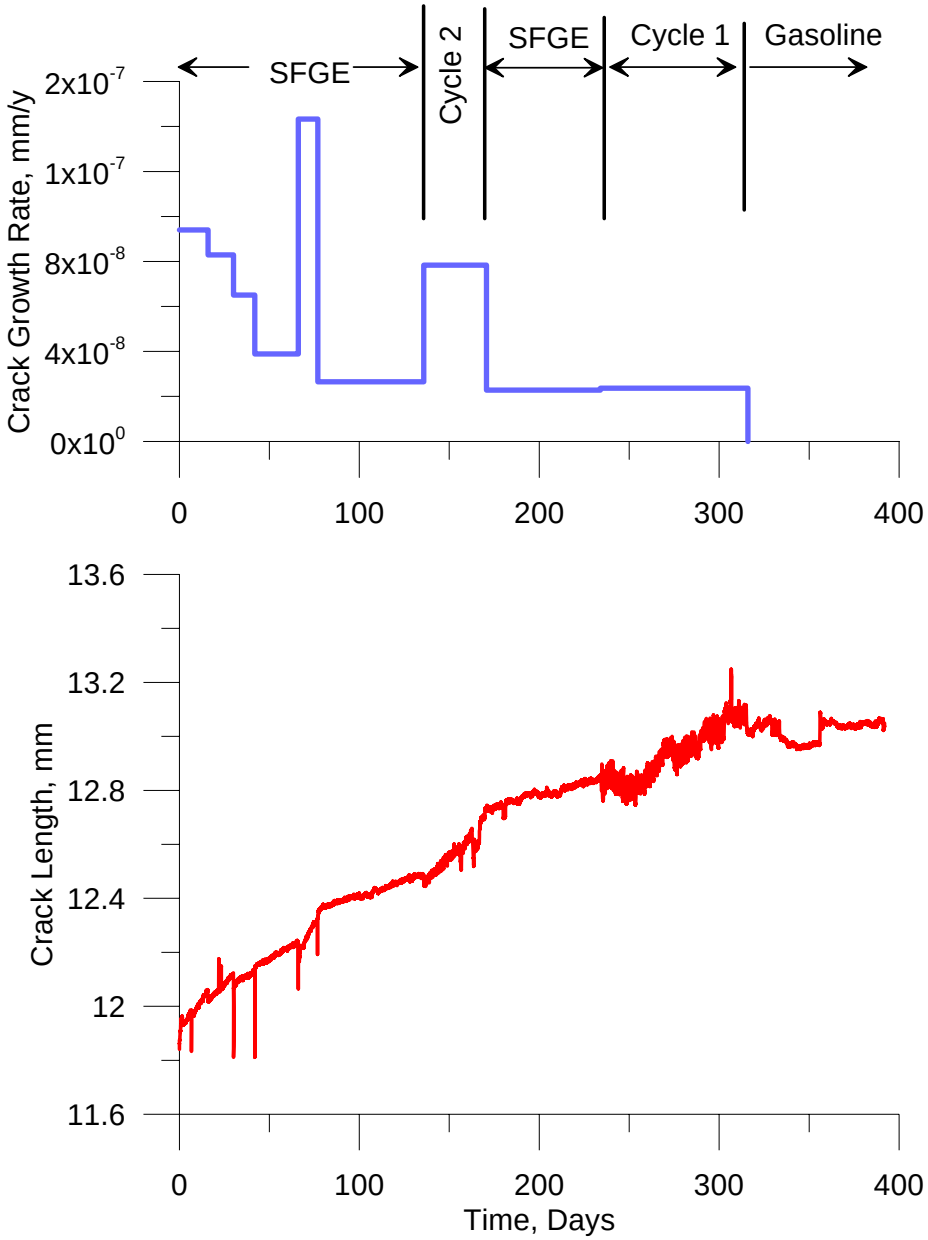

Figure 16. Crack growth rate changes due to different batching cycles.

A fair amount of disruption in the EPD data was observed in all tests, as a result of the batching process but the behavior in the tests could be estimated from the peaks of the EPD data. Figure 17 shows the average crack growth rates observed for the five tests.

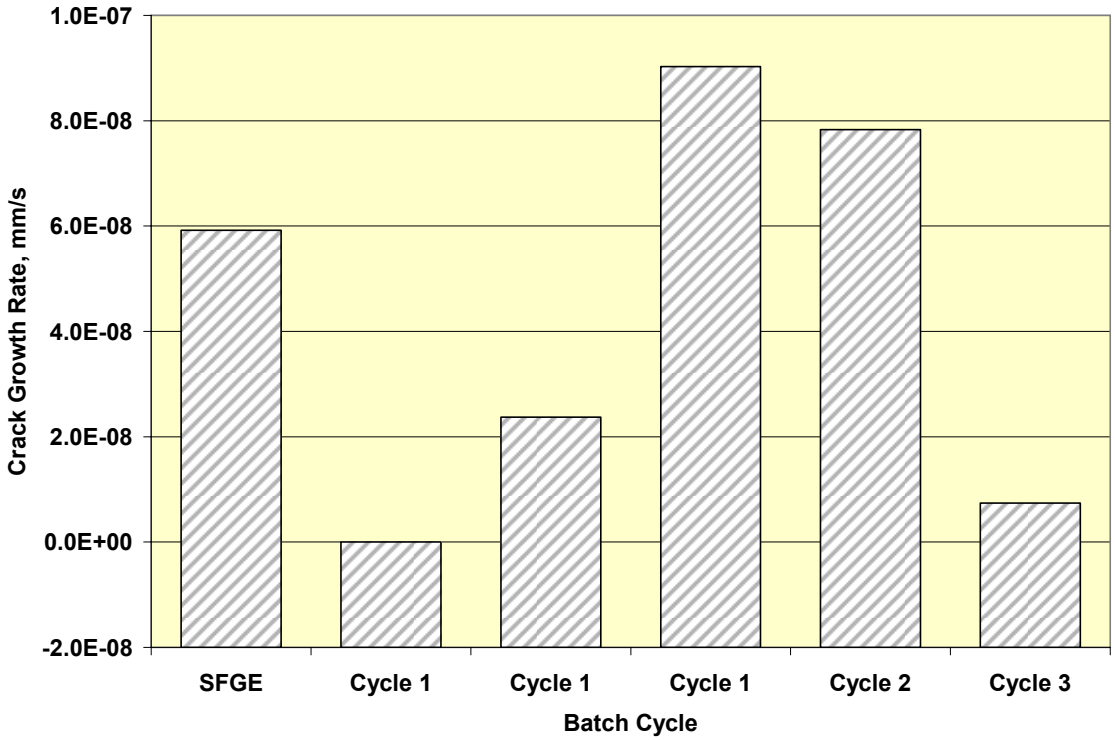

Figure 17. Time average crack-growth rate for various batch cycles. Value for SFGE (no batching) is an average for a number of observations.

This figures shows that measurable crack growth was observed for the single tests with Cycles 2 and 3 and two of the three tests with Cycle 1. Data for the long cycle test are shown in Figure 16. Batch Cycle 3 was started on Day 237 and the growth rate declined only slightly from that which was observed in SFGE. A reasonable estimate of the average crack growth could be made for the long batch cycle based on the relative ratio of exposure time in FGE and in gasoline, assuming that no SCC growth occurs in the gasoline phase.

This approach does not appear to be applicable to the short batch cycle. Surprisingly, a fair amount of growth was observed for two of the three tests with Batch Cycle 1 in which there was very little exposure time to SFGE. Data for Specimen 4-4 Base 7 are shown in Figure 47. Batch Cycle l was started on Day 234 and cracking appeared to have arrested over the next 30 days. However, cracking reinitiated and the average crack growth rate over the Batching period (Day

234 to Day 315) was 2.37×10^{-8} mm/s, which is lower than the rate observed in SFGE, but never the less, quite significant.

4.0 TASK 4 - ELASTOMERIC MATERIALS

4.1 BACKGROUND

Elastomers are amorphous polymers, characterized by their ability to display large and reversible extensions. They are usually above their glass transition temperature, T_g, at ambient temperature but they have to be crosslinked by vulcanization to prevent flow. Due to their crosslinked nature, permanent chain slippage is largely avoided during deformation of elastomers such that virtually all polymer chains return back to their original location upon release of the strain [4]. This elastic feature associated with high deformation renders elastomers very attractive for sealing applications.

Usually, the affinity a polymer has for a fluid depends on the chemical nature of the polymer's repeat unit. Elastomers are more susceptible to fluid uptake than thermoplastics. Dissolved liquids diffuse into the elastomer bulk over a period of time depending on both the value of the diffusion coefficient (which depends on the fluid and the elastomer) and the seal cross section and geometry [5]

Volume swelling of elastomers is one of the most critical measurements when considering tolerances for housing design [7]. Volumetric swelling of elastomers over 20 % are reported to cause several problems including overfill of the seal housing groove, seal extrusion damage, extremely high stresses in the seal and in the housing, occasional fracture of metal components and progressive degradation of elastomers.

Some of the factors influencing the swelling of elastomers [5], [7] are reported as:

- Both the rate of absorption and the level of equilibrium mass uptake of elastomers are found to decrease as the fluid viscosity increases.

- Swelling of elastomers can accelerate by a modest amount with an increase in temperature.

- Maximum absorption of a liquid by an elastomer depends on the difference in solubility parameter, δ values; the closer they are, the more likely fluid absorption is to occur. An elastomer exposed to an immiscible liquid mixture will eventually swell as if it's exposed to the more compatible liquid (i.e., the one with the nearest δ), even if the sample does not directly contact that liquid in a pure form.

The objective of this project is not only to document the performance of several fluoroelastomers of varying fluorine content and a thermoplastic polymer tested in two fuel blends of varying ethanol amount but also to evaluate the effect of sequential fuel transitions on the performance of these seal materials used in the fuel dispensing equipment upon subjecting them first to the ethanol blends and then to the neat gasoline. The study also enables an assessment on whether the swelling of tested polymers is reversible or not.

4.2 Experimental Procedures

Previous research studies indicated that the effect of ethanol-fuel blends on rubber sealing materials such as fluoroelastomers has been investigated up to 10% blends, but has not been well documented for various levels of ethanol. Experiments to measure the changes in volumetric swelling, hardness and compression-set properties of several fluoroelastomers typically used in fuel systems were conducted in this research when their exposure to fuel blends with as low ethanol content as E20.

Three different fluoroelastomers, two copolymers of acrylonitrile and butadiene, as well as a Teflon polymer were selected for evaluation in this study. The FKMs varied in monomer and fluorine content from a low of 66% F to a high of 70%F. This test matrix provided a broad spectrum of polymers to evaluate. Detailed description of each of the test materials is provided as below:

Viton® GF: 70.2% fluorine standard fluoroelastomer (FKM) polymer of vinylidene fluoride-hexafluoropropylene- tetrafluoroethylene.

Viton® GFLT: 67% fluorine low temperature, Peroxide cured, specialty FKM polymer of vinylidene fluoride-perfluoromethylvinylether-tetrafluoroethylene.

Viton® A: 66% fluorine standard molded, Bisphenol cured FKM polymer of vinylidene fluoride- tetrafluoroethylene-hexafluoropropylene.

Teflon: Polytetrafluroethylene.

Buna N: Copolymer of 22 % acrylonitrile and butadiene, cold polymerized.

Low Swell Buna N: Copolymer of 36% acrylonitrile & butadiene, cold polymerized.

FGE : Fuel grade ethanol: **E95**: approximately 95 % Ethanol and 5 % neat gasoline, by volume.

E20 : 20 % Ethanol and 80 % neat gasoline, by volume.

Neat Gas: 100 % Gasoline.

4.2.1 Testing Conditions

All of the test materials were exposed to three sequential fuel immersion phases at room temperature in a round aging oven starting from ethanol (Et-OH) immersion followed by neat gasoline and Et-OH immersions for 28 days in each phase. Twenty eight test tubes situated in the aging oven were equipped with condensers and exit traps filled with ethanol to prevent the moisture pick up of ethanol fuel blends during the long term exposure experiments. All of the measurements were conducted during periodic exposure intervals.

Volumetric swelling measurements were conducted with rectangular bars of 25 x 50 x 2 ± 0.1 mm as per the ASTM D 471 test standard which covers how to measure and calculate a variety of properties including but not limited to the percentage volumetric swell of elastomers, mass percentage change after swelling, mass of soluble matters in elastomers extracted by fluids [6].

Circular disks of 13.0 ± 0.2 mm diameter with 6.0 ± 0.2 mm thickness were used for the compression-set measurements as per ASTM D 395 Method B [6]. This test procedure outlines the testing of rubber to be used in applications where it will be subjected to compressive stresses in liquid media or air. The test method applies to the rubbers used in seals, vibration dampers and machinery mountings. Method B involves the testing for permanent set under constant compressive force in air or liquids.

Durometer hardness measurements were conducted with rectangular bars of 12 x 12 x 6 mm following the ASTM D 2240 [6]. This test method allowed measurement of the indentation resistance of elastomeric or soft polymeric materials based on the depth of penetration of a conical indentor. While the hardness of Teflon samples were measured using Durometer D since Durometer A results were found to be greater than 90, the hardness of all other samples were measured with Durometer A as Durometer D results were observed to be less than 20. Both of these criteria were recommended in ASTM D 2240 [6].

4.2.2 Results and discussion

The compatibility of six polymeric materials with E95, E20 fuel blends and neat gasoline have been investigated both during single fuel exposure of 28 days and during sequential fuel transition exposures under static loading conditions. Swelling, hardness and compression set tests were conducted as per ASTM test standards. The results of all of the static test measurements are provided in Figures 18 - 20.

Comparison of the volumetric swelling of all test materials upon 28 days of exposure to E95 Fuel Blend with that of E20 Fuel Blend and the Neat Gasoline (Figure 18) indicates that all test materials except *Buna N* were found to have less than 5 % volumetric swelling upon their exposure to E95 fuel for 28 days at ambient temperature, whereas, up to 9.8 % of volumetric

swelling was observed upon their exposure to E20 blends. In contrast, the volume swelling in neat gasoline attained a value as high as 125 percent.

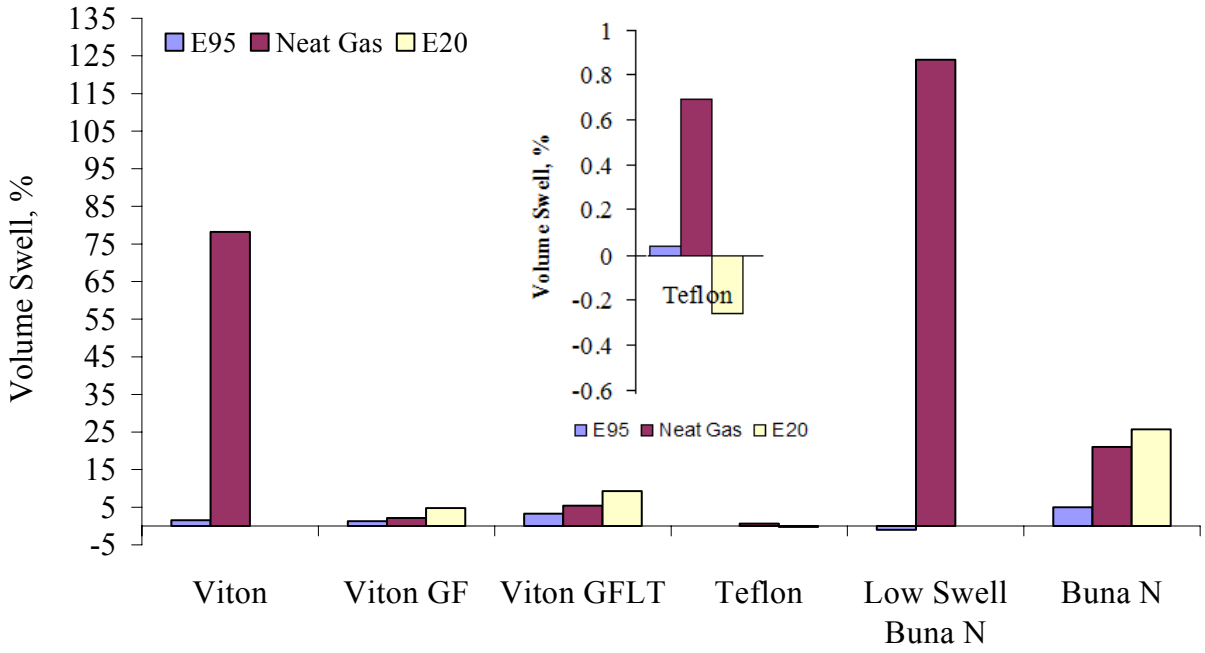

Figure 18. Comparison of the swelling of non-metallic materials upon 28 days of exposure to E95 Fuel Blend with that of E20 Fuel Blend and the Neat Gasoline.

The results of swelling tests during sequential fuel transition phases are provided in Figure 19 and Figure 20. The volumetric swelling plots in Figure 19 clearly show that sequential fuel transition from E-95 to Neat Gasoline is observed to have a substantial effect on the volume swell of *Viton* and *Low Swell Buna N* samples.

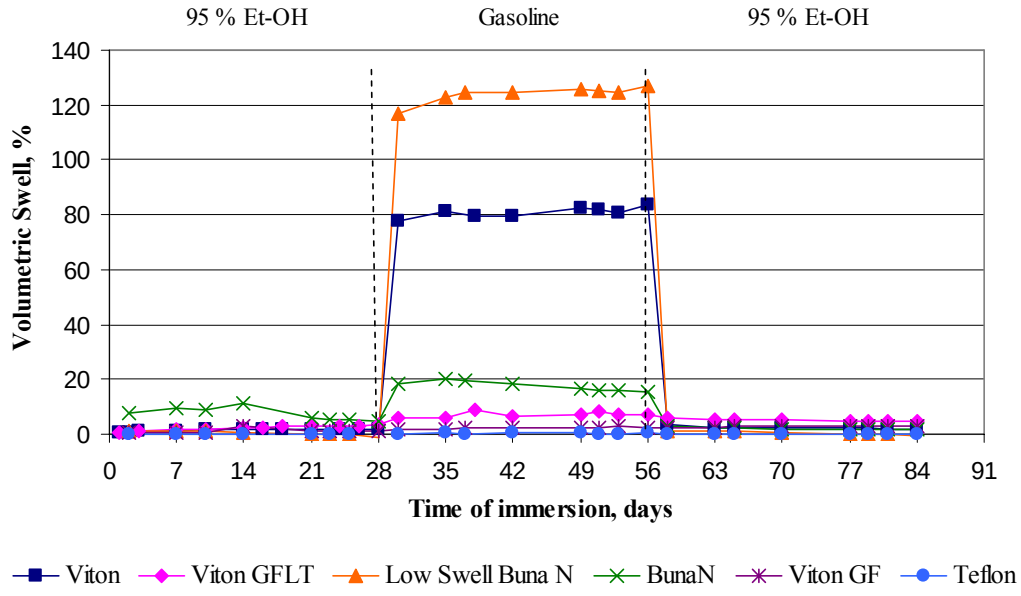

Figure 19. Effect of sequential fuel transitions from E95 fuel blend to neat gasoline followed by E95 fuel blend on the swelling of non-metallic materials.

The comparison of Figures 19 and 20 also indicates that the volumetric swelling of all elastomers are found to increase as the amount of gasoline in the ethanol (Et-OH) blends increases such that % volumetric swelling of elastomers in E95 blends were much smaller than % volumetric swelling of elastomers in E20 blends.

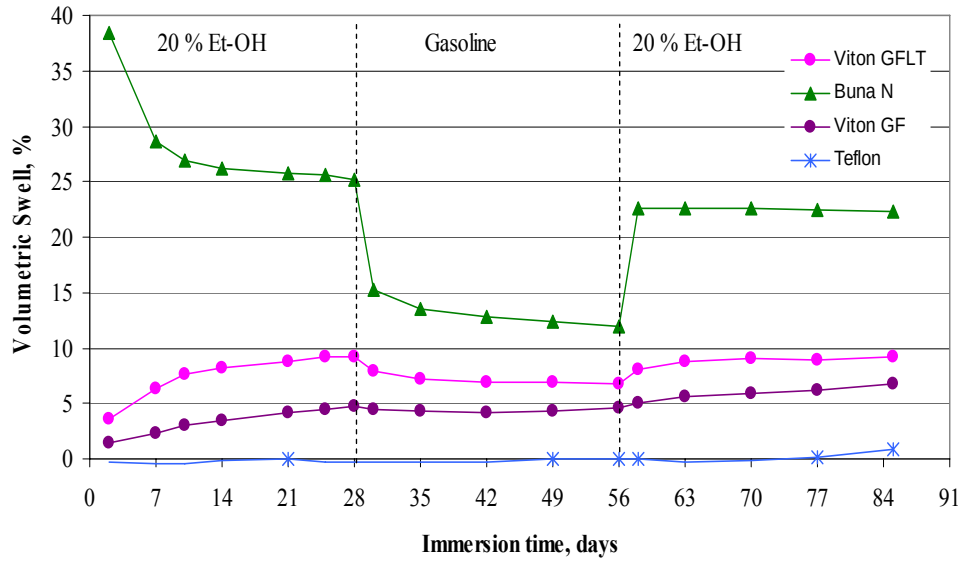

Figure 20. Effect of Sequential Fuel Transitions from E20 Fuel Blend to Neat Gasoline followed by E20 Fuel Blend on the Swelling of Non-Metallic Materials.

Another important result which is noteworthy to mention is that swelling of elastomers in the Et-OH blends was usually determined to be more than that of neat fuel systems (i.e., neat gasoline or neat Et-OH), such that % volumetric swelling of elastomers in E20 > % volumetric swelling of elastomers in Neat Gas > % volumetric swelling of elastomers in E95. This finding was observed to be also in alignment with the earlier literature survey results. When the non-metallic samples are exposed to fuels containing higher gasoline content, i.e. E-20 fuel, the subsequent exposure of these non-metallic samples to Neat Gasoline is found to be less severe in the swelling behavior.

A visual comparison of swollen elastomeric samples upon exposure to sequential fuel immersions of E95 fuel and neat gas can be seen in Figure 21.

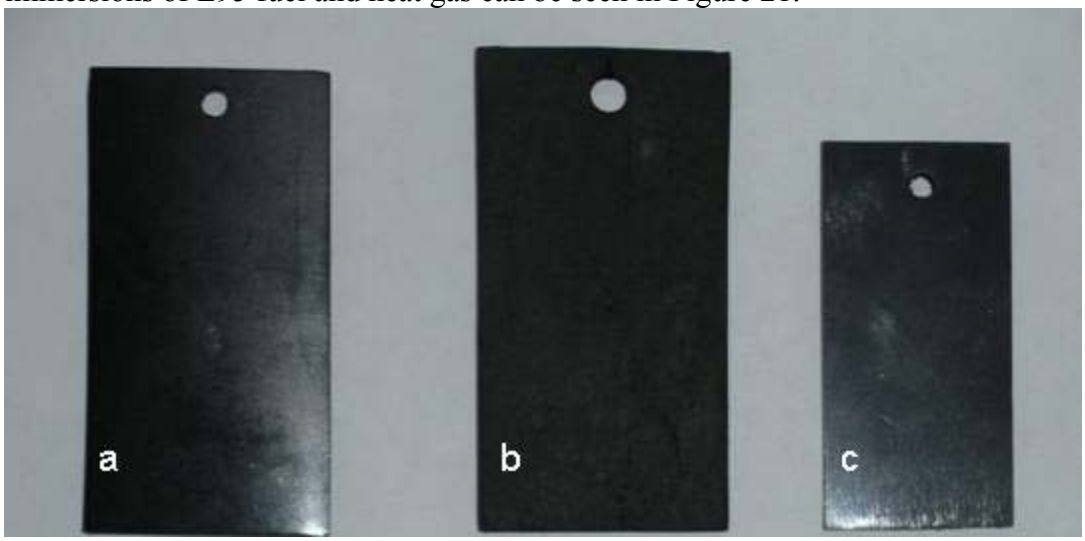

Figure 21. Comparison of the swollen elastomeric samples upon exposure to sequential fuel immersions of E95 fuel and gasoline (a) Viton Sample after 28 days of exposure to E95 followed by 28 days in Gasoline & 7 days in E95, (b) Low-Swell Buna N Sample after 28 days of exposure to E95 followed by 7 days of exposure to Gasoline and (c) Initial dimensions of a Viton sample.

Figure 22 indicates a photographic illustration of the severity of swelling & eventually tearing of a Low swell Buna N sample after 28 days of exposure to E95 Fuel followed by 28 days of exposure to neat gasoline.

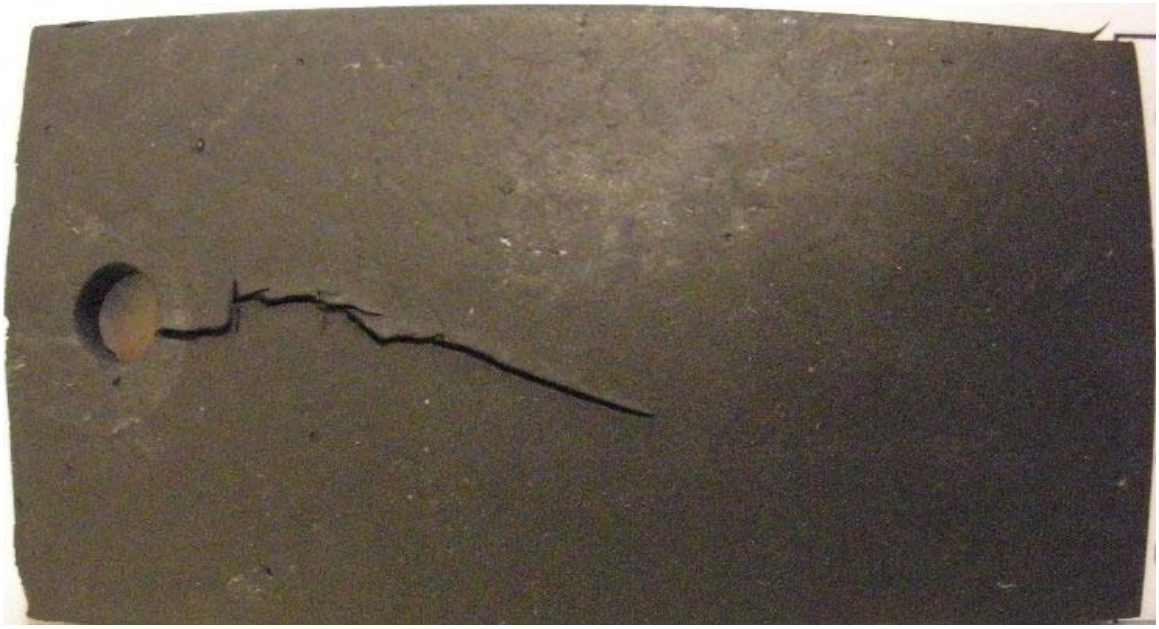

Figure 22. Tearing of a Low-swell Buna N sample after 28 days of exposure to E95 Fuel followed by 28 days of exposure to Neat Gasoline.

The effect of leaching of some non-metallic test materials on the immersion test fluids at the end of the last E95 fuel exposure phase is shown in Figure 23. Leaching of the soluble non-bound ingredients of some elastomers, such as *Viton and Low Swell Buna-N and Buna-N* samples was witnessed by coloration of test fluids during immersion tests. It's believed that the GC/MS analysis of Et-OH Blends used in the immersion tests could provide a better understanding of which ingredients of elastomers are leaching out during their exposure.

The results of hardness tests were presented from Figures 24 to 26. Figure 24 illustrates that up to 60 % of lack of hardness retention was observed with the *Low Swell Buna N* samples upon sequential fuel transition from E-95 fuel to Neat Gasoline during the immersion tests. A comparison of Figure 24 with Figure 25 clearly indicates that the effect of fuels containing higher gasoline content, such as, E-20 fuel on the hardness retention of non-metallic materials are found to be more severe than that of fuels containing less gasoline content, ie. E-95 fuel.

Figure 23. Effect of leaching of non-metallic materials on the immersion test fluids at the end of the last E95 fuel exposure, Phase III.

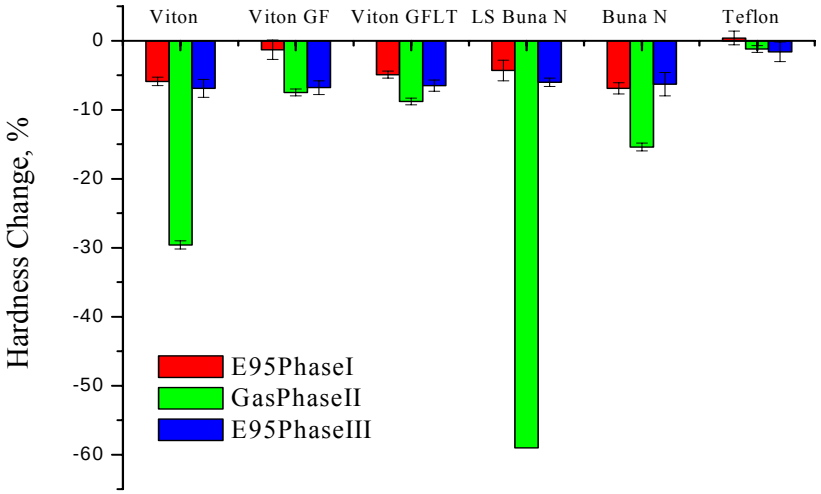

Figure 24. Effect of Sequential Fuel Transitions from E95 Fuel to Neat Gasoline followed by E95 Fuel for 28 days on the Hardness Loss of Non-Metallic Materials.

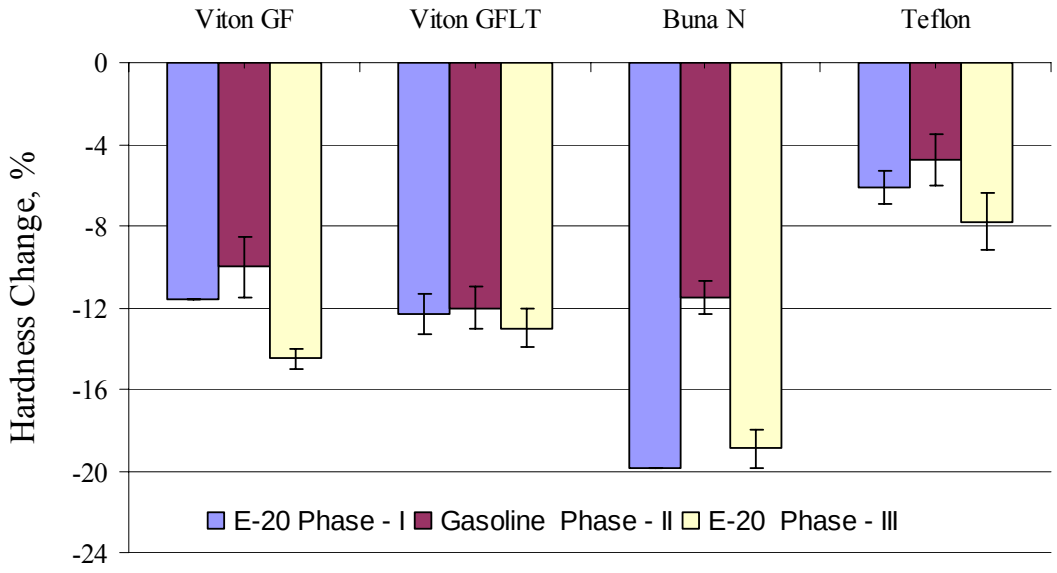

Figure 25. Effect of sequential fuel transitions from E20 Fuel to neat gasoline followed by E20 Fuel for 28 days on the hardness loss of non-metallic materials.

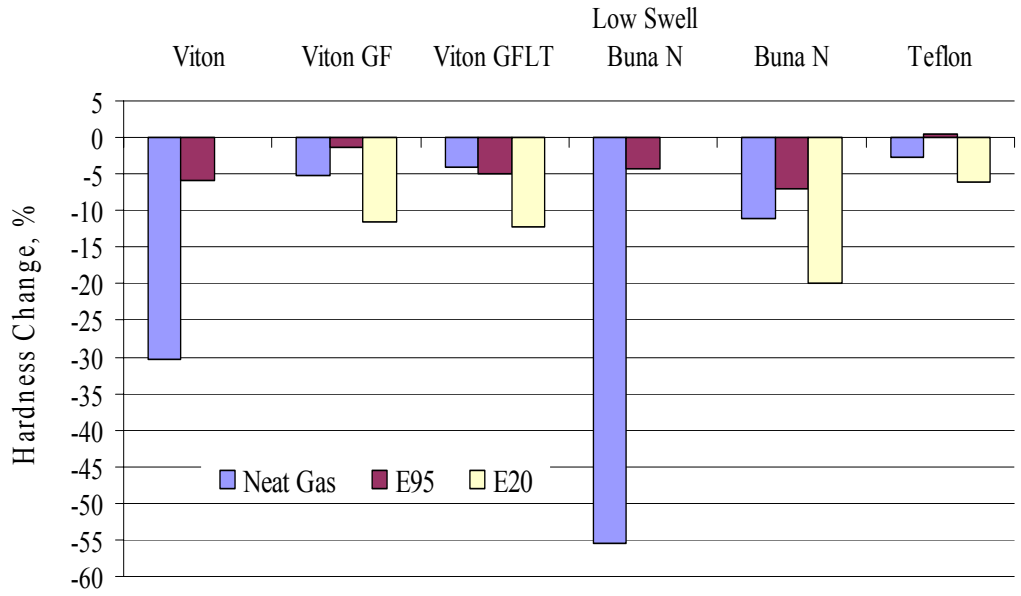

Figure 26. Comparison of hardness retention of non-metallic materials upon 28 days of exposure to E95 fuel blend with that of E20 fuel blend and the neat gasoline.

The results of compression set measurements during single fuel exposure of 28 days and during sequential fuel transition exposures are plotted for E95 and E20 fuel immersions in Figure 26 and Figure 27, respectively.

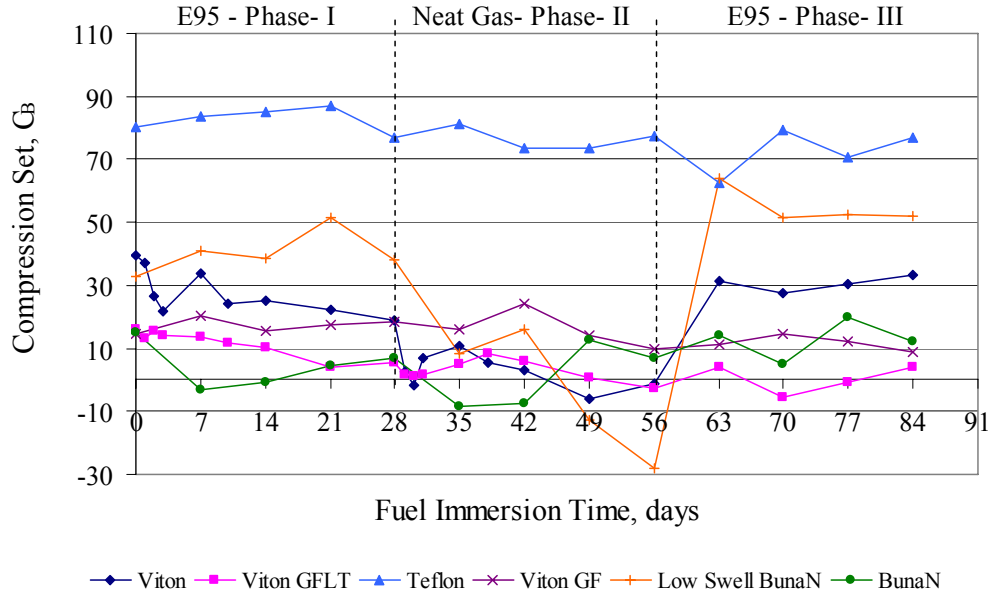

Figure 27. Comparison of compression-set properties of non-metallic materials upon 28 days of exposure to E95 fuel blend followed by neat gasoline and E95 fuel blend.

Compression Set Tests measure the ability of a rubber to return to its original thickness after prolonged compressive stresses at a given temperature and deflection. Compression-set tests are generally used to determine the ability of elastomeric materials to maintain elastic properties and to measure somewhat permanent deformation of test specimens after prolonged compressive stress. As a rubber material is compressed over time, it loses its ability to return to its original thickness. This loss of resiliency (memory) may reduce the capability of an elastomeric gasket, seal or cushioning pad to perform over a long period of time.

Compression Set results for each test materials are expressed as a percentage maximum figure. Usually, the lower the percentage figure, the better the material resists permanent deformation under a given deflection and temperature range. The unusually high compression set test results of Teflon samples plotted in Figure 26 and Figure 27 were attributed to the fact that Teflon isn't a rubbery material but it's a thermoplastic material and ASTM D 395 Method B may not necessarily be the best way of determining its compression set properties. Thus, a comparison of the compression set test results of Teflon with those of elastomers may not be viable.

Comparison of the compression set results of all elastomeric test materials in Figure 26 has followed similar trends with the results of swelling and hardness retention such that both Viton and Low Swell Buna-N samples exhibited high compression set values while the other elastomers showed lower compression set values upon their 28 days of exposure to E95 Fuel Blend followed by Neat Gasoline and E95 Fuel Blend. The fluctuations in the compression set test data both in E95 and in E20 fuel immersion tests are attributed to the fact that the test results might have been influenced by the effects of swelling and the changes in chemical structures of test materials over long periods of fuel immersion phases. All of the test results indicated that *Viton GF, Viton GFLT and Teflon* samples were determined to offer the best hardness retention and least volume swelling upon exposure to both pure fuel systems and subsequent transition of fuel systems under static loading conditions.

4.2.3 Summary of Elastomer Testing

The major findings of this research along with some recommendations are outlined as:

- As the amount of gasoline in the ethanol (Et-OH) blends increases, the Volumetric Swelling of all elastomers are found to increase such that % volumetric swelling of elastomers in E95 Blends were much smaller than % volumetric swelling of elastomers in E20 Blends. Thus, it is concluded that the use of higher Ethanol containing blends (ie., using E95 instead of E20) would be safer in terms of less volumetric swell.

- Swelling of elastomers in the Et-OH blends was determined to be more than that of Neat Fuel Systems (i.e., Neat Gasoline or Neat Et-OH), in general such that % Volumetric Swelling of elastomers in E20 > % Volumetric Swelling of elastomers in Neat Gas > % Volumetric Swelling of elastomers in E95. This finding was observed to be also in alignment with the earlier literature survey results.

- *Viton GF, Viton GFLT and Teflon* samples were determined to offer the best hardness retention and least volume swelling upon exposure to both pure fuel systems and subsequent transition of fuel systems under static loading conditions.

- All test materials except *Buna N* were found to have less than 5 % volumetric swell upon exposure to E-95 for 28 days at ambient temperature.

- Sequential fuel transition from E-95 to Neat Gasoline was observed to have a substantial effect on the volume swell of *Viton* and *Low Swell Buna N* samples.

- Lack of hardness retention up to 60 % was observed in *Low Swell Buna N* samples upon subsequent fuel transition from E-95 fuel to Neat Gasoline.

- Leaching of the ingredients of some elastomers, such as *Viton and Low Swell Buna-N and Buna-N* samples was witnessed by coloration of test fluids. GC/MS analysis of Et-OH Blends used in tests will be valuable for better understanding of which ingredients of elastomers are leaching out during exposure.

- *Viton and Low Swell Buna-N* samples were found to be highly incompatible for use when switching from E-95 fuel to neat gasoline in various sections of fuel dispensing equipment. Thus, they are eliminated from other blend tests.

- When the non-metallic samples are exposed to fuels containing higher gasoline content, ie. E-20 fuel, the subsequent exposure of these non-metallic samples to Neat Gasoline is found to be less severe in the swelling behavior.

- The effect of fuels containing higher gasoline content, ie. E-20 fuel on the hardness retention of non-metallic materials are observed to be more severe than that of fuels containing less gasoline content, ie. E-95 fuel.

5.0 TASK 5 - EVALUATION OF MITIGATION METHODS FOR EXISTING PIPELINES

In this task, both slow strain rate (SSR) and crack growth tests (similar to those in Task 3) are being performed. Most of the SSR tests in Task 5, to date, have been performed on base metal specimens machined from one X-60 line pipe steel. This line pipe steel was previously evaluated in PRCI SCC 4-3 and was shown to be susceptible to ethanol SCC. The majority of the testing is being performed with un-notched specimens, but a few SSR tests are being performed with notched specimens of the same line pipe steel as that being evaluated in Task 3.

The un-notched specimens have a gage length of 25 mm (1 inch) and a gage diameter of 3.2 mm (0.125 inches). A displacement rate of 1×10^{-6} inches/sec is being used, which produces a strain

rate of 1×10^{-6} sec^{-1}. The notched specimens have a gage length of 12.5 mm (0.5 inches) and a gage diameter of 4.75 mm (0.187 inches). The notch has a depth and width of 0.25 mm (0.01 inches) and a radius of 0.127 mm (0.005 inches). A displacement rate of 9.53×10^{-6} mm/s (3.75×10^{-7} inches/s) is being used for all of the SSR tests with notched specimens. The SSR tests with both types of specimens are performed in stainless steel test cells with a total volume of 400 ml; 350 ml of solution is filled and the vapor space is 50 ml.

The testing is being performed using FGE and the SFGE containing 5 ppm Cl^-. Specimens are tested under freely corroding conditions and the corrosion potential is monitored in each test using an Ag/AgCl/EtOH reference electrode. Based on independent measurements of chloride leakage rate from the reference electrode, it is estimated that the chloride concentration in the test cell increased by about 1 ppm during the course of the SSR tests. A piece of rusted pipe steel is placed in the test cell and galvanically connected to the test specimen to more closely simulate the native corrosion potential of a mill scaled/rusted pipe wall. The rusted steel to specimen area ratio is approximately 5 to 1. The specimen and rusted steel piece are electrically isolated from the specimen grips and test cell in the SSR test machine. The tests are performed at room temperature and the cell is actively sparged with breathing air at a flow rate of approximately 4 ml/minute. Ethanol bubbler traps are used on the inlet and outlet to the test cell to remove/exclude any moisture. Posttest analyses are not performed on the test solutions but extensive previous water analyses of test solutions from the SSR tests indicates that there is negligible pick-up of water in the tests.

After testing, the specimens are examined and optically photographed. The fracture surfaces are examined in the scanning electron microscope (SEM) and the depths of the stress corrosion cracks on the fracture surfaces are measured. The depth of the second deepest crack in each specimen is recorded. Other parameters that are recorded for each test included the time to failure, ultimate tensile strength, and reduction in area (un-notched specimens only).

5.1 Results

Appendix A (Table 8) provides the detailed results of the tests performed in this task. The following SSR tests were control tests performed in air (or in a non-cracking environment) on the three steels; Test C-18 and 4-3-22 [Steel 1229 (X60 line pipe steel)], Test KM-12 [Steel 1228 (X-52 line pipe steel)], and Test 1238N-3 [Steel 1238 (X46 line pipe steel)]. The data from these tests are used to calculate the mechanical property ratios for the SSR tests performed in the cracking environments.

Test 4-3-3 was a base line test performed in the SFGE. Note that the time to failure ratio and reduction in area ratio were all less than the values in the air tests and relatively deep stress corrosion cracks were present on the fracture surface. Secondary stress corrosion cracks also

were present on the gage length of the specimen. Test 4-3-0 was a base line test performed in one lot of actual FGE. Note that the extent of SCC in this specimen was very similar to that observed in SFGE, validating the use of SFGE for most of the inhibitor work.

Tests 1229-02 and 1229-03 were performed in SFGE containing 150 ppm by weight of NH_4OH (500 ppm by weight of reagent grade [30%] aqueous ammonium hydroxide). Previous research has indicated that amines are capable of inhibiting ethanol SCC and a series of tests is being performed in this task to investigate the mechanism of inhibition. Specifically, amines can raise the pHe and we wanted to determine whether the inhibition of SCC by the amines is simply the result of a pH increase. What we found was very surprising and potentially groundbreaking. The 150 ppm NH_4OH didn't just inhibit the SCC; it completely eliminated it. No SCC was observed on either specimen. Test 1229-04 was performed in SFGE containing 75 ppm by weight of NH_4OH and SCC was completely mitigated in this test as well. Inhibition of SCC also was observed in a second line pipe steel examined (Sample 1228-36) at 150 ppm NH_4OH concentration, but not at a concentration of 38 ppm. Therefore, the threshold inhibitor concentration appears to be between 38 ppm and 75 ppm.

Test 1229-05 was performed in SFGE containing 3.38mM LiOH. This is the same molar concentration of OH as that found in the test with 150 ppm NH_4OH. While the cracking severity was diminished from the base line test in SFGE, SCC never the less was observed in this test. Test 1229-8 was performed with 165 ppm ammonium acetate (1.69 mM acetate) to investigate the effect of the ammonium ion. Again, cracking was observed. The behavior in these tests suggests that both the pH increase and the presence of the ammonium ion are required for the observed inhibition.

Test 1229-7 was performed to better understand the role of oxygen in the SCC process. A non-oxygen containing oxidizer ($FeCl_3$) was added to the SFGE and the test was run under deaerated conditions. The corrosion potential in the test was within the previously established cracking range yet no SCC was observed. This behavior suggests that oxygen may play more of a role in the cracking process that just modifying the corrosion potential. Because the ferric chloride also is acidic, and therefore affected the pH, additional testing (outside the scope of this task) is necessary to better understand this issue.

Tests 1229-51 through 1229-59, and 1229-X1 were performed with several inhibitors supplied by three commercial vendors. The inhibitors were added at the concentration recommended by the supplier. None of the inhibitors completely stopped cracking but several exhibited evidence of SCC inhibition, including two from one vendor (030509-5 and 030509-4) and two from a second vendor. However, one of the latter caused severe crevice corrosion and pitting.

Four SSR tests using notched specimens were performed and the results are shown in Table 8. Also included in Table 8 are two tests from PRCI SCC 4-4, Task 1 that are used as control and base line tests. The results were quite surprising in that none of the inhibitors tested, even those that were effective in SSR tests using smooth specimens (e.g., 150 ppm NH_4OH and diethanol amine (DEA)), inhibited SCC with this specimen geometry. One test (1238N-1) was performed in an attempt to understand the behavior. This test was performed with ammonium hydroxide at a concentration that completely inhibited SCC with smooth specimens. It had been noted that the corrosion potential in most of the SSR tests with un-notched specimens tended to drop with time as the gage section strained. A similar drop was not observed with the notched specimens. It was hypothesized that this potential dropped reduced the aggressiveness of the SSR test with un-notched specimens. This was evaluated by coating the gage section of the notched specimen (except the notch) to eliminate the large noble surface. Cracking was observed in this test as well. While a potential drop later in the test only was observed with the coated sample, that sample also had a more noble average potential. Additional research is needed to understand why the SSR tests with notched specimens are so aggressive. However, because of this aggressiveness, the technique does not appear to be useful for screening corrosion inhibitors. Accordingly, this technique will not be used for future inhibitor screening. The crack growth tests are probably the most realistic, yet aggressive, technique for inhibitor assessment. Results from these tests are given below.

5.1.1 Crack Growth Test Results

Crack growth tests with two of the commercial inhibitors, ammonium hydroxide, and diethanol amine (DEA) were started this reporting period. The commercial inhibitors were added at the concentration recommended by the supplier. DEA was shown to be an effective inhibitor in PRCI SCC 4-1, based on SSR tests of un-notched specimens. Results, to date are promising. Inhibitor 030509-5 (500 ppm) and Inhibitor 154 (250 ppm) appear to have arrested cracking while crack growth rates are decreasing with time for NH_4OH (150 ppm). In the latter test, cracking might also eventually stall out. Surprisingly, the DEA inhibitor did not appear to decrease the crack growth rate. These tests are now being conducted as a part of a new PHMSA project whose objective it is to evaluate various commercial inhibitors under realistic conditions.

6.0 SUMMARY AND RECOMMENDATIONS

Referring to the overall project objectives, the following are the conclusions of SCC 4-4:

- All pipelines made of common line pipe steels are susceptible to ethanol SCC and any differences in susceptibility are not significant from an integrity perspective (Section 2.2.2).

- While differences in susceptibility were noted for some weld types, in general, the base metal, heat affected zone, and weld metal were all susceptible to SCC in SFGE (Section 2.2.2).
- The threshold stress intensity factor for SCC initiation, K_{thSCC}, in the base metal is approximately 30 ksi $in^{1/2}$ in SFGE (Section 3.2.1).
- In the cyclic load tests, the crack growth rates in SFGE followed a Weibull distribution with the 50th percentile for the distribution of 5.55×10^{-8} mm/s. This rate is about three times higher than maximum rates measured for near neutral pH SCC of underground pipelines (Section 3.2.2).
- The only blends that can be safely transported in existing pipelines without significant modification of the system or operations (Case 1) are those containing less than 15% (by volume) ethanol (Section 2.2.3 and 3.2.3). All other blends require significant modifications of the system or operations (Case 2), or specially designed systems (Case 3).
- Case 2 (operational changes) could include deaeration of the SFGE, or the addition of inhibitors. Some commercial inhibitors and ammonium hydroxide have been found to be effective in mitigating SCC. It is not clear whether the addition of these inhibitors will take the ethanol out of ASTM Specification since the D-4806 specification includes inhibitors, but only for corrosion and not SCC. These are being studied, in detail, as a part of a new PHMSA project (Section 5.1.1).
- Case 3 is the subject of ongoing research by PRCI and Honeywell, Inc..
- Batching does not appear to be a viable method for SCC mitigation (Section 3.2.4). Different batching cycles did not produce any major change in crack growth behavior. This is because, For sharp cracks, SCC initiation times are short once the line pipe steel is exposed to FGE or FGE blends capable of promoting SCC. The re-initiation process is not always reproducible, as occasionally an arrested crack did not re-initiate in the presence of ethanol without a superimposed load change (e.g., a load-unload cycle). However, it is presumed that some cyclic loading always exists in pipelines and therefore, continued arrest of a crack in the presence of ethanol cannot be relied upon.
- Volumetric swelling of elastomers in the Et-OH blends was determined to be more than that of Neat Fuel Systems (i.e., Neat Gasoline or Neat Et-OH), in general such that % Volumetric Swelling of elastomers in E20 > % Volumetric Swelling of elastomers in

Neat Gas > % Volumetric Swelling of elastomers in E95. This finding was observed to be also in alignment with the earlier literature survey results (Section 4.2.2).

- All test materials except Buna N were found to have less than 5 % volumetric swell upon exposure to E-95 for 28 days at ambient temperature. Viton GF, Viton GFLT and Teflon samples were determined to offer the best hardness retention and least volume swelling upon exposure to both pure fuel systems and subsequent transition of fuel systems under static loading conditions (Section 4.2.2).

- Sequential fuel transition from E-95 to Neat Gasoline was observed to have a substantial effect on the volume swell of Viton and Low Swell Buna N samples. Lack of hardness retention up to 60 % was observed in Low Swell Buna N samples upon subsequent fuel transition from E-95 fuel to Neat Gasoline. Leaching of the ingredients of some elastomers, such as Viton and Low Swell Buna-N and Buna-N samples was witnessed by coloration of test fluids.

- The effect of fuels containing higher gasoline content, i.e. E-20 fuel on the hardness retention of non-metallic materials are observed to be more severe than that of fuels containing less gasoline content, i.e. E-95 fuel (Section 4.2.3).

7.0 REFERENCES

1. National Renewable Fuels Standard Program for 2010 and Beyond, Environmental Protection Agency, http://www.epa.gov/otaq/renewablefuels/index.htm.
2. National Commission on Energy Policy's Task Force on Biofuels Infrastructure, Bipartisan Policy Center, Washington D.C., U.S., www.energycommission.org, (2008).
3. H. H. Johnson, "Calibrating the Electric Potential Drop Method for Studying Slow Crack Growth," Materials Research and Standards, Vol. 5, No. 9, Sept. 1965, pp. 442-445.
4. R.J. Young and P.A. Lovell, Introduction to Polymers, Second Edition, Chapman & Hall, (1992).
5. MERL Ltd. Research Report 320, "Elastomers for Fluid Containment in Offshore Oil and Gas Production: Guidelines and Review", (2005).
6. http://www.astm.org/Standard/index.shtml
7. A. Ertekin and N. Sridhar, NACE Corrosion Conference Paper & Presentation, "Performance of Elastomeric Materials in Gasoline-Ethanol Blends- A Review", GA, USA, (March 2009).

APPENDIX A: SCREENING TEST DATA

Table A-5 summarizes the results of the SSR tests performed with un-notched base metal specimens of two line pipe steels, an X60 DSAW line pipe steel and an X52 ERW line pipe steels. These tests were performed with base metal specimens so the weld type is not significant. The first column in the table is the sample number. The second column in the table is the line pipe steel used for the testing. The third column in the table is the test solution; which, in all tests with un-notched specimens, was simulated FGE with varying chloride concentrations. The SFGE was sparged with air at a flow rate of approximately 4 ml/minute.

The fourth column in the table is the maximum stress sustained by the specimen, which is the maximum load divided by the cross sectional area. The fifth column in Table A-5 is the total time to failure in the SSR test, in hours. The sixth column in the table is the percent elongation to failure, which was the elongation, measured using the displacement transducer on the test frame, divided by the gage length of the specimen. The seventh column in the table is the reduction in area of the cross section of the specimen. After each test was completed, calipers were used to measure the diameter of the specimen at the fracture surface. This value was converted to an area and compared with the initial cross sectional area.

Column 8 of the table is the severity of SCC. As shown in the table, severe SCC, in which the SCC extends along the gage section of the specimen, was observed in most of the tests with un-notched specimens. A typical example is shown in Figure A-4. Very minor SCC was observed in Test (4-4)-1. In this test, no stress corrosion cracks were present on the fracture surface but crack-like fissures were present in the necked region of the gage section of the specimen, see Figure A-5.

The ninth column of Table A-5 is the average corrosion potential. In each test, corrosion potential readings were recorded every two minutes using a data acquisition system. The potential data for each test were averaged and the result is shown in Column 9.

The tenth column in the table is the crack depth, in micrometers, measured on the fracture surface in the SEM. A typical example of a measurement is shown in Figure A-6. Note that the depth of the second deepest thumbnail crack was recorded in Table A-5; in some cases, the deepest crack was not representative of the other cracks found on the fracture surface. The eleventh column in the table is the pseudo-crack growth rate, in mm/s, calculated by dividing the crack depth by the time to failure. The last column in the table contains brief comments indicating the goal of each test.

Table A-6 summarizes the results of the SSR tests performed with notched specimens. These tests were performed to evaluate the effects of ethanol-gasoline blend ratio and weld microstructure on SCC susceptibility. The first column in Table 6 is the sample number. The

second column is the grade of line pipe steel used for the testing. The third column in the table is the longitudinal seam weld type. Several different types of longitudinal seam welds were evaluated, including double submerged arc weld (DSAW), low frequency electric resistance weld (LFERW), and high frequency electric resistance weld (HFERW). Seamless line pipe, cast steel, and girth welds were included in the test matrix. The fourth column in the table is the notch location with respect to the weld. The fifth column in the table is the test solution, which was either a SFGE-gasoline blend, or an actual FGE-gasoline blend (Tests 33-36).

The sixth column in the table is the maximum stress sustained by the specimen, which is the maximum load divided by the cross sectional area at the notch root. The seventh column in Table 6 is the total time to failure in the SSR test, in hours. The eighth column in the table is the elongation to failure, which was measure using the displacement transducer on the test frame.

The ninth column of Table A-6 is the average corrosion potential. In each test, corrosion potential readings were recorded every two minutes using a data acquisition system. The potential data for each test were averaged and the result is shown in Column 9.

The tenth column in the table is the crack depth, in micrometers, measured on the fracture surface in the SEM. As with the un-notched specimens, the depth of the second deepest thumbnail crack was recorded. A typical example of a measurement is shown in Figure A-6 and A-7. Figure A-8 is a higher magnification SEM photograph of the fracture surface, which shows that the cracking was mixed mode, with both intergranular and transgranular features. SEM photographs of the fracture surfaces of all of the notched SSR specimens are shown in Appendix E. The eleventh column in the table is the pseudo-crack growth rate, in mm/s, calculated by dividing the crack depth by the time to failure. The last column in the table contains brief comments indicating the goal of each test.

Unlike Table A-5, Table A-6 does not contain a description of the severity of SCC, based on the optical examination of the gage section, or a reduction in area calculation. In the notched specimens, the cracking is confined to the notch and there is no appreciable necking of the specimen, regardless of the extent of SCC.

Table 2. Chemical compositions of steels used in SSR testing.

ELEMENT		X60 * DSAW	X52 * ERW	X46 ** DSAW	X42 ** SMLS	X46 ** HFERW	X52 ** HFERW	X52 ** LFERW	CAST ** STEEL
C	(Carbon)	0.198	.229	.191	0.226	.255	0.225	0.250	.237
Mn	(Manganese)	1.12	.960	.097	0.880	.091	1.24	1.08	.064
P	(Phosphorus)	0.009	.016	.006	0.007	.010	0.005	0.012	.022
S	(Sulfur)	0.017	.032	.017	0.016	.002	0.015	0.022	.015
Si	(Silicon)	0.216	.018	.017	0.038	.021	0.016	0.000	.636
Cu	(Copper)	0.085	.036	.016	0.016	.012	0.068	0.10	.109
Sn	(Tin)	0.007	.003	.002	0.002	.002	0.005	0.008	.010
Ni	(Nickel)	0.029	.041	.016	0.010	.010	0.035	0.038	.062
Cr	(Chromium)	0.042	.034	.029	0.029	.026	0.024	0.024	.186
Mo	(Molybdenum)	0.006	.002	.000	0.002	.001	0.012	0.010	.017
Al	(Aluminum)	0.020	.006	.003	0.029	.077	0.002	0.017	.053
V	(Vanadium)	0.001	.001	.001	–	.001	0.003	0.000	.005
Nb	(Niobium)	0.037	.001	.001	0.001	.001	0.026	0.000	.002
Zr	(Zirconium)	0.001	.001	.000	0.001	.000	0.000	0.000	.001
Ti	(Titanium)	0.002	.000	.000	–	.002	0.003	0.000	.002
B	(Boron)	0.0001	.000	.000	–	.000	0.0000	0.0001	.000
Ca	(Calcium)	0.0001	.000	.000	–	.002	0.0002	0.000	.000
Co	(Cobalt)	0.003	.005	.006	0.003	.001	0.007	0.004	.011
Fe	(Iron)	Balance	Balance	Balance	Balance	Balance	Balance	Balance	Balance

*Un-notched base metal specimens
** Notched specimens

Table 3. Matrix of Slow Strain Rate SCC Tests for Task 1.

Test ID	Steel Source	Pipe Type	Pipe Diameter, inches	Pipe Wall, inches	Pipe Grade	Notch Location	Ethanol	Ethanol Blend			
								E10	E20	E30	E50
SCC4-4-1	A	DSAW	36	0.500	X46	Base	PRCI SFGE *				
SCC4-4-2	A	DSAW	36	0.500	X46	Base	PRCI SFGE				X
SCC4-4-3	A	DSAW	36	0.500	X46	Base	PRCI SFGE			X	
SCC4-4-4	A	DSAW	36	0.500	X46	Base	PRCI SFGE		X		
SCC4-4-5	A	DSAW	36	0.500	X46	Base	PRCI SFGE	X			
SCC4-4-6	C	Seamless	22	0.281	X42	Base	PRCI SFGE			X	
SCC4-4-7	C	Seamless	22	0.281	X42	Base	PRCI SFGE				
SCC4-4-8	A	DSAW	36	0.500	X46	DSAWweld	PRCI SFGE				
SCC4-4-9	A	DSAW	36	0.500	X46	DSAW weld	PRCI SFGE				
SCC4-4-10	A	DSAW	36	0.500	X46	DSAW HAZ	PRCI SFGE				
SCC4-4-11	A	DSAW	36	0.500	X46	DSAW HAZ	PRCI SFGE				
SCC4-4-12	A	DSAW	36	0.500	X46	DSAW weld	PRCI SFGE			X	
SCC4-4-13	A	DSAW	36	0.500	X46	DSAW weld	PRCI SFGE			X	
SCC4-4-14	A	DSAW	36	0.500	X46	DSAW HAZ	PRCI SFGE			X	
SCC4-4-15	A	DSAW	36	0.500	X46	DSAW HAZ	PRCI SFGE			X	
SCC4-4-16	A	HFERW	12	0.375	X46	Base	PRCI SFGE				
SCC4-4-17	A	HFERW	12	0.375	X46	Girth,Weld	PRCI SFGE			X	
SCC4-4-18	A	HFERW	12	0.375	X46	Girth,Weld	PRCI SFGE				
SCC4-4-19	A	HFERW	12	0.375	X46	GW, HAZ	PRCI SFGE			X	
SCC4-4-20	A	HFERW	12	0.375	X46	GW, HAZ	PRCI SFGE				
SCC4-4-21	B	HFERW	24	0.312	X52	Base	PRCI SFGE				
SCC4-4-22	B	HFERW	24	0.312	X52	Weld	PRCI SFGE			X	

Test ID	Steel Source	Pipe Type	Pipe Diameter, inches	Pipe Wall, inches	Pipe Grade	Notch Location	Ethanol	Ethanol Blend			
								E10	E20	E30	E50
SCC4-4-23	B	HFERW	24	0.312	X52	Weld	PRCI SFGE				
SCC4-4-24	B	HFERW	24	0.312	X52	HAZ	PRCI SFGE			X	
SCC4-4-25	B	HFERW	24	0.312	X52	HAZ	PRCI SFGE				
SCC4-4-26	D	LFERW	20	0.250	X52	Base	PRCI SFGE				
SCC4-4-27	D	LFERW	20	0.250	X52	Weld	PRCI SFGE			X	
SCC4-4-28	D	LFERW	20	0.250	X52	Weld	PRCI SFGE				
SCC4-4-29	D	LFERW	20	0.250	X52	HAZ	PRCI SFGE			X	
SCC4-4-30	D	LFERW	20	0.250	X52	HAZ	PRCI SFGE				
SCC4-4-31	TBD	Casting	N/A	N/A	TBD	Casting	PRCI SFGE			X	
SCC4-4-32	TBD	Casting	N/A	N/A	TBD	Casting	PRCI SFGE				
SCC4-4-33	A	DSAW	36	0.500	X46	Base	Company A				
SCC4-4-34	A	DSAW	36	0.500	X46	Weld	Company A				
SCC4-4-35	A	DSAW	36	0.500	X46	Base	Company A			X	
SCC4-4-36	A	DSAW	36	0.500	X46	Weld	Company A			X	

* Containing 5 ppm Cl.

Table 4. Additives used to prepare SFGE .

200-Proof Ethanol	Water	Methanol	Denaturant	Chlorides	Acetic Acid
3785 ml	40 ml	20 ml	150 ml gasoline	0.0265 g NaCl	0.3 ml

Table 5. Target composition of SFGE.

Requirement	ASTM D 4806 Limits		PRCI SFGE
	Minimum	Maximum	
Ethanol, vol. %	92.1	–	
Methanol, vol. %	–	0.5	0.5
Solvent-washed gum, mg/100 ml	–	5.0	–
Water content, vol. %	–	1.0	1.0
Denaturant content, vol. %	1.96	5.00	3.75
Inorganic chloride, ppm (mg/L)	–	40 (32)	5 ppm
Copper, mg/kg	–	0.1	–
Acidity (as Acetic Acid CH_3COOH), mass % (mg/L)	–	0.007 (56)	(75)
pH_e	6.5	9.0	–

Table 6. Summary of results of SSR tests performed with un-notched base metal specimens

Sample №	Steel	Solution	Max Stress, MPa	Time-to-Failure, hours	Elongation to Failure, %	Reduction in Area %	Severity of SCC	Average Corrosion Potential, mV (Ag/AgCl)	Crack Depth, µm	Crack Growth Rate, mm/s	Comment
(4-4)-X0	X60 DSAW	None	589.9	52.7	17.5	69.5	None	–	0	0	Control (No Solution)
(4-4)-X1	X60 DSAW	SFGE w/o Cl	588.2	59.5	19.2	70.4	Very Minor	97	0*	0*	Evaluate Effect of Chloride
(4-4)-X2	X60 DSAW	SFGE (40 ppm Cl)	593.0	40.9	14.0	48.6	Severe	48	336	2.28×10^{-6}	Evaluate Effect of Chloride
(4-4)–X3	X60 DSAW	SFGE (80 ppm Cl)	606.8	38.1	13.1	44.7	Severe	29	461	3.36×10^{-6}	Evaluate Effect of Chloride
(4-4)-X4	X52 ERW	SFGE (4 ppm Cl)	540.8	38.0	18.8	37.1	Severe	90	354	2.58×10^{-6}	Evaluate Effect of Chloride
(4-4)-X5	X52 ERW	SFGE (8 ppm Cl)	536.5	38.0	18.1	37.3	Severe	84	327	2.39×10^{-6}	Evaluate Effect of Chloride
(4-4)-X7	X52 ERW	None	523.1	64.5	21.3	60.1	None	–	0	0	Control (No Solution)

* Some SCC on gage section in necked region.

Table 7. Summary of results of SSR tests performed with notched test specimens.

Sample №	Steel	Weld Type	Notch Location	Solution [b]	Maximum Stress, Mpa	Time-to-Failure, hours	Elongation to Failure, mm	Average Corrosion Potential, mV (Ag/AgCl)	Crack Depth, µm	Crack Growth Rate, mm/s	Comment
(4-4)-1	X46	DSAW	Base	E-95	453.4	44.5	1.27	-74	727	4.54×10^{-6}	Evaluate DSAW base metal performance with blends
(4-4)-2	X46	DSAW	Base	E-50	448.5	38.5	1.68	233	584	4.21×10^{-6}	Evaluate DSAW base metal performance with blends
(4-4)-3	X46	DSAW	Base	E-30	461.3	45.7	1.60	–	643	3.90×10^{-6}	Evaluate DSAW base metal performance with blends
(4-4)-4	X46	DSAW	Base	E-20	453.2	41.1	1.32	221	355	2.40×10^{-6}	Evaluate DSAW base metal performance with blends
(4-4)-5	X46	DSAW	Base	E-10	501.8	61.2	1.98	–	0	0	Evaluate DSAW base metal performance with blends
(4-4)-6	X42	SMLS[a]	–	E-30	501.2	52.3	1.73	284	454	2.41×10^{-6}	Evaluate seamless pipe
(4-4)-7	X42	SMLS[a]	–	E-95	470.6	50.0	0.99	262	456	2.53×10^{-6}	Evaluate seamless pipe
(4-4)-8	X46	DSAW	Weld	E-95	503.5	50.3	1.65	302	578	3.19×10^{-6}	Evaluate DSAW weld metal performance
(4-4)-9	X46	DSAW	Weld	E-95	558.6	43.3	1.60	196	549	3.52×10^{-6}	Evaluate DSAW weld metal performance
(4-4)-10	X46	DSAW	HAZ	E-95	508.5	31.2	0.61	208	419	3.73×10^{-6}	Evaluate DSAW HAZ performance
(4-4)-11	X46	DSAW	HAZ	E-95	521.6	34.9	1.65	272	492	3.92×10^{-6}	Evaluate DSAW HAZ performance
(4-4)-12	X46	DSAW	Weld	E-30	573.8	51.8	1.78	298	447	2.40×10^{-6}	Evaluate DSAW weld metal performance with blend
(4-4)-13	X46	DSAW	Weld	E-30	579.4	51.3	1.68	282	478	2.59×10^{-6}	Evaluate DSAW weld metal performance with blend

Table 7 (continued). Summary of results of SSR tests performed with notched test specimens.

Sample №	Steel	Weld Type	Notch Location	Solution [b]	Maximum Stress, Mpa	Time-to-Failure, hours	Elongation to Failure, mm	Average Corrosion Potential, mV (Ag/AgCl)	Crack Depth, µm	Crack Growth Rate, mm/s	Comment
(4-4)-14	X46	DSAW	HAZ	E-30	526.7	39.4	1.63	342	530	3.73×10^{-6}	Evaluate DSAW HAZ performance with blend
(4-4)-15	X46	DSAW	HAZ	E-30	526.2	36.3	1.24	354	532	4.07×10^{-6}	Evaluate DSAW HAZ performance with blend
(4-4)-16	X46	HFERW	Base	E-95	469.0	55.9	1.83	58	845	4.20×10^{-6}	Evaluate X46 HFERW base metal Performance
(4-4)-17	X46	HFERW	Girth Weld	E-30	506.7	58.2	1.63	147	489	2.33×10^{-6}	Evaluate girth weld metal performance with blend
(4-4)-18	X46	HFERW	Girth Weld	E-95	529.3	64.0	1.80	145	513	2.23×10^{-6}	Evaluate girth weld metal performance
(4-4)-19	X46	HFERW	GWHAZ	E-30	507.1	55.7	1.80	–	719	3.59×10^{-6}	Evaluate GW HAZ performance with blend
(4-4)-20	X46	HFERW	GWHAZ	E-95	525.1	61.2	1.75	214	852	3.87×10^{-7}	Evaluate GW HAZ performance
(4-4)-21	X52	HFERW	Base	E-95	541.6	37.7	–	244	650	4.79×10^{-6}	Evaluate HFERW base metal performance
(4-4)-22	X52	HFERW	Weld	E-30	485.6	21.8	0.64	239	0	0	Evaluate HFERW weld metal performance with blend
(4-4)-23	X52	HFERW	Weld	E-95	358.8	15.8	0.63	134	0	0	Evaluate HFERW weld metal performance
(4-4)-24	X52	HFERW	HAZ	E-30	541.1	21.7	0.79	281	0	0	Evaluate HFERW HAZ performance with blend
(4-4)-25	X52	HFERW	HAZ	E-95	590.0	24.6	0.81	307	30	3.39×10^{-7}	Evaluate HFERW HAZ performance
(4-4)-26	X52	LFERW	Base	E-95	557.1	39.5	1.07	306	353	2.48×10^{-6}	Evaluate LFERW base metal performance

Table 7 (continued). Summary of results of SSR tests performed with notched test specimens.

Sample №	Steel	Weld Type	Notch Location	Solution [b]	Maximum Stress, Mpa	Time-to-Failure, hours	Elongation to Failure, mm	Average Corrosion Potential, mV (Ag/AgCl)	Crack Depth, µm	Crack Growth Rate, mm/s	Comment
(4-4)-27	X52	LFERW	Weld	E-30	785.5	63.3	1.55	380	0	0	Evaluate LFERW weld metal performance with blend
(4-4)-28	X52	LFERW	Weld	E-95	848.2	57.7	1.52	174	291	1.41×10^{-6}	Evaluate LFERW weld metal performance
(4-4)-29	X52	LFERW	HAZ	E-30	884.4	33.6	0.97	550	136	1.13×10^{-6}	Evaluate LFERW HAZ performance with blend
(4-4)-30	X52	LFERW	HAZ	E-95		28.5	0.48	260	219	2.13×10^{-6}	Evaluate LFERW HAZ performance
(4-4)-31	Cast	–	–	E-30	520.3	82.7	2.78	235	491	1.65×10^{-6}	Evaluate cast steel performance with blend
(4-4)-32	Cast	–	–	E-95	541.0	100.1	3.49	-46	442	1.23×10^{-6}	Evaluate cast steel performance
(4-4)-33	X46	DSAW	Base	E-95 [c]	483.2	42.6	0.81	78	438	2.86×10^{-6}	Evaluate DSAW base metal performance with actual FGE
(4-4)-34	X46	DSAW	Weld	E-95 [c]	560.8	47.4	1.35	151	463	2.71×10^{-6}	Evaluate DSAW weld metal performance with actual FGE
(4-4)-35	X46	DSAW	Base	E-30 [c]	476.9	42.6	1.60	192	346	2.26×10^{-6}	Evaluate DSAW base metal performance with actual FGE blend
(4-4)-36	X46	DSAW	Weld	E-30 [c]	592.8	67.8	2.26	276	414	1.70×10^{-6}	Evaluate DSAW weld metal performance with actual FGE blend
(4-4)-37	X46	HFERW	Base [d]	E-30	483.0	58.4	1.83	416	533	2.53×10^{-6}	Evaluate X46 HFERW base metal performance in blend

a. Seamless
b Prepared with Modified Simulated FGE containing 5 ppm Cl, unless otherwise specified.
c Prepared with actual FGE
d Base metal for pipe used for girth weld evaluation

Table 8. Summary of results of SSR tests performed in Task 5. All testes were performed in SFGE unless noted.

Sample №	Time-to-Failure, Hours	Reduction in Area, %	UTS, MPa	Time-to-Failure, Ratio*	Reduction in Area Ratio*	UTS Ratio *	Crack Depth, µm	Crack Growth Rate, mm/s	Average Corrosion Potential, mV, Ag/AgCl	Comment
Un-Notched Specimens										
C-18	52.7	69.5	590	0.971	0.982	0.999	–	–	–	Control test in air (1229 steel)
4-3-22	55.8	72.1	591	1.029	1.018	1.001	–	–	–	Duplicate control test in air (1229 steel)
Average	54.25	70.8	590.5	1.000	1.000	1.000	–	–	–	Average for Air Tests
4-3-0	49.7	49.3	602	0.916	0.696	1.019	365	2.04E-06	166	Base line test in Lot 4 FGE
4-3-3	50.7	50.4	591	0.935	0.712	1.001	376	2.06E-06	128	Base line test in PRCI SFGE
1229-2	57.4	69.5	616	1.058	0.982	1.043	NC	NC	163	150 ppm NH_4OH
1229-3	55.8	69.5	613	1.029	0.982	1.038	NC	NC	195	150 ppm NH_4OH
1229-4	55.7	72.1	602	1.027	1.018	1.019	NC	NC	128	75 ppm NH_4OH
1229-5	51.7	69.5	601	0.953	0.982	1.018	284	1.53E-06	199	3.38 mM LiOH (same OH molarity as 1229-2 and 1229-3)
1229-7	56.6	71.3	602	1.043	1.007	1.019	NC	NC	42	100 ppm $FeCl_3$
1229-8	47.6	53	616	0.877	0.749	1.043	339	1.98E-06	231	165 ppm NH_4Acetate
1229-51	47.2	47.7	611	0.870	0.674	1.035	358	2.11E-06	200	500 ppm 030509-2
1229-52	55.6	66.7	609	1.025	0.942	1.031	155	7.74E-07	91	500 ppm 030509-4
1229-53	50.4	61.2	616	0.929	0.864	1.043	272	1.5E-06	84	500 ppm 030509-6
1229-54	53.4	69.3	615	0.984	0.979	1.041	86	4.47E-07	68	500 ppm 030509-5
1229-55	53.8	57.3	596	0.992	0.809	1.009	331	1.71E-06	175	500 ppm M 119
1229-56	51.1	55.2	604	0.942	0.780	1.023	309	1.68E-06	80	500 ppm 82870
1229-57	50.8	49.1	611	0.936	0.694	1.035	272	1.49E-06	81	500 ppm 81321
1229-58	52.6	49.1	615	0.970	0.694	1.041	598	3.16E-06	182	500 ppm Y9BH1261
1229-59	55.9	66.2	618	1.030	0.935	1.047	186	9.24E-07	89	250 ppm 154
1229-X1	57.3	68.1	616	1.056	0.962	1.043	185	8.97E-07	96	750 ppm Q (pitting and crevice corrosion observed)
KM-12	64.5	60.1	523	1.000	1.000	1.000	NC	NC	–	Control test in air (1228 steel)
1228-35	60.8	53	534	0.943	0.882	1.021	303	1.38E-06	203	38 ppm NH_4OH
1228-36	64	67.7	491	0.992	1.126	0.939	NC	NC	163	150 ppm NH_4OH
Notched Specimens										
4-4-5	61.2	–	502	1.000	–	1	NC	NC	–	Control test in E-10 (no SCC)
4-4-1	44.5	–	453	0.727	–	0.90239	727	4.54E-06	-74	SFGE
1238-8	33.8	–	616	0.552	–	1.227092	284	2.33E-06	-15	250 ppm NaOH (5mM NaOH/L)
1238-10	46.8	–	526	0.765	–	1.047809	496	2.94E-06	19	150 ppm NH_4OH
1238N-1	50.1	–	550	0.819	–	1.095618	585	3.24E-06	221	150 ppm NH_4OH (Coated gage section)
1238N-2	44.6	–	514	0.729	–	1.023904	635	3.95E-06	162	500 ppm DEA

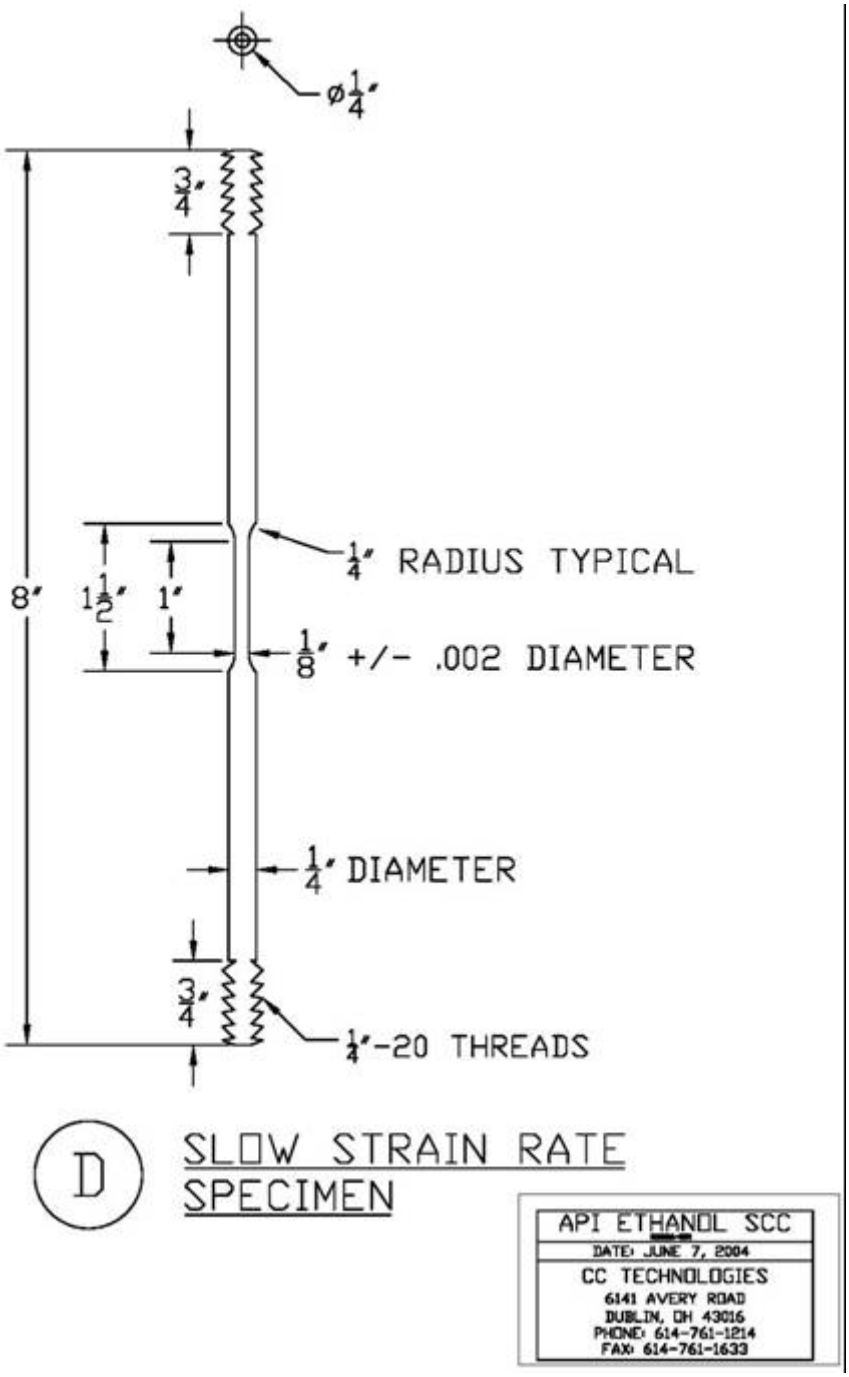

Figure 28. Drawing of un-notched SSR test specimen.

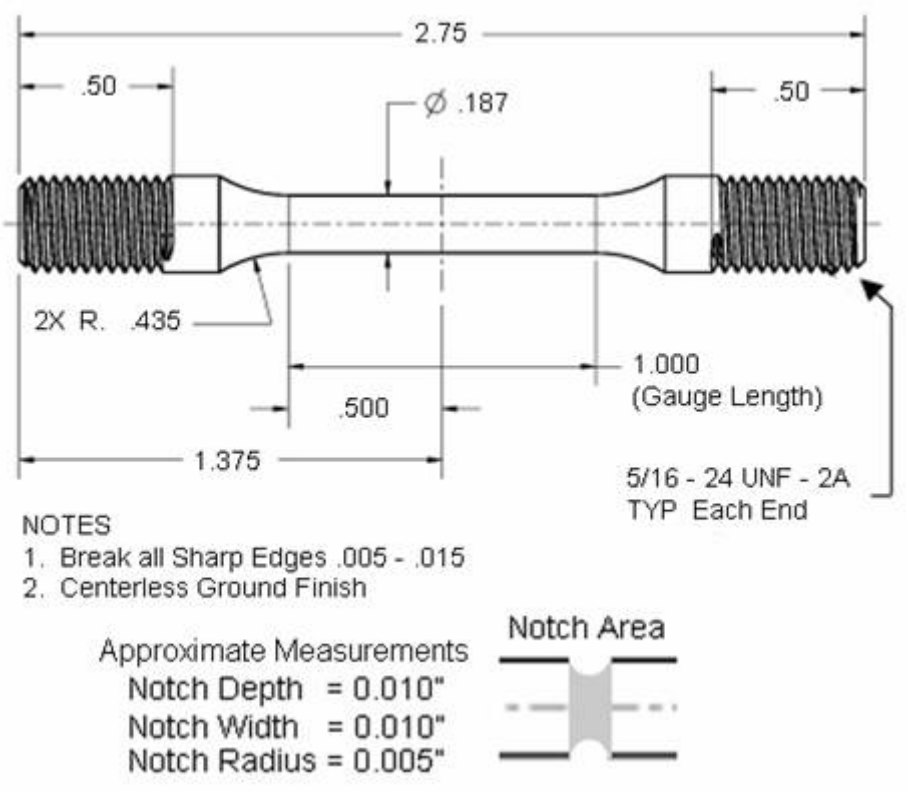

Figure 29. Drawing of notched SSR test specimen.

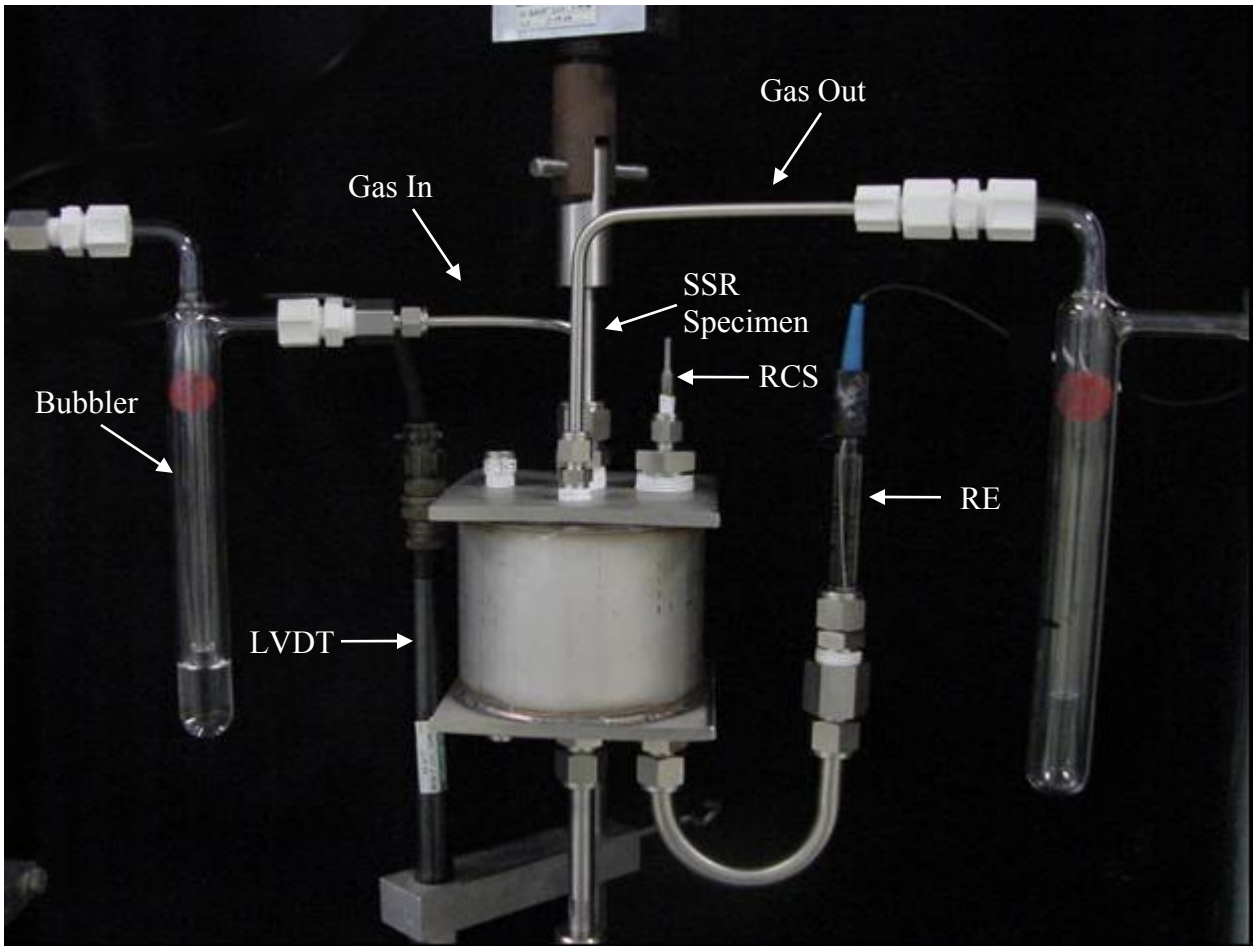

Figure 30. Photograph of cell used for testing the notched specimens; RE – Reference Electrode, LVDT – Displacement transducer, RCS – Connection to rusted carbon steel sample, SSR Specimen – Slow Strain Rate specimen.

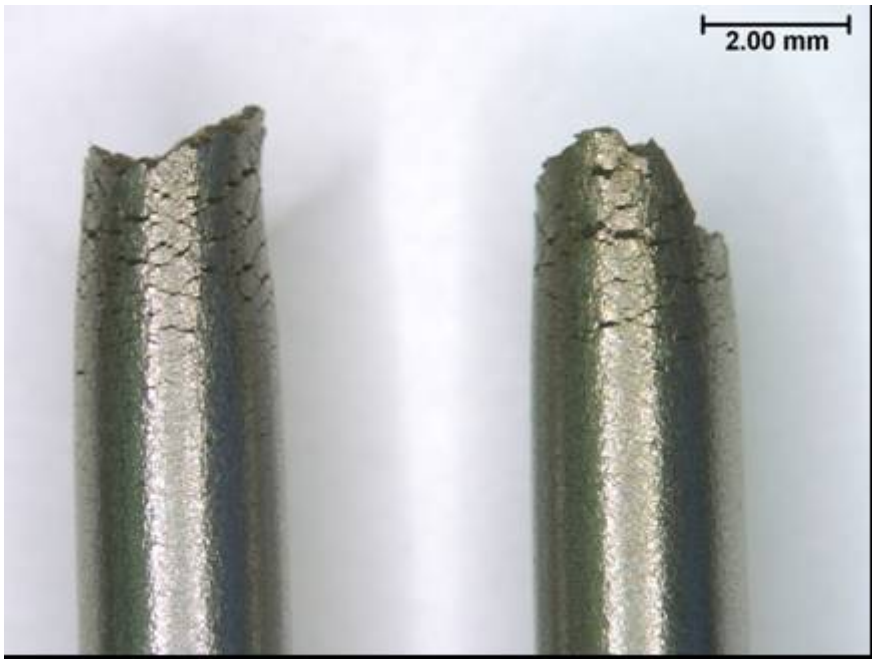

Figure 31. Optical Photograph of gage section of SSR Specimen (4-4)-X4, showing severe cracking.

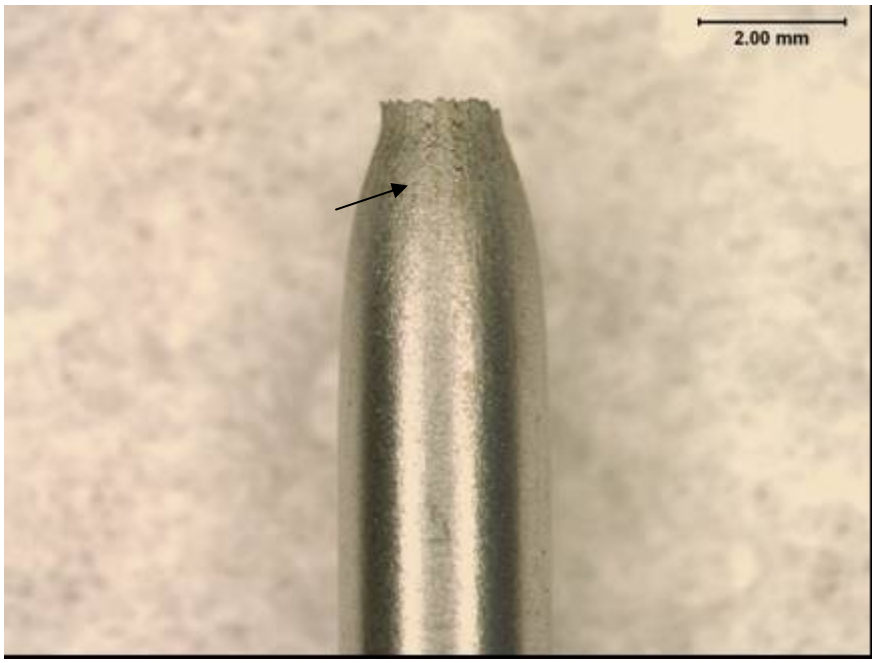

Figure 32. Optical Photograph of gage section of SSR Specimen (4-4)-X1, showing very minor crack-like fissures (arrow) in necked region of gage section.

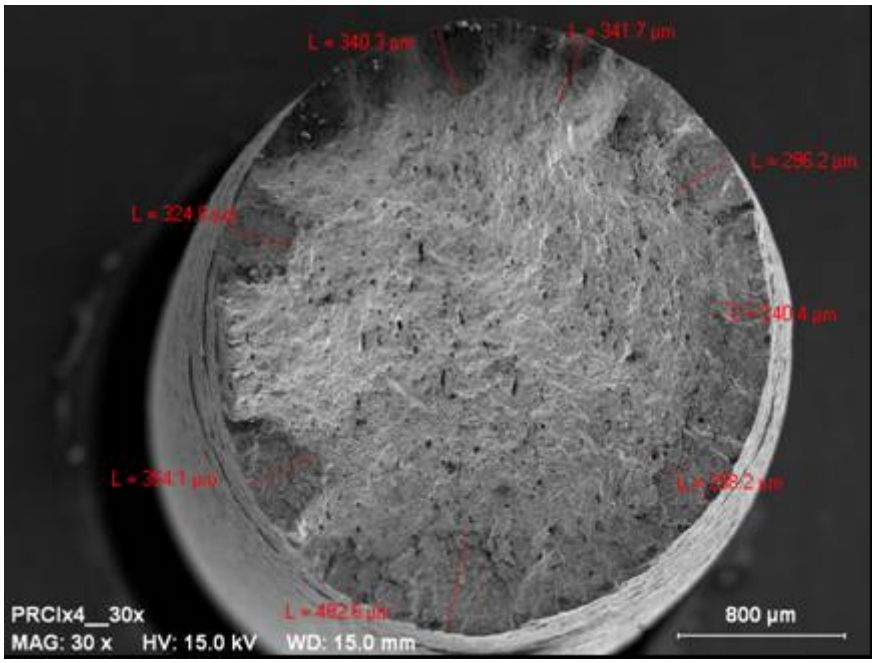

Figure 33. Low magnification SEM photograph of the fracture surface of base metal Specimen (4-4)-X4, tested in SFGE containing 4 ppm Cl, showing SCC crack depth measurements.

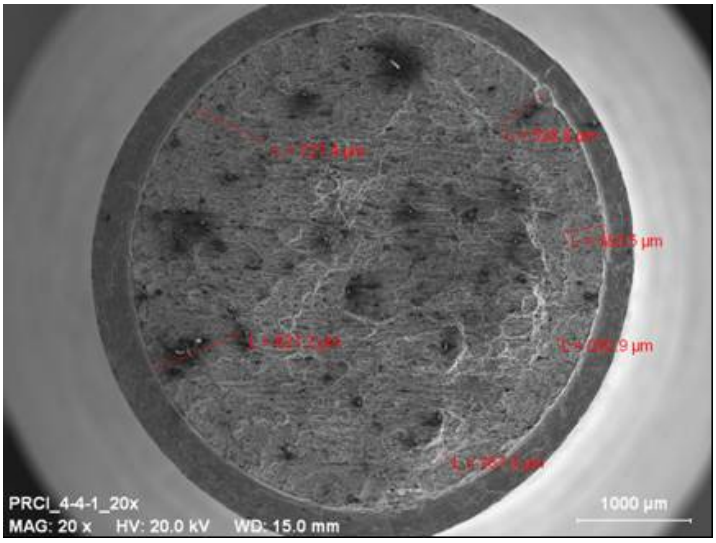

Figure 34. Low magnification SEM photograph of the fracture surface of Specimen (4-4)-1, with notch located in base metal, tested in SFGE containing 5 ppm Cl (E-95), showing SCC crack depth measurement.

Figure 35. High magnification SEM photograph of the fracture surface of Specimen (4-4)-1, with notch located in base metal, tested in SFGE containing 5 ppm Cl (E-95), showing mixed mode cracking.

APENDIX B – CRACK GROWTH MEASUREMENTS

Table 11 summarizes the results of all of the Phase 2 crack growth tests. The first column in the table is the specimen number. The term Base in the specimen number refers to the location of the pre-crack in the specimen with respect to the weld; Base = pre-crack located in the base metal, HAZ = pre-crack located in the heat affected zone of the weld, and Weld = pre-crack located in the weld metal. The second column in the table is the time period over which the test was conducted using a specific test condition. As described above, the test conditions are changed periodically for each specimen in order to asses the effects of the parameters on SCC behavior. The third column is the R ratio, which is the ratio of the minimum to maximum load. Testing has been performed at R ratios of 0.6 and 0.8. Initial tests were performed at an R ratio of 0.8 but cracking did not initiate in some tests so it was decided to run the majority of the later tests under more aggressive cycling, with an R ratio of 0.6. The fourth column in the table is the test environment. All tests are being started with the simulated FGE, and; in some tests, the environment is changed during the test. The fifth and sixth columns are the maximum K and range in K (ΔK), in ksi $in^{1/2}$ for the test period. The seventh column is the amount of crack growth measured from the EPD during the test period and the eighth column is the resulting crack growth rate. Crack length versus time data for all of the crack growth tests are given in Appendix A. The last column contains comments about the test period. Corrosion potential data for the tests are given in Appendix B. The majority of the measured potentials were within the range where SCC has been observed in SSR tests. Detailed descriptions of each test are given below.

Table 9. Summary of results of Phase 2 crack growth tests.

Specimen Number	Time Period, days	R Ratio	Test Environment	K_{max} Start-End, Ksi $in^{1/2}$	ΔK Start-End Ksi $in^{1/2}$	Crack Growth, inches	Crack Growth Rate, mm/s	Note
4-4 Base 1	4 – 39	0.8	SFGE	35.7 – 36.8	7.2 – 7.4	0.0089	7.46E-08	Good Cracking
4-4 Base 1	39 – 60	0.8	Gasoline	36.8 – 36.9	7.4 – 7.4	0.0000	0	No Obvious Crack Growth
4-4 Base 1	60 – 96	0.8	SFGE	36.8 – 36.9	7.4 – 7.6	0.0013	1.07E-08	SCC reinitiated at a slower rate.
4-4 Base 1	96 – 115	0.8	SFGE	37.0 – 36.8	7.6 – 7.3	0.0060	7.52E-08	Unloaded/Reloaded at Day 96
4-4 Base 1	116 – 132	0.64	SFGE	36.8 – 37.0	13.4 – 13.7	0.0057	1.04E-07	Day 116 Switch to R=0.6
4-4 Base 1	132 – 194	0.64	Gasoline	37.0 – 37.3	13.1 – 13.3	0.0000	0.00E+00	Day 132 Changed to 100% Gasoline
4-4 Base 1	194 – 211	0.64	Gasoline	36.6 – 36.8	13.9 – 13.9	0.0000	0.00E+00	Unload/Reload
	211							Test Over
4-4 Base 2	0 – 40	0.8	SFGE	35.7 – 35.9	6.6 – 6.6	0.0022	1.62E-08	Minor SCC Growth
4-4 Base 2	40 – 59	0.6	SFGE	35.9 – 35.9	13.2 – 13.5	0.0000	0.00E+00	Changed to R=0.6 at Day 40
4-4 Base 2	60 – 96	0.6	SFGE	35.9 – 36.8	13.5 – 14.25	0.0105	8.93E-08	Unload-Reload at Day 59
4-4 Base 2	96 – 119	0.6	50% Blend	37.2 – 40.5	14.3 – 14.9	0.0256	3.33E-07	Changed to 50/50 Blend at Day 96
4-4 Base 2	119 – 180	0.6	E10	39.7 – 40.6	15.5 – 16.0	0.0063	3.04E-08	Day 119 Change to E-10 – Day 144-180 CGR was 0
4-4 Base 2	180 – 205	0.61	E10	41.0 – 40.6	16.0 – 16.0	0.0000	0.00E+00	Unload/Reload – End Test Day 205
	205							Test Over
4-4 Base 3	0 – 16	NA	SFGE	0 – 32.6	32.6	0.0030	5.45E-08	Constant Displacement Rate, Loading Stopped at Day 16
4-4 Base 3	16 – 20	NA	SFGE	32.6	0.0	0.0017	2.41E-08	Displacement Held Day 16 to Day 35
4-4 Base 3	20 – 35	NA	SFGE	32.6	0.0	0.0000	0.00E+00	Displacement Held Day 16 to Day 35
	35							Test Over
4-4 Base 4	0 – 29	0.8	SFGE	35.6 – 35.7	6.5 – 6.5	0.0006	2.03E-08	Noisy Crack Growth Data
4-4 Base 4	29 – 37	0.8	SFGE	35.9 – 35.9	7.3 – 7.3	0.0000	0.00	Unload-Reload at 29 Days
4-4 Base 4	37 – 73	0.63	SFGE	36.4 – 37.1	13.6 – 13.9	0.0088	7.26E-08	Changed to R=0.6 at Day 37

Specimen Number	Time Period, days	R Ratio	Test Environment	K_{max} Start-End, Ksi $in^{1/2}$	ΔK Start-End Ksi $in^{1/2}$	Crack Growth, inches	Crack Growth Rate, mm/s	Note
4-4 Base 4	73 – 126	0.62	E20	37.1 – 38.4	13.9 – 14.4	0.0109	5.98E-08	Changed to E-20
4-4 Base 4	126 – 199	0.63	E10	38.3 – 38.2	14.4 – 14.4	0.0000	0.00E+00	Changed to E-10
4-4 Base 4	199 – 218	0.63	SFGE	37.9 – 38.9	14.2 – 14.5	0.0072	1.11E-07	Changed to SFGE
4-4 Base 4	218 – 298	0.63	E15	38.9 – 39.3	14.5 – 14.7	0.0037	1.36E-08	Changed to E-15; CGR was 0 last 45 days
4-4 Base 4	298 – 324	0.63	SFGE	39.3 – 39.9	14.7 – 14.9	0.0045	5.16E-08	Changed to SFGE, Day 298
4-4 HAZ 1	0 – 84	0.8	SFGE	36.5 – 37.8	7.1 – 7.4	0.0105	3.72E-08	Good Cracking but Slower than Base-1
4-4 HAZ 1	84 – 115	0.8	E50	37.8 – 37.8	7.4 – 7.4	0.0003	2.75E-09	Changed to E-50 at 84 Days
4-4 HAZ 1	115 – 132	0.8	E50	37.6 – 38.2	7.3 – 7.5	0.0052	9.17E-08	Unload/Reload Day 115
4-4 HAZ 1	132 – 172	0.81	Gasoline	38.0 – 38.0	7.3 – 7.4	0.0000	0.00	Change to 100% Gasoline
4-4 HAZ 1	172 – 236	0.81	SFGE	38.3 – 38.7	7.4 – 7.4	0.0034	1.56E-08	Changed to SFGE
4-4 HAZ 1	236 – 304	0.81	Batching	38.7 – 38.8	7.6 – 7.5	0.0017	7.37E-09	Batching 7 days Gasoline 5 Days SFGE
4-4 HAZ 1	304 – 329	0.81	SFGE	38.8 – 39.0	7.5 – 7.5	0.0012	1.41E-08	Changed to SFGE
4-4 HAZ 1	329 – 403	0.81	Inhibitor	39.0 – 39.0	7.5 – 7.5	0.0005	1.99E-09	500 ppm 30% NH_4OH
4-4 HAZ 1	403 – 455	0.81	SFGE	39.1 – 39.1	7.5 – 7.6	0.0003	1.70E-09	Changed to SFGE
4-4 HAZ 1	455 – 517	0.8	SFGE	37.4 – 37.4	7.6 – 7.6	0.0002	2.94E-09	Unload-Reload Lowered Load Day 455
4-4 HAZ 1	517							Test Over
4-4 Base 5	0 – 20	NA	SFGE	0 – 32.8		0.0024	3.54E-08	Constant Displacement Rate, Loading Stopped at Day 19
4-4 Base 5	19 – 80	NA	SFGE	32.6		0.0000	0.00E+00	Displacement Held Day 19 to Day 70
	80							Test Over
4-4 Base 6	0 – 17	0.61	SFGE	33.0 – 34.3	13.0 – 12.9	0.0055	9.64E-08	
4-4 Base 6	17 – 30	0.60	SFGE	34.3 – 36.5	12.9 – 13.3	0.0007	1.58E-08	Day 17 Unload-Reload
4-4 Base 6	30 – 42	0.60	SFGE	36.3 – 36.6	14.3 – 14.8	0.0015	3.74E-08	Day 30 Unload-Reload
4-4 Base 6	42 – 66	0.60	SFGE	36.6 – 36.9	14.8 – 14.9	0.0027	3.27E-08	Changed Solution
4-4 Base 6	66 – 77	0.60	SFGE	36.8 – 37.6	14.5 – 14.8	0.0072	1.97E-07	Changed to Fast Cycle Frequency

Specimen Number	Time Period, days	R Ratio	Test Environment	K_{max} Start-End, Ksi $in^{1/2}$	ΔK Start-End Ksi $in^{1/2}$	Crack Growth, inches	Crack Growth Rate, mm/s	Note
4-4 Base 6	77 – 135	0.60	SFGE	36.8 – 38.1	15.0 – 15.2	0.0044	2.20E-08	Returned to Standard Cycle Frequency
4-4 Base 6	135 – 154	0.60	SFGE	38.1 – 38.8	15.3 – 15.5	0.0056	9.03E-08	Batching 23 hrs Gasoline 1 hr SFGE
	154							Test Over
4-4 Base 7	0 – 16	0.61	SFGE	35.4 – 35.8	13.7 – 13.9	0.0051	9.40E-08	
4-4 Base 7	16 – 30	0.62	SFGE	35.8 – 36.6	13.8 – 13.9	0.0040	8.29E-08	Day 16 Unload-Reload
4-4 Base 7	30 – 42	0.61	SFGE	36.3 – 36.6	13.9 – 14.1	0.0026	6.50E-08	Day 30 Unload-Reload
4-4 Base 7	42 – 66	0.61	SFGE	36.6 – 36.8	14.1 – 14.2	0.0032	3.88E-08	Changed Solution
4-4 Base 7	66 – 77	0.61	SFGE	36.8 – 37.2	14.2 – 14.2	0.0053	1.43E-07	Changed to Fast Cycle Frequency
4-4 Base 7	77 – 136	0.62	SFGE	37.2 – 37.9	14.2 – 14.3	0.0053	2.65E-08	Returned to Standard Cycle Frequency
4-4 Base 7	136 – 170	0.62	Batching	37.9 – 38.9	14.3 – 14.7	0.0093	7.83E-08	Batching 1 hr Gasoline 23 hrs SFGE
4-4 Base 7	170 – 234	0.62	SFGE	38.9 – 39.4	14.7 – 14.9	0.0049	2.28E-08	Batching Stopped
4-4 Base 7	234 – 316	0.62	Batching	39.5 – 40.1	15.0 – 15.2	0.0066	2.37E-08	Batching 23 hrs Gasoline 1 hr SFGE
4-4 Base 7	316 – 356	0.62	Gasoline	40.1 – 40.1	15.2 – 15.2	0	0.00E+00	Changed to Gasoline, Day 356
4-4 Base 8								Test Over No Data
4-4 Base 9	45 – 93	0.63	SFGE	38.0 – 38.7	14.1 – 14.6	0.0061	3.74E-08	
4-4 Base 9	93 – 195	0.63	Inhibitor	38.7 – 39.5	14.6 – 14.8	0.0082	2.36E-08	500 ppm DEA
4-4 Base 9	195 – 243	0.63	SFGE	39.5 – 40.3	14.8 – 15.1	0.0066	4.04E-08	Flushed cell New SFGE, Day 195
4-4 Base 9	243 – 281	0.61	SFGE	38.6 – 39.1	15.2 – 15.3	0.0034	2.63E-08	Lowered Load, Day 243
4-4 Base 10	26 – 68	0.66	LTV-200	33.5 – 33.4	11.3 – 11.4	0	0	LTV (mineral oil)
4-4 Base 10	72 – 80	0.61	SFGE	33.2 – 35.7	13.1 – 14.1	0.0246	9.04E-07	Changed to Fast Cycling, Day 72
4-4 Base 10	80 – 131	0.61	SFGE	36.6 – 37.2	14.2 – 14.5	0.0073	4.30E-08	Changed to Regular Cycling, Day 80
4-4 Base 10	131 – 148	0.61	SFGE	37.2 – 37.2	14.5 – 14.5	0.0006	1.04E-08	Added 500 ppm 30% NH_4OH, Day 131
4-4 Base 10	148		SFGE					Changed to SFGE, Day 148

Specimen Number	Time Period, days	R Ratio	Test Environment	K_{max} Start-End, Ksi $in^{1/2}$	ΔK Start-End Ksi $in^{1/2}$	Crack Growth, inches	Crack Growth Rate, mm/s	Note
4-4 Base 11	22 – 68	0.62	SFGE	34.1 – 34.9	13.0 – 13.3	0.0098	5.01E-08	Establishing Cracking
4-4 Base 11	68 – 126	0.62	Batching	34.9 – 34.0	13.3 – 13.2	0	0.00E+00	Batching 23 hrs Gasoline 1 hr SFGE
4-4 Base 11	126 – 141	0.61	SFGE	34.0 – 34.0	13.2 – 13.2	0	0.00E+00	Changed to SFGE, Day 141
4-4 Base 11	141 – 159	0.62	SFGE	34.0 – 33.7	13.2 – 12.9	0.0002	3.17E-09	Unload-Reload, Day 141
4-4 Base 12	0 – 121	0.61	SFGE	34.9 – 37.9	13.7 – 15.1	0.0315	7.65E-08	Start
4-4 Base 12	121 – 132	0.6	SFGE	37.9 – 37.9	15.1 – 15.0	0	0.00E+00	Added Inhibitor MCC 062909-1, Day 121
4-4 Base 13	0 – 32	0.58	SFGE	32.7 – 33.1	13.7 – 13.8	0.0066	6.06E-08	Establishing Cracking
4-4 Base 14	65 – 105	0.65	SFGE	34.0 – 34.4	11.9 – 12.0	0.0058	4.32E-08	Establishing Cracking
4-4 Base 14	105 – 127	0.65	E-50	34.4 – 37.0	12.0 – 12.8	0.0262	3.50E-07	Changed to E-50, Day105
4-4 Weld 1	0 – 17	0.7	SFGE	36.4 – 36.0	11.3 – 10.9	0.0000	0.00E+00	Establishing Cracking
4-4 Weld 1	17 – 30	0.7	SFGE	37 – 36.6	11.4 – 10.8	0.0000	0.00E+00	Day 17 Unload-Reload
4-4 Weld 1	30.0 – 42	0.7	SFGE	36.6 – 36.9	10.9 – 10.9	0.0000	0.00E+00	Day 30 Unload-Reload
4-4 Weld 1	42 – 64	0.71	SFGE	36.9 – 36.6	10.9 – 10.5	0.0000	0.00E+00	Changed Solution
4-4 Weld 1	64 – 77						0	Changed to Fast Cycling Day 64
4-4 Weld 2	0 – 33	0.62	SFGE	34.2 – 39.2	12.9 – 14.7	0.0422	3.79E-07	Establishing Cracking
4-4 Weld 2	33 – 61	0.63	Gas	39.2 – 41.8	14.7 – 15.6	0.0178	1.87E-07	Changed to Gasoline, Day 33
4-4 Weld 2	61 – 84	0.62	Gas	40.9 – 40.9	15.4 – 15.4	0	0.00E+00	Lowered Load, Day 61
4-4 Weld 2								Test Over
4-4 Weld 3	8 – 32	0.64	SFGE	32.7 – 33.6	11.9 – 12.2	0.0096	1.18E-07	Establishing Cracking
	32 – 50	0.64	Gasoline	33.6 – 33.6	12.2 – 12.2	0.0002	3.27E-09	Changed to Gasoline on Day 32

Specimen Number	Time Period, days	R Ratio	Test Environment	K_{max} Start-End, Ksi $in^{1/2}$	ΔK Start-End Ksi $in^{1/2}$	Crack Growth, inches	Crack Growth Rate, mm/s	Note
4-4 Weld 3	50 – 59	0.64	Gasoline	33.6 – 33.7	12.2 – 12.3	0.0015	4.79E-08	Crack Growth Rate Increased, Beginning Day 32
4-4 Weld 3	59 – 72	0.64	Gasoline	33.7 – 33.7	12.3 – 12.3	0.0000	0.00E+00	Crack Growth Rate Decreased to 0 Day 59-72
4-4 Weld 3	32 – 72	0.64	Gasoline	33.6 – 33.7	12.3 – 12.3	0.0017	1.25E-08	Gasoline Period
4-4 Weld 3	72 – 84	0.64	SFGE	33.7 – 34.0	12.3 – 12.3	0.0027	6.61E-08	Changed to SFGE on Day 72, Running

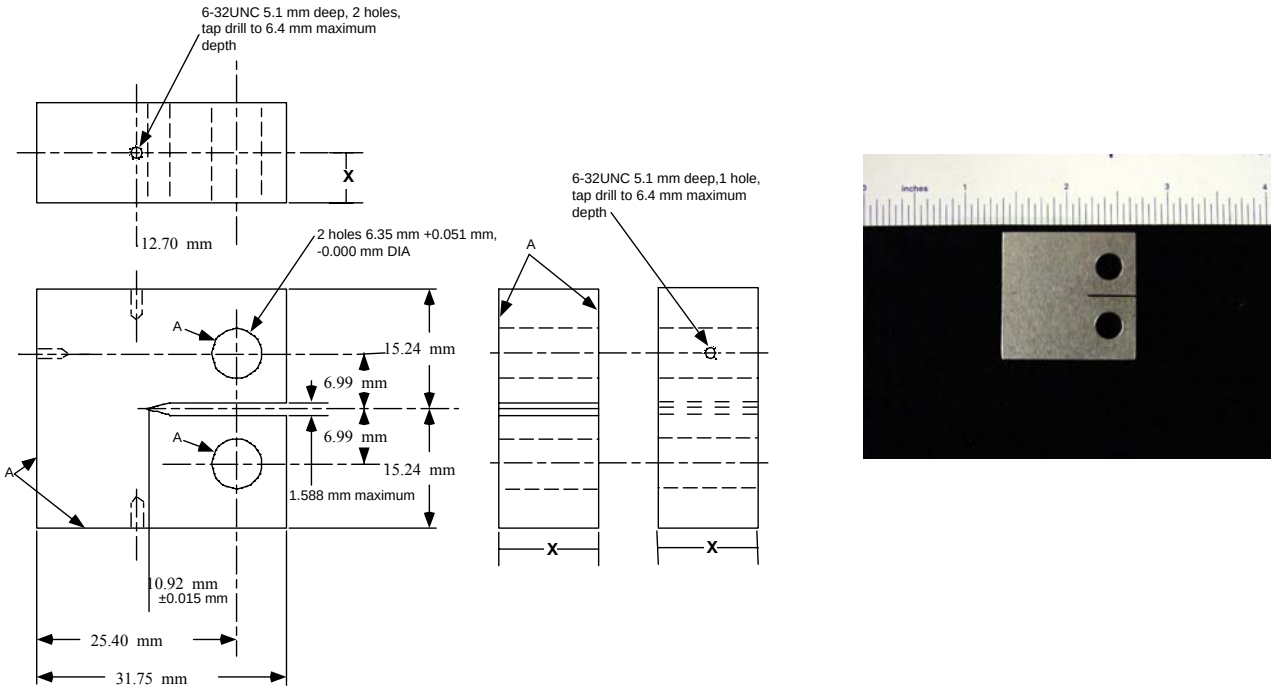

Figure 36. Schematic drawing of the crack growth specimen and photograph.

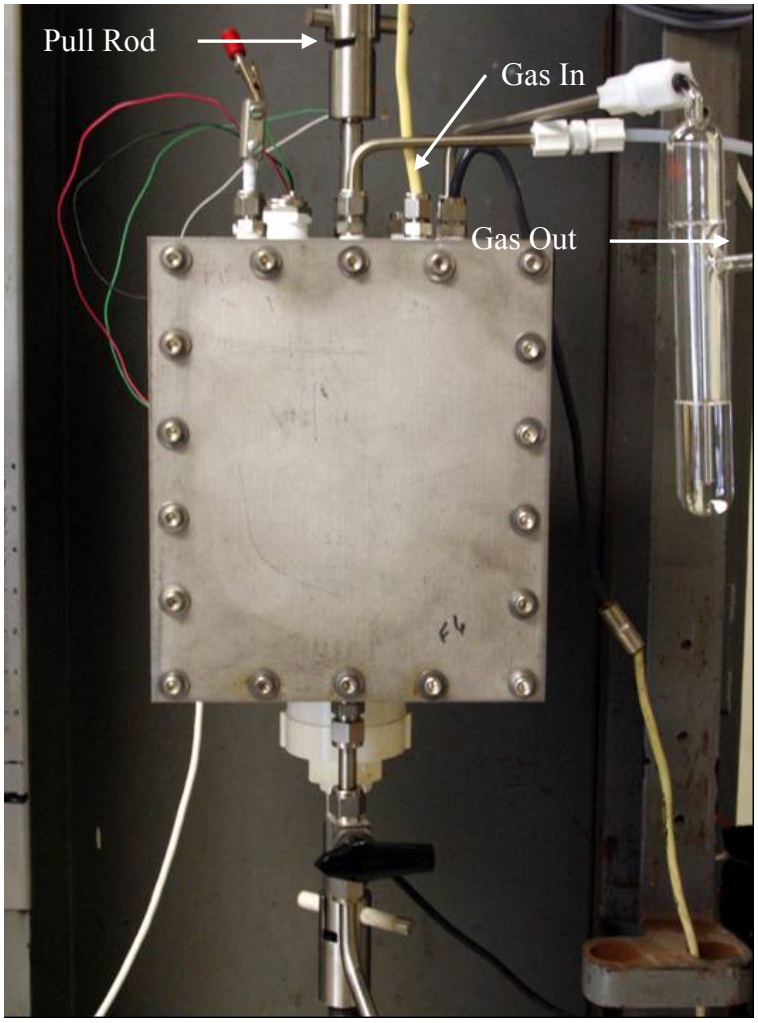

Figure 37. Photograph of cell used for crack-growth testing.

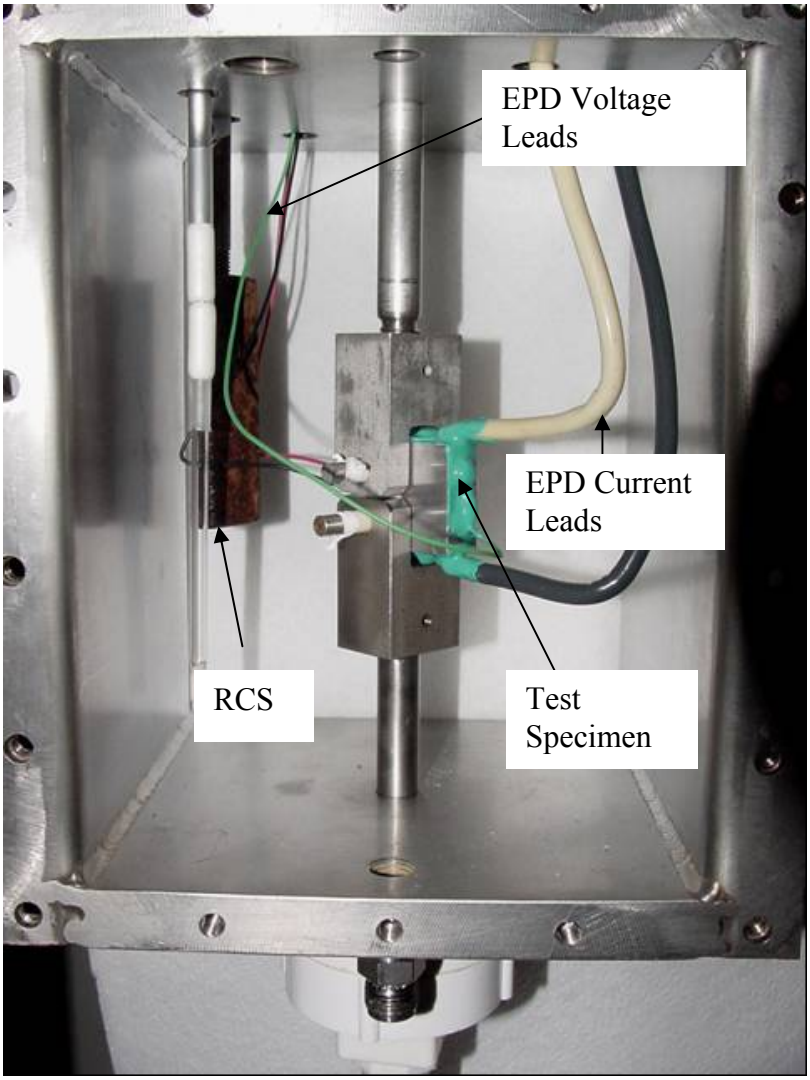

Figure 38. Photograph of the inside of the test cell used for crack-growth testing, showing the test specimen and cell internals; RCS –Rusted Carbon Steel Sample, EPD – Electric Potential Drop.

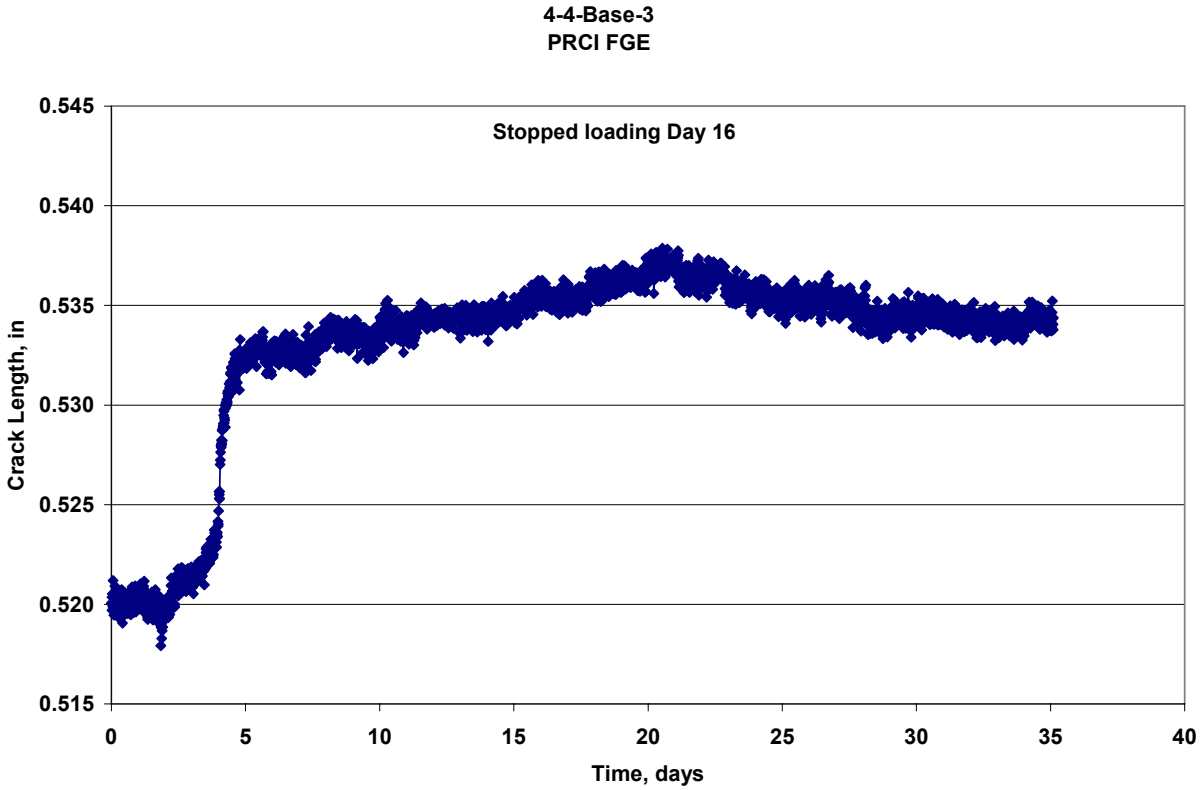

Figure 39. Crack length as a function of time for Specimen 4-4 Base 3.

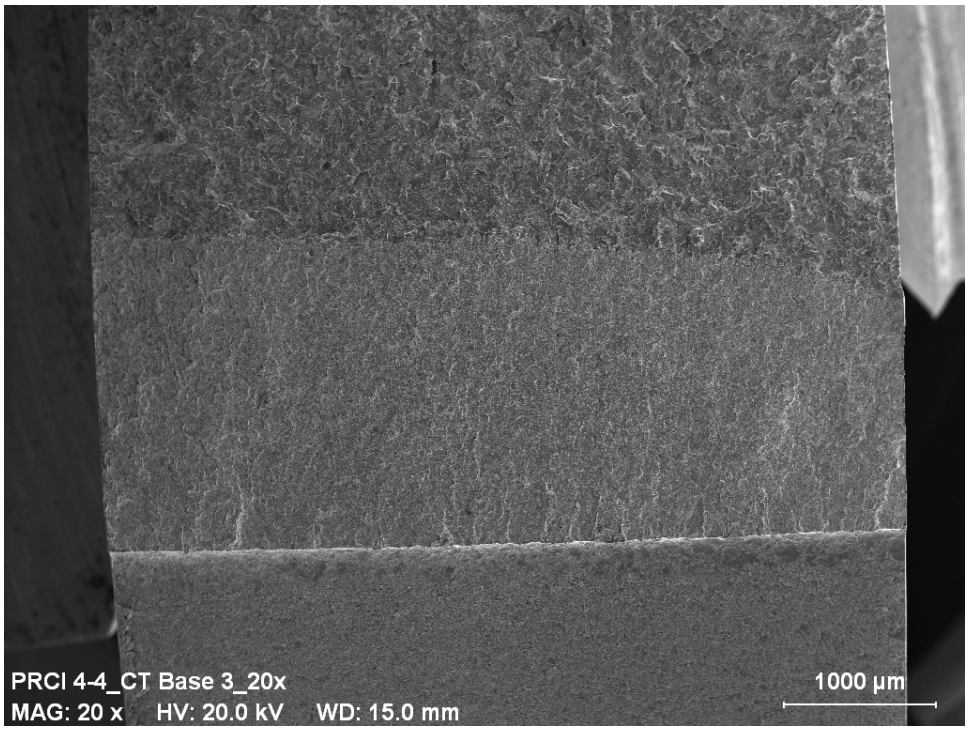

Figure 40. Low magnification SEM photograph of fracture surface of Specimen 4-4 Base 3.

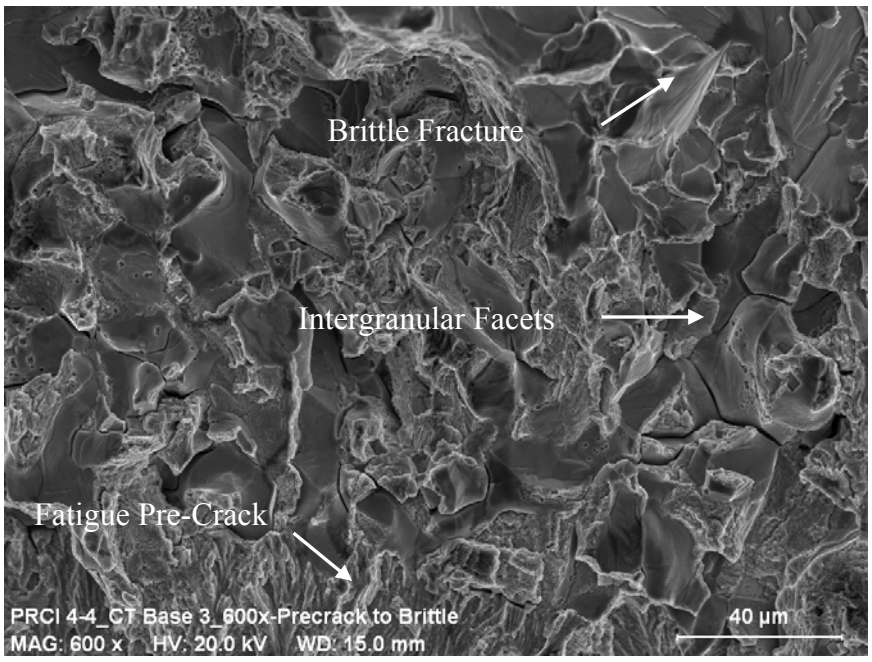

Figure 41. SEM photograph of fracture surface of Specimen 4-4 Base 3 showing the SCC zone.

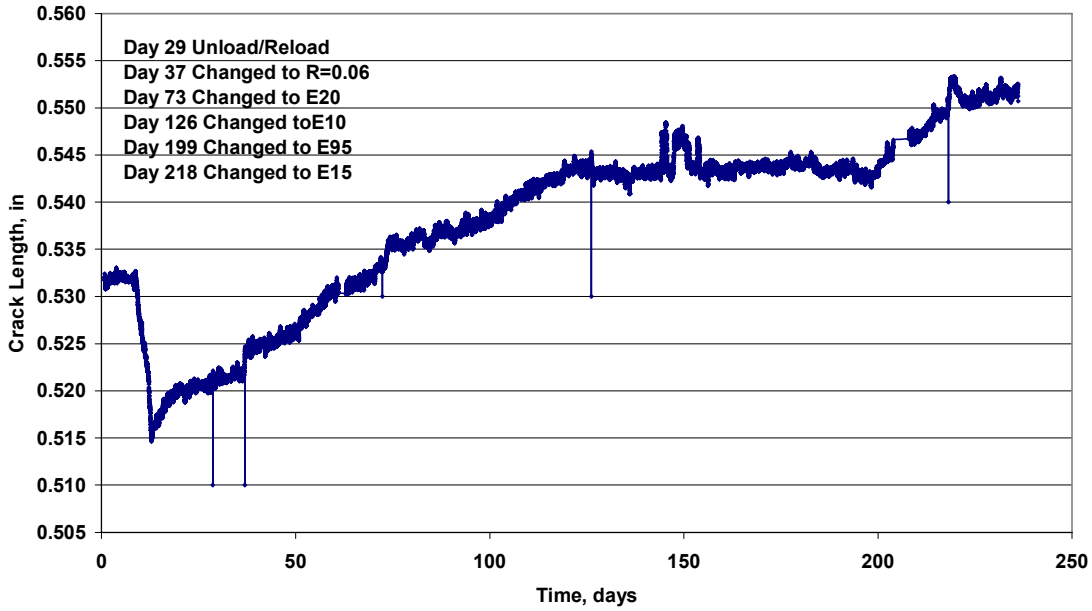

Figure 42. Crack length as a function of time for Specimen 4-4 Base 4 (0 to 240 hours).

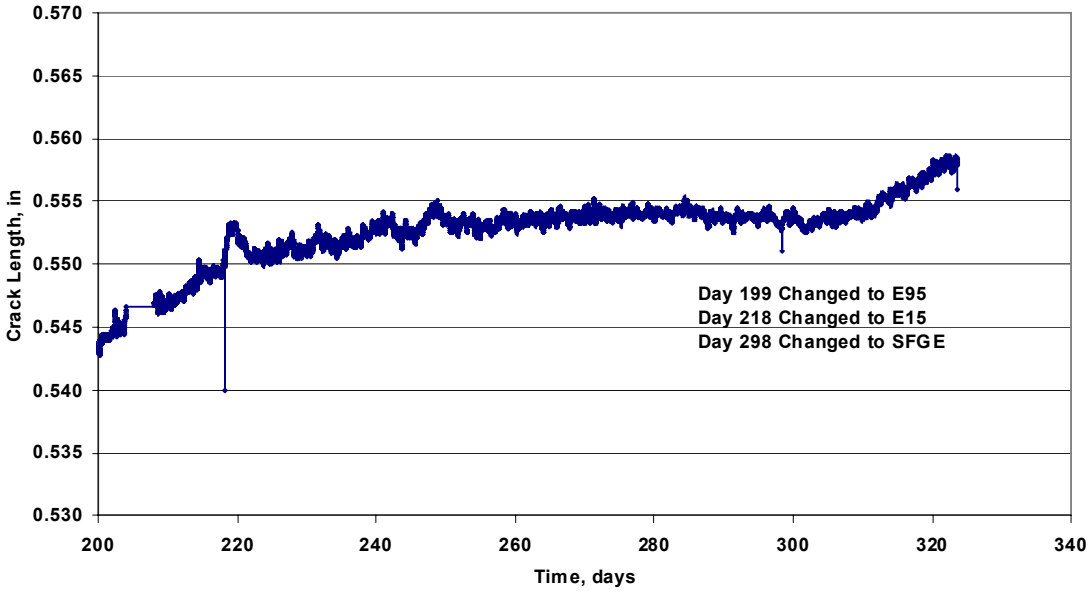

Figure 43. Crack length as a function of time for Specimen 4-4 Base 4 (200 to 325 hours).

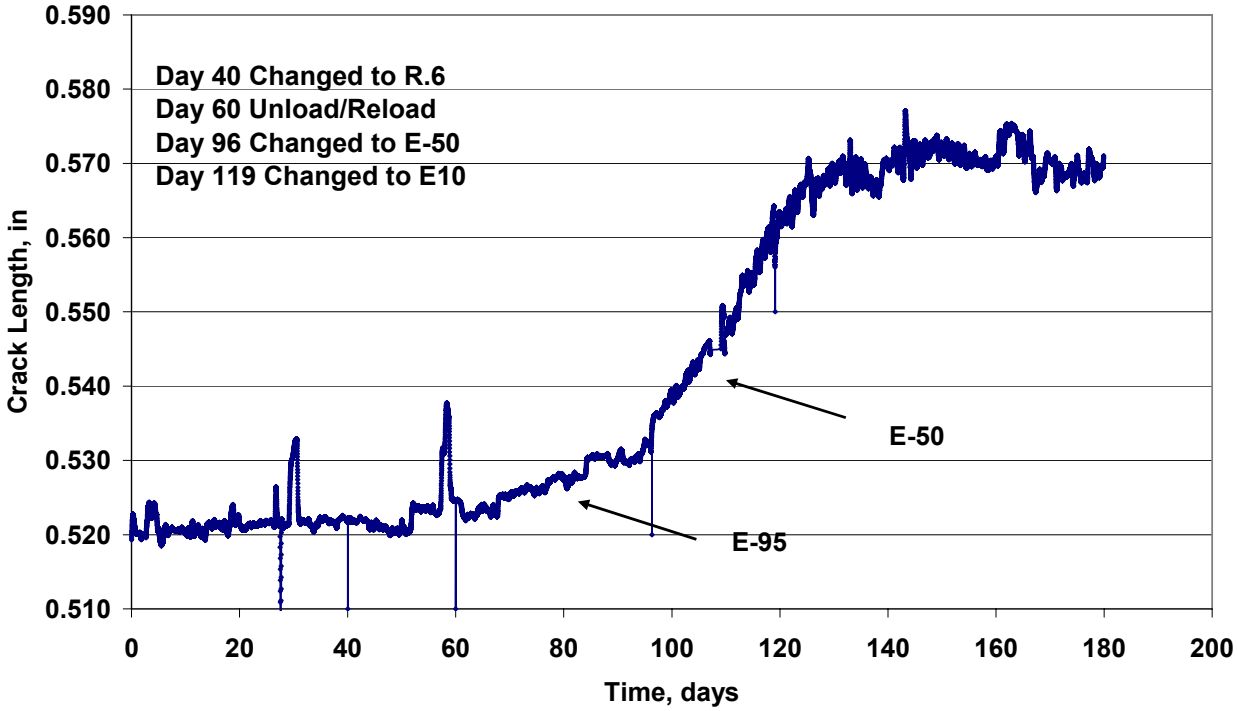

Figure 44. Crack length as a function of time for Specimen 4-4 Base 2 (0 to 190 hours).

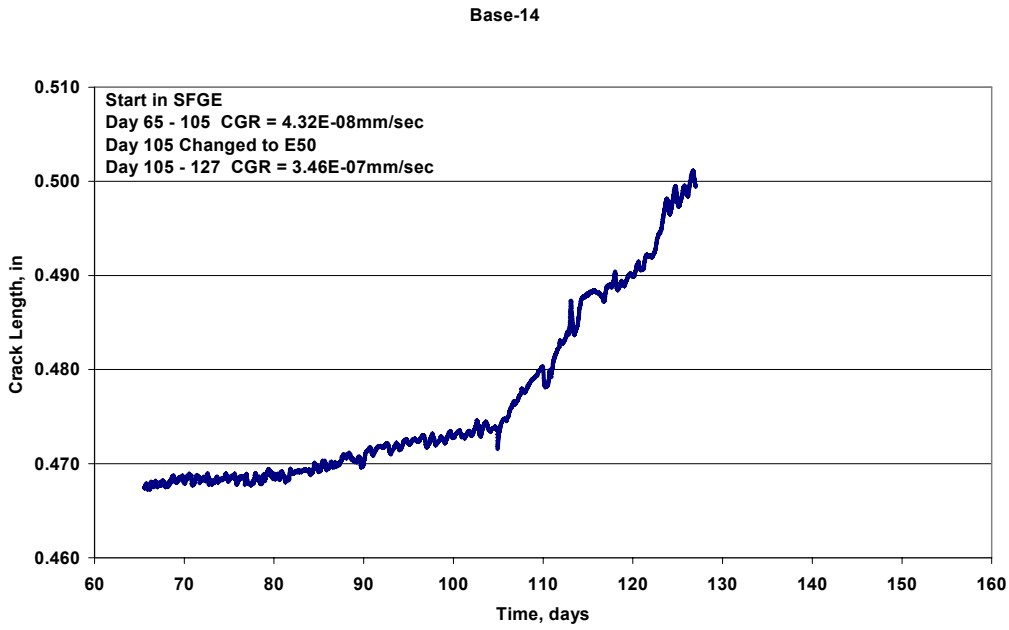

Figure 45. Crack Length as a function of time for Specimen 4-4 Base 14 (65 to 130 hours).

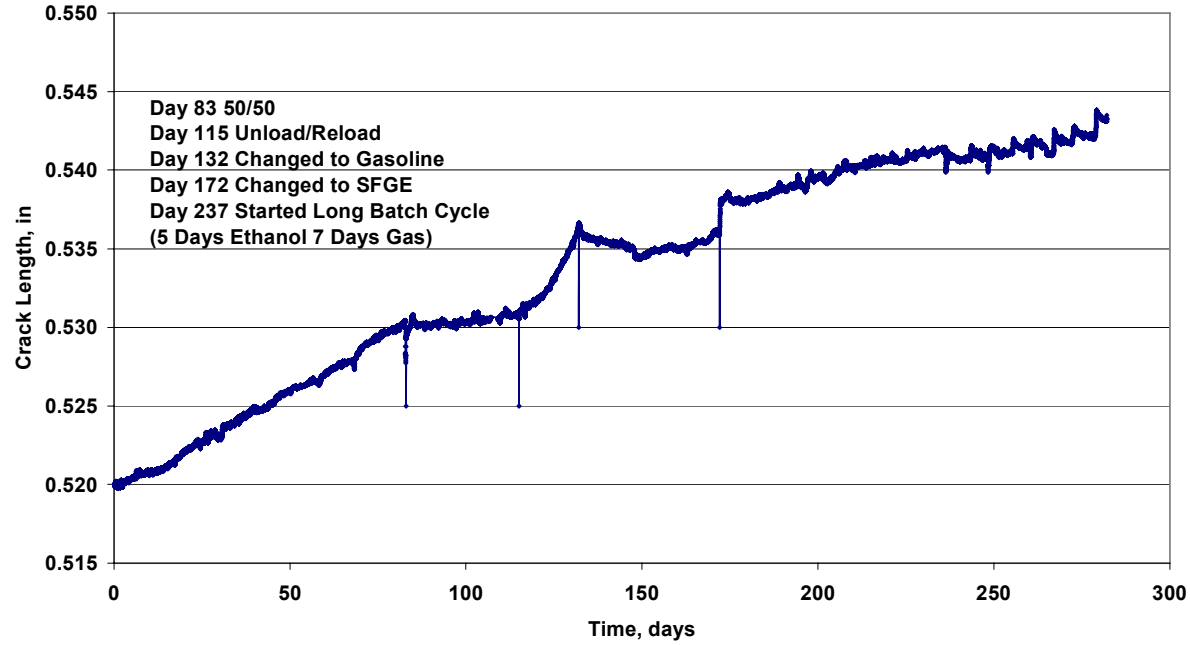

Figure 46. Crack length as a function of time for Specimen 4-4 HAZ 1. Long batch cycle (5 days SFGE – 7 Days Gasoline) started on Day 237.

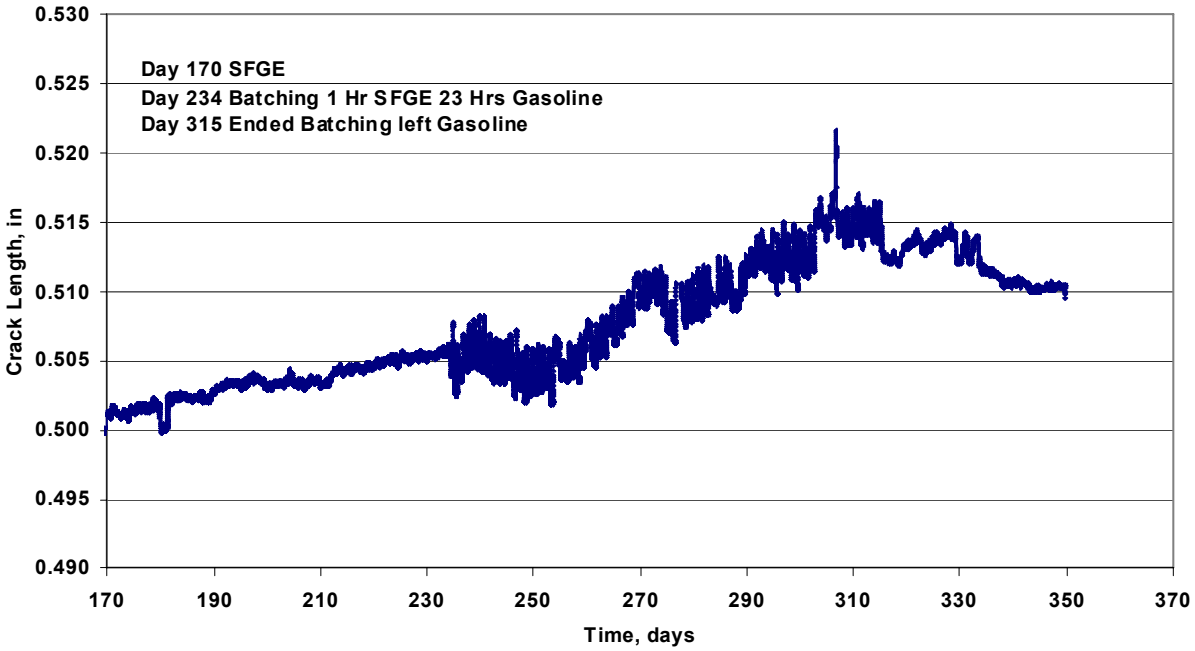

Figure 47. Crack length as a function of time for Specimen 4-4 Base 7. Short batch cycle (1 hour SFGE – 23 hours Gasoline) started on Day 234.

DNV Energy

DNV Energy is a leading professional service provider in safeguarding and improving business performance, assisting energy companies along the entire value chain from concept selection through exploration, production, transportation, refining, and distribution. Our broad expertise covers Asset Risk & Operations Management, Enterprise Risk Management; IT Risk Management; Offshore Classification; Safety, Health and Environmental Risk Management; Technology Qualification; and Verification.

DNV Energy Regional Offices:

Asia and Middle East
Det Norske Veritas Sdn Bhd
24th Floor, Menara Weld
Jalan Raja Chulan
50200 Kuala Lumpur
Phone: +603 2050 2888

North America
Det Norske Veritas (USA), Inc.
1400 Ravello Drive
Katy, TX 77449
United States of America
Phone: +281-396-1000

Europe and North Africa
Det Norske Veritas Ltd
Palace House
3 Cathedral Street
London SE1 9DE
United Kingdom
Phone: +44 20 7357 6080

Offshore Class and Inspection
Det Norske Veritas AS
Veritasveien 1
N-1322 Hovik
Norway
Phone: +47 67 57 99 00

Cleaner Energy & Utilities
Det Norske Veritas AS
Veritasveien 1
N-1322 Hovik
Norway
Phone: +47 67 57 99 00

South America and West Africa
Det Norske Veritas Ltda
Rua Sete de Setembro
111/12 Floor
20050006 Rio de Janeiro Brazil
Phone: +55 21 2517 7232

Nordic and Eurasia
Det Norske Veritas AS
Veritasveien 1
N-1322 Hovik
Norway
Phone: +47 67 57 99 00